TESIS DE LA UNIVERSIDAD DE ZARAGOZA

2023

157

Hasan Md Rafiul

Metal-organic framework (mof)-pebax-based mixed matrix membranes for post-combustion CO2 capture

Director/es

Malankowska, Magdalena

Coronas Ceresuela, Joaquín Juan

ISSN 2254-7606

Prensas de la Universidad Universidad Zaragoza

ISSN 2254-7606

Universidad Zaragoza
1542

Tesis Doctoral

METAL-ORGANIC FRAMEWORK (MOF)-PEBAX-BASED MIXED MATRIX MEMBRANES FOR POST-COMBUSTION CO2 CAPTURE

Autor

Hasan Md Rafiul

Director/es

Malankowska, Magdalena
Coronas Ceresuela, Joaquín Juan

UNIVERSIDAD DE ZARAGOZA
Escuela de Doctorado

2023

Doctoral Thesis

In the area of Chemical Engineering

METAL-ORGANIC FRAMEWORK (MOF)-PEBAX-BASED MIXED MATRIX MEMBRANES FOR POST-COMBUSTION CO_2 CAPTURE

Report to obtain Doctor of Philosophy from University of Zaragoza,
Presented by:

Md Rafiul Hasan

Supervisors:

Magdalena Malankowska
Joaquín Coronas Ceresuela

Chemical and Environmental Engineering Department

University of Zaragoza, Spain

March 2023

METAL ORGANIC FRAMEWORK (MOF)-PEBAX-BASED MIXED MATRIX MEMBRANES FOR POST-COMBUSTION CO_2 CAPTURE

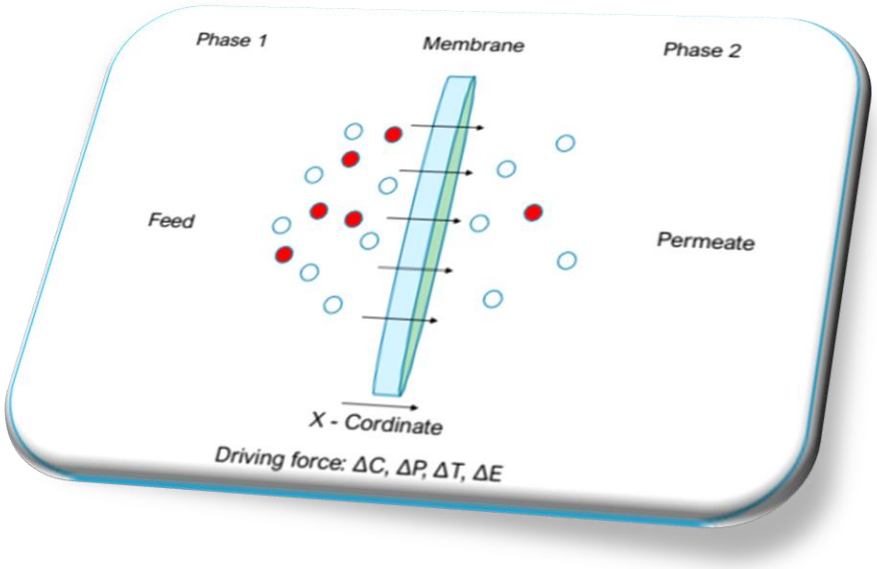

Md Rafiul Hasan

Doctoral Thesis

March 2023

Prof. Joaquín Coronas Ceresuela, Professor in the Department of Chemical and Environment Engineering of the University of Zaragoza and Dr. Magdalena Malankowska, Postdoctoral Researcher, Department of Chemical and Biochemical Engineering of Technical University of Denmark,

Certify for the report entitled:

METAL-ORGANIC FRAMEWORK (MOF)-PEBAX-BASED MIXED MATRIX MEMBRANES FOR POST COMBUSTION CO_2 CAPTURE

That the work has been carried out by Md Rafiul Hasan in the Department of Chemical and Environment Engineering of the University of Zaragoza and authorize its presentation to qualify for the degree of doctor by the University of Zaragoza.

For the record, they signed this certificate in Zaragoza on March 15th, 2023

Fdo.: Dr. Joaquín Coronas Ceresuela **Fdo.: Dr. Magdalena Malankawska**

To my Grandparents

Because your love was unconditional

To my Parents

You sacrificed your life for me

Mehenaz

Your faith inspires me!!

Acknowledgements

To my supervisors, Magdalena Malankowska and Joaquín Coronas, for their advice, cooperation and teaching.

To Carlos Téllez, for all his ideas and support in the different meetings.

To Dr. Md. Zaved Hossain Khan, mentor of my life.

To all my colleagues at CREG with whom I shared both lab and office, who offered me wonderful workplace, without their help and support, it would have been difficult to complete my such a beautiful journey.

To my wife, who has sacrificed her career for me.

To my sisters, who always backed me with their unconditional love and support.

To those, who keep/kept me in their prayers.

To you all, my heartiest Thanks!!!

Table of Contents

Chapter 1

1 Context, objectives and structure of the report

This doctoral thesis entitled "**Metal-Organic Framework (MOF)-Pebax-based Mixed Matrix Membranes for Post-combustion CO_2 Capture**" has been carried out in the research group CREG (Catalysis, Molecular Separations and Reactor Engineering) at the University of Zaragoza (UZ), which is part of the Department of Chemical Engineering Environmental Technologies (IQTMA) of the UZ and the Institute of Nanoscience and Materials of Aragon (INMA) (it is a mixed institute of Spanish National Research Council (CSIC) and UZ). The CREG group has worked since the early 90s on the development and modification of nanostructured materials (porous silicas, zeolites, titano-silicates and related materials, MOFs and graphene) to apply them to different fields such as gas separation, membrane reactors, pervaporation, heterogeneous catalysis, encapsulation, membrane reactors and nanofiltration, to name a few. In 2005, the group began its research on hybrid membranes initially using inorganic porous materials as fillers and later other nanostructured materials such as those mentioned above. Development of MOFs ("metal-organic frameworks") in the group began in 2009, initially for use in hybrid membranes toward gas separation, but later, due to excellent properties of MOFs, their use was extended. Since 2005, the following doctoral theses were supervised in the group related to the fields of porous materials, membranes and mixed matrix membranes:

- "Development of Porous Sheet Materials for the Preparation of Hybrid Membranes". Patricia Gorgojo Alonso (2010).
- "Porous Nanostructured Material-Polymer Hybrid Membranes for the Separation of Gaseous Mixtures". Beatriz Zornoza Encabo (2011).
- "Synthesis and Application of Layered and Delaminated Titanosilicates and Stanosilicates". César Rubio Hortells (2012).
- "Structural Study of Laminar Materials and their Application in Mixed Laminar Material-Polymer Membranes". Alejandro Galve Guinea (2013).
- "Nanocomposite Materials for Membrane Separations Processes". Daniel Sieffert (2013).
- "Encapsulation in Porous Inorganic Materials to Additive Polyamide Fibers". Eduardo Pérez García (2013).
- "New Strategies to Synthesize Zeolites and MOFs. Application to Gas Separation with Micromembranes". Marta Navarro Rojas (2013).
- "Synthesis of Porous Nanostructured Materials in the Presence of Caffeine with Application to Controlled Release". Nuria Liédana Pérez (2014).
- "New MOF Synthesis Strategies and their Application as Filler in Polymeric Membranes for Gas Separation". Beatriz Seoane de la Cuesta (2014).
- "Laminar and Porous Materials for their Application to Sustainable Development". Sonia Castarlenas Sobreviela (2014).
- "Development of Porous Nanostructured Materials for Application in Separation Processes by Polymeric Matrix Hybrid Membranes". Sara Sorribas Roca (2015).

- “Modelling Study of Vanadium Bases Alloys and Crystalline Porous Materials for Gas Separation Membranes”. Jenny Borisova Evtimova (2016).
- “Innovations in Mesoporous Silica, Layered Silicates and MOFs for the Transformation of Sugars into Lactic Acid and Derivatives”. Beatriz Murillo Esteras (2017).
- “Continuous and Supported MOF Membranes for the Separation of Gaseous Mixtures”. Luis Fernando Cacho Bailo (2017).
- “Coordination Polymers: Crystalline Transformations and Gas Separation Through Membranes”. Adelaida Perea Cachero (2017).
- “Synthesis and Characterization of Polyimide-Based Mixed Matrix Membranes for CO_2/CH_4 Separation”. Mohd Zamidi Ahmad (2018).
- “Preparation and Characterization of Mixed Matrix Membranes for Gas Separation and Pervaporation”. Roberto Castro Muñoz (2018).
- “Synthesis of Metal-Organic Materials and Encapsulation of Bioactive Molecules”. Rebeca Monteagudo Oliván (2018).
- “MOF-Based Polymeric Membranes for CO2 Capture”. Javier Sánchez Laínez (2019).
- “Development of Thin Film Nanocomposite Membranes Based on Porous Metal-Organic Materials and Graphene for Application in Nanofiltration”. Lorena Paseta Martínez (2019).
- “Synthesis Strategies for Polyamide and MOF-Polyamide Thin Layers on Flat and Hollow Fiber Supports for Application in Nanofiltration of Organic Solvents and Water”. Carlos Echaide Górriz (2020).
- “Advances in Membranes Based on MOFs and Carbon Nanotubes Focused on Sustainable Separation Processes”. D. Víctor Berned Samatán (2022).
- “CO_2 Capture with Ultrafine Membranes Modified with Porous Metal Organic Compounds”. Lidia Martínez Izquierdo (2022).
- “More Efficient and Sustainable Membrane Osmotic Distillation to Partial Dealcoholization of Wine and Beer”. Javier Esteras Saz (2023).

This thesis reflects the research carried out in CREG group, presenting innovations in the preparation of novel membranes based on MOFs, covering their applications related to sustainability, including the recycling and reuse of the waste materials. Specifically, the thesis focuses on the use of ZIF-94, ZIF-8 and MIL-178(Fe) to form mixed matrix membranes and then the application for the separation of gases for the capture of CO_2 from post-combustion streams and the purification of natural gas or biogas.

Finally, a recycling method for recovering components of MMMs and their reuse has been developed. The completion of this thesis has been possible, thanks to the "MEMBER/Advanced MEMBranes and membrane assisted process for pre and postcombustion CO_2 captuRe (Aid H2020 nº GA 760944)/PIP-MODALIDAD A, as well as the following projects are greatly acknowledged:

- Grant PID2019-104009RB-I00 funded by MCIN/AEI/10.13039/501100011033 is gratefully acknowledged (Agencia Estatal de Investigación (AEI) and MCIN (Ministerio de Ciencia e Innovación), Spain).
- Research Group on Catalysis, Molecular Separations and Reactor Engineering (CREG)" (T43_17R, T43_20R) financed by the Government of Aragon and the European Social Fund.
- Servicio General de Apoyo a la Investigación (SAI).
- Use of instrumentation as well as the technical advice provided by the National Facility ELECMI ICTS, node "Laboratorio de Microscopías Avanzadas" at the University of Zaragoza.

The results presented in this report comprise the following publications that correspond to chapters 4, 5, 6 and 7, respectively:

1. **M.R. Hasan**, L. Paseta, M. Malankowska, C. Téllez, J. Coronas, Synthesis of ZIF-94 from Recycled Mother Liquors: Study of the Influence of Its Loading on Post-combustion CO_2 Capture with Pebax Based Mixed Matrix Membranes, Adv. Sustain. Syst. (2021) 2100317. https://doi.org/10.1002/adsu.202100317.

2. **M.R. Hasan**, A. Moriones, M. Malankowska, & J. Coronas, Study on the Recycling of Zeolitic Imidazolate Frameworks and Polymer Pebax® MH 1657 from their Mixed Matrix Membranes Applied to CO_2 Capture, *Sep. Purif. Technol.* (2023) *122355*. https://doi.org/10.1016/j.seppur.2022.122355.

3. M. Benzaqui, M. Wahiduzzaman, H. Zhao, **M.R. Hasan**, T. Steenhaut, A. Saad, J. Marrot, P. Normand, J.-M. Grenèche, N. Heymans, G. de Weireld, A. Tissot, W. Shepard, Y. Filinchuk, S. Hermans, F. Carn, M. Manlankowska, C. Téllez, J. Coronas, G. Maurin, N. Steunou, C. Serre, A robust eco-compatible microporous iron coordination polymer for CO_2 capture, J. Mater. Chem. A (2022) 8535–8545. https://doi.org/10.1039/d1ta10385g.

4. **M.R. Hasan**, H. Zhao, N. Steunou, C. Serre, M. Malankowska, C. Téllez, & J. Coronas, Optimization of MIL-178(Fe) and Pebax® 3533 loading in mixed matrix membranes for CO_2 capture, *Int. J. Greenhouse Gas Control* (2022) 103791. https://doi.org/10.1016/j.ijggc.2022.103791.

1.1 Context

Membrane technology is said to be one of the optimistic solutions in controlling global warming caused by industrial revolution, due to their lower production cost, affordable operation cost, efficient separation performance and lower carbon footprint. Simultaneously, membrane technology could reduce the ecological impact of toxic solvents to the environment, which were formerly being used for carbon capture and storage (CCS) applications. The progress of the membrane modernization involves improvement of their adaptability to the operating conditions and enhancement of their performance in terms of both permeability and selectivity for the target components. Membranes can be either polymeric, inorganic or mixed, wherein the mixed is a combination of the first two. Polymeric membranes are cheap and easy to scale-up but limited in CCS application due to their plasticization tendency (which reduces durability of the membranes) and chemical stability at the operating condition. Inorganic membranes on the other hand, are attractive due to their mechanical and chemical stability, adaptable to harsh application condition, but they are brittle and expensive (due to the difficulties in the scale-up). Considering all these limits and prospects, more emphasize is growing towards the improvement of the existing mixed matrix membranes. There is a different type of filler available, which can be dispersed in the polymeric matrices to obtain mixed matrix membranes (MMMs). Best dispersion of the fillers and defect free membranes depend on the affinity of the fillers with the matrices and inter-chain void size. However, the incorporation of inorganic fillers may improve the thermal and chemical stability of the membranes, but they still suffer from lack of better dispersion in the matrices (organic phase). On the other hand, metal-organic frameworks (MOFs), that are hybrid (organic-inorganic) porous materials formed by ions or metallic clusters coordinated with organic ligands, giving rise to uni-, di- or three-dimensional crystal lattices, overcome such dispersion related drawbacks. Their crystallinity, high surface area, synthesis flexibility, pore size variability, and compatibility with organic materials, make them suitable fillers for fabrication of defect free mixed matrix membranes. Following such excellent properties of MOFs, this research focusses on studying MMMs based on MOFs and to recycle waste products obtained in the process.

1.2 Objectives

Based on the above, the purpose of this thesis is to innovate in the fabrication of MMMs through the use of MOFs, that can be applied to CCS to ensure sustainable development. In brief, objectives of this thesis are to cooperate in achieving sustainable development goals (SDGs): G - 6 (clean water and sanitation), G - 7 (affordable and clean energy), G - 13 (climate action) and G - 14 (life below water). More specifically, to ensure green synthesis of one of the MOF (i.e. ZIF-94) by reusing mother liquors (produced after synthesis of MOFs), which contain unreacted chemicals due to limiting reagent phenomenon, may disrupt life below water. Since their direct discharge will contaminate water and destroy natural sanitation process. In such approach, the intended project opts to satisfy SDGs related to water, sanitation and life below water: G - 6 (clean water and sanitation) and G - 14 (life bellow water). Subsequently, both

fresh and that obtained from recycling of the mother liquors, ZIF-94 materials were aimed to incorporate into MMMs to investigate their performance on CO_2 separation application by separation of CO_2 from CO_2/N_2 mixture. Such comparison of fresh and recycled ZIF-94 in terms of their CO_2 separation performance was aimed to confirm the viability of the recycling of the mother liquor. This study opts to ensure that the rest of SDGs related to environmental concern (G - 7 (affordable and clean energy) and G - 13 (climate action)) are met. Finally, the research pursued to reduce the carbon foot print caused by using MMMs by recycling their components. Next, another MOF named as MIL-178(Fe) was incorporated in the MMMs to investigate its applicability towards CO_2 separation (from CO_2/N_2 mixture). Then optimization of the fillers and polymer matrices was performed, wherein purification of natural gas or biomethane (CO_2/CH_4 mixture) was also investigated. Partial objectives of the thesis are defined as follows:

- Synthesis of ZIF-94 following a conventional and well-developed method.

- Synthesis of ZIF-94 by recycling mother liquor (produced from synthesis of ZIF-94) and its incorporation into MMMs.

- Comparison of fresh and recycled ZIF-94 in MMMs (in terms of their CO_2 separation performance), to confirm the viability of the proposed method of recycling of mother liquor.

- Development of a recycling method for ZIF-94 and Pebax® MH 1657 matrix based MMMs to recover their components.

- Investigation of the reusability of the recycled products in new MMMs.

- Validation of the proposed recycling method for ZIF-8 from its Pebax® MH 1657 based MMMs.

- Investigation of recently developed 1-dimensional MIL-178(Fe) in Pebax® 3533 based MMMs towards CO_2 separation application

- Optimization of MIL-178(Fe) and Pebax® 3533 dose in MMMs for CO_2 separation from the CO_2/N_2 mixture and in purification of natural gas or biomethane.

- Characterization of the materials and membranes using various techniques, among others:

  • Thermogravimetric analysis (TGA)

  • Fourier transform infrared spectroscopy (FTIR-ATR)

  • X-ray diffraction (XRD)

  • Scanning electron microscopy (SEM)

  • Transmission electron microscopy (TEM)

1.3 Structure of the report

Apart from the chapter 1 "Context, objectives and structuring of the report", the thesis report consists of the following chapters:

Chapter 2 "Introduction" which describes the importance of carbon capture, review on the membrane technology, modes of gas transportation and their mechanisms through membranes and review on polymeric matrices. It also mentions metal organic frameworks (MOFs) (in particular the ZIFs ("zeolitic imidazolate framework") and MIL-178(Fe)), used in this thesis.

In chapter 3 "Experimental procedures and characterization techniques" describes the synthesis of the MOFs and preparation of the MMMs in detail. It also explains the system used for gas separation experiments and experimental techniques used to characterize the filler materials and membranes.

In chapters 4, 5, 6 and 7, the results obtained are presented and discussed. Chapter 4 discusses the green synthesis of MOF ZIF-94 from its mother liquors (waste produced after the crystallization of MOFs), which contains unreacted chemicals due to limiting reagent phenomenon. Subsequently, ZIF-94 (both fresh and those obtained from recycling of the mother liquors) was incorporated into MMMs to investigate their performance in the separation of CO_2 from CO_2/N_2 mixture. In chapter 5, the report is focused on the development of a recycling method for ZIF-94 and Pebax® MH 1657 based MMMs, then reincorporated recycled ingredients (filler and polymer) into membranes to investigate their response in gas separation (CO_2/N_2). Finally, this method was repeated for ZIF-8 and Pebax® MH 1657 based MMMs for validation of the methodology. Chapters 6 and 7 focus on the application of MIL-178(Fe) in the MMMs to investigate its applicability towards CO_2 separation (from CO_2/N_2 mixture) and then optimization of the filler (MIL-178(Fe)) and polymer matrix, respectively. For these chapters, a collaboration was carried out with the groups of Profs. Nathalie Steunou and Christian Serre from the Institut Lavoisier de Versailles and the Institut des Matériaux Poreux de Paris, both from CNRS, France.

Chapter 8 "Summary and Conclusions" presents a summary of the thesis and the most relevant conclusions on it.

Chapter 9 corresponds to the "Bibliography" accessed throughout the thesis and used in the writing of the report.

Chapter 10 corresponds to "Abbreviations" shortlisted all the acronyms being used in the report.

Chapter 2: General Introduction

2.1 Introduction to CO_2

Carbon dioxide (CO_2) is characterized as a colorless and odorless gas but industrially a major pollutant due to two different aspects (for energy and for the environmental concern). CO_2 is especially dangerous because it decreases the calorific value of gaseous fuel mixtures in which it is present and makes the gas streams acidic and corrosive, thus separation of CO_2 is essential to increase fuel efficiency and pipelines endurance. Secondly, CO_2 is a greenhouse gas contributor to climate change and global warming. Consequently, its capture from processes, which emit CO_2 to the atmosphere, is a must. Herein, CO_2 will be studied as a pollutant, describing the process industries in which it is produced and the conditions in which its separation is a must.

2.1.1 CO_2 as an atmospheric pollutant in power generation

Globally, power generation is intensively dependent on fossil fuels which cause immense generation of CO_2. Although CO_2 is one of the minor gases in the atmosphere, it has a strong influence on the global warming because of giant volume of flue gas discharge. Even though, methane or water vapor have superior radiation absorption capacities, extend of the CO_2 emissions to the atmosphere are much higher than these other gases since the first industrial revolution [1]. Consequently, the hazard of CO_2 to climate change has triggered a political movement around the world. The European Union already agreed in 2011 through the Strategic Energy Technology Plan (SET-Plan) and the CCS Technology Roadmap 2050 [2], to support the progress of carbon capture and storage (CCS) that would be competitive as of 2020 [3]. An ambitious goal which is envisioned to cut CO_2 emissions by 80 - 95 % compared to those of 1990. Additionally, the protocol was updated in 2015 by the meeting of the Climate Conference in Paris (COP 21), where the objective was set to maintain the rise in the average temperature of the planet below 2 °C with respect to the pre-industrial levels [4]. Moreover, this agreement was indorsed during the climate summit (COP 24) in December 2018 in Katowice (Poland). In follow-up, COP27 (November 2022), held in Egypt with representatives from 190 countries, agrees on policies to adopt impacts associated with climate changes (loss and damage fund being created) and to restrict global temperature rise [5]. CCS can play an essential role in the power sector and in other industries (cement, steel or plastic production) where large amounts of CO_2 are generated, to bring this goal into a reality. CCS technologies consist of three stages: separation, transport and storage of CO_2. The separation methods can be classified into three different groups depending on their application phase at the combustion process: post-combustion. Precombustion and oxyfuel combustion.

- Post-combustion

This process implies the separation of a CO_2/N_2 mixture by integrating a capture stage after the fuel combustion phase. The flue gases containing CO_2 pass through an absorption unit, wherein target gas selectively reacts with an absorbent (chemical absorption) and ensures separation from the rest (**Figure 2.1(A)**). Although there are several solvents which favor CO_2 absorption: potassium carbonate, sodium hydroxide, ammonia, among others, the most functional are the solutions of amines (a mixture of

primary and secondary amines with water). This process is advantageous due to the possibility of its easy installation into existing power plants, since minimal modifications of the plant are required. However, there are impurities such as SOx and NO_x which should be taken into consideration. Moreover, it is worthy to mention that CO_2 is very diluted in the exhaust gases (3-20 %) and comes out at low pressure (around 1 bar), which makes it challenging towards CCS application [6], since a potential gradient is required between inlet and outlet streams to lead the membrane performance.

- Pre-combustion

Pre-combustion capture involves the separation of H_2 from H_2/CO_2 mixtures at elevated operating conditions (around 15-20 bar and 190-210 °C) before feeding in the combustion chamber, wherein H_2 is approximately ~45 (by vol %) [7]. Initially, the fuel mixture (for example: natural gas) undergoes a gasification process wherein it becomes a synthesis gas (a mixture of carbon monoxide (CO) and hydrogen (H_2) called syngas). The CO is subsequently oxidized with water vapor (often called steam reforming reaction), which produces CO_2 (**Figure 2.1 (B)**). Finally, H_2 is separated from the produced stream (called pre-combustion capture) and fed in the combustion chamber as a fuel. Consequently, the exhaust gas is free from CO_2, since the combustion of hydrogen produces only water vapor. Such overall process is called integrated gasification combined cycle (IGCC) [8]. Although pre-combustion capture is more efficient than post-combustion, the extreme operating conditions and energy penalty resulted from gasification makes it challenging [9].

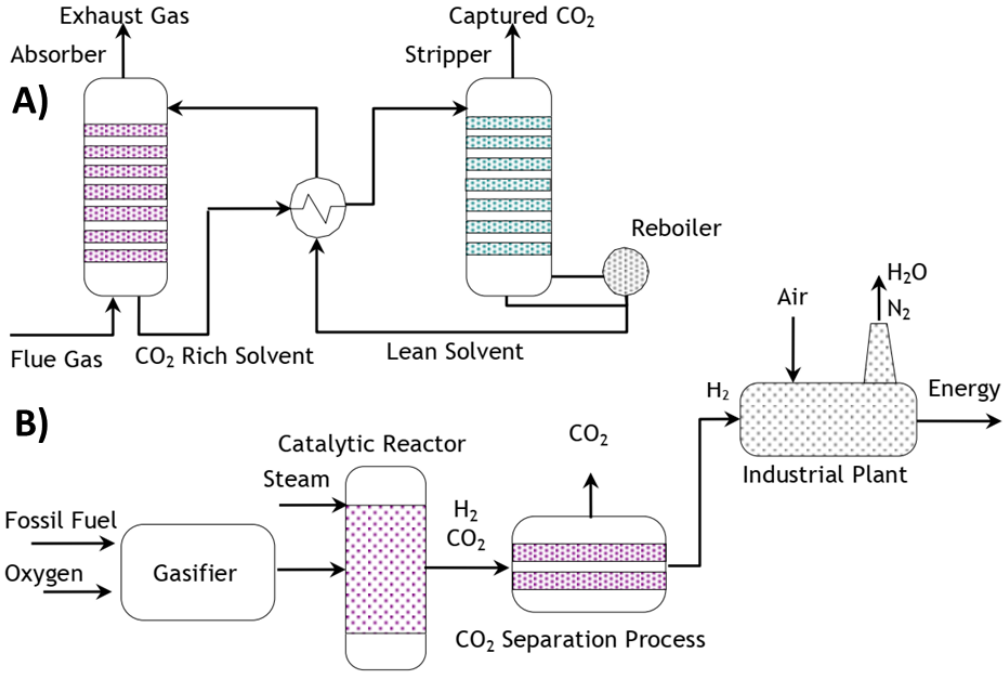

Figure 2.1. Schematic represntation of A) post-combustion CO_2 capture, B) pre-combustion CO_2 capture [10], reproduced with permission from University of Manchester Library.

- Oxyfuel combustion

This technology is characterized by feeding pure oxygen to the reactor, instead of air, together with the fuel. Thus, the oxy-combustion process deals with the separation of oxygen (O_2) from air (O_2/N_2). Owing to the high flammability of O_2, a part of the exhaust gases (generally CO_2) are recirculated to the reactor to dilute the incoming O_2. Flue gas composition from such process mostly depends on fuels being used. If complete combustion of the fuels (free from NO_x, SO_x) can be confirmed, CCS becomes easy. However, additional cost involved in fractionating of the air to obtain pure O_2 makes it challenging to adopt this technology [11].

2.1.2 CO_2 as a contaminant in biogas and natural gas

Both biogas and natural gas are mixtures rich in CH_4, an appropriate fuel for generation of power and heat. Natural gas, a fossil fuel (non-renewable), is a mixture of light gaseous hydrocarbons accompanied by minor other gases such as CO_2, N_2, He, ethane, propane, butane, impurities and traces of heavier hydrocarbons, extracted from certain reservoirs (either oilfield or coal mine). Its composition varies depending on the reservoir, but often comprises of 70-80 % of CH_4 (by vol.%). However, over depletion of the mine, CH_4 content is reduced while percentile for impurities is increased. Consequently, purification of a natural gas prior to feeding in the main transport stream is a must, which becomes difficult by the exhaustion of the mine (CO_2 content peaks).

On the other hand, biogas (calorific value varies between 15 - 30 MJ/Nm^3) [12], is an alternative energy source over fossil fuels, generated either in natural environments or by anaerobic (in absence of oxygen) biodegradation of organic matter over the action of microorganisms. The materials being the feed and the technology adopted for the anaerobic digestion generally decide on the biogas composition [13]. However, CO_2 and CH_4 content in biogas are usually 50 % by volume along with traces of other gases. Once the gas is properly purified, it can be used in multipurpose: to produce electricity, to heat in ovens, stoves, dryers, boilers or other properly adapted systems for household cooking. Generally, an upgrading process has been installed (see **Figure 2.2**) [14], that increases CH_4 content from 55 % to 90 vol.%, which is often named biomethane, suitable to be injected into the natural gas network.

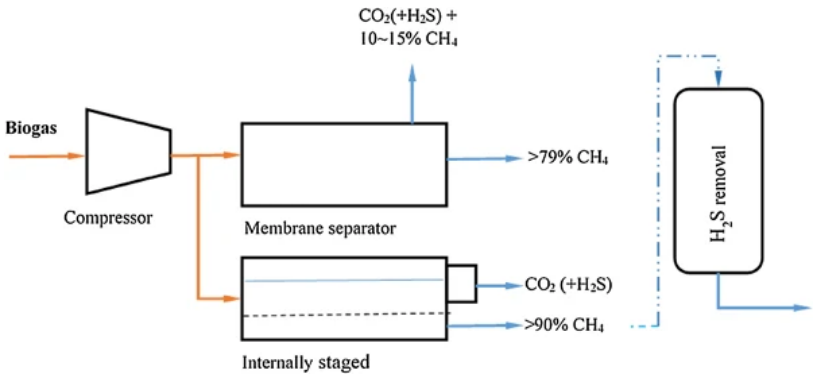

Figure 2.2. Schematic representation of Biogas upgrading system [14] reproduced with permission form Springer Nature.

As we already know, CO_2 is the key impurity of both the natural gas and biogas, which decreases fuel calorific value and makes the gas streams acidic and corrosive towards transporting pipelines. Additionally, CO_2 has an adverse effect to the ambient, act as a stimulator to greenhouse effect and global warming. Therefore, elimination of the CO_2 is necessary to avoid global temperature rise less than 2%[4] .

2.1.3 Conventional technologies in the separation of CO_2 mixtures

Among current technologies, CO_2 capture based on chemical absorption (arises due to a chemical interaction between absorbate and absorbend) for mixtures: CO_2/N_2 and CO_2/CH_4, is more efficient than physical absorption (absorption occures without chemical interaction) (in the market 90 % share of CCS is amine-based absorption). Eventually, blended solvent provides better capture throughput than a single solvent [12,15]. Among them, amines are very effective in CO_2 capture, thanks to high absorption capacity, high reactivity and selectivity with CO_2. The chemisorption process starts with feeding of gas stream into an absorber where 85-90 % of the CO_2 can be retained (see **Figure 2.3**) [16]. After that the absorbent is regenerated in a second reactor, where heat is applied in the form of water vapor to desorb CO_2. However, absorption with amines possesses few severe disadvantages, such as: high vapor pressure, emission of water-soluble toxic compounds (toxic secondary components formed during generation process, (i.e. amides, nitroimines, nitrosamines)), excessive recycling costs due to high reaction heat and large volume of water losses.

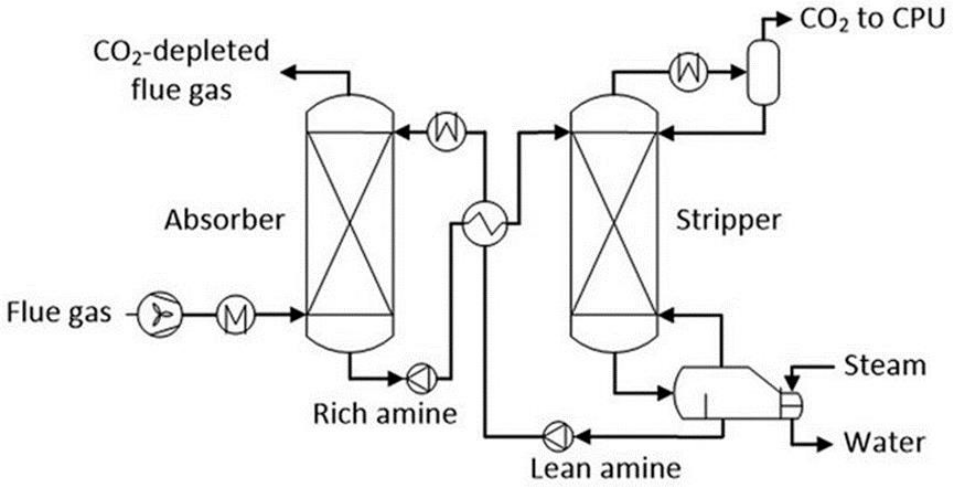

Figure 2.3. Schematic representation of amin-based CCS process, reproduced with permission from [16], Society of Chemical Industry and John Wiley & Sons, Ltd

Cryogenic separation (are classified as: flash liquefaction, distillation and liquefaction combined with distillation), another predominant process which results 99.99 % capture of CO_2 from flue gas or biogas[17]. However, this technology has its own limitations as well: it is not suitable for diluted CO_2 streams since refrigeration and compression requirement increases its operation cost [15], it has problems related to corrosion and low capacity.

Having seen the limitations of the current CO_2 capture technologies, membrane-based technology, a fast growing and environmentally friendly separation process is suitable for CO_2 capture from gas mixture stream due to its easy operation, facile scaling, small carbon footprint, and inexpensiveness [18]. Large-scale industrial application of polysulfone based hollow fiber membrane was initiated for gas separation (for the recovery of H_2) for ammonia production in the 1980s by Permea (now a subsidiary of Air Products) [19]. Moreover, the first cellulose acetate-based membrane system for the removal of CO_2 from natural gas was introduced in the mid-1980s by Cynara (now part of Natco) [20]. Nowadays, different companies such as UOP, Air Products and Chemicals, Dow, DuPont and Grace produce industrial scale membranes for gas separation applications.

Even though power plants based on pre-combustion processes (separation of H_2/CO_2 mixtures) are sophisticated and more expensive than traditional plants, membrane-based CCS is easier to install and operate and cheaper. Using membranes produces CO_2 stream at high pressure, which is ready for transport. On the contrary, CO_2/N_2 separation in post-combustion processes becomes more complicated because the exit gas conditions are just the opposite. It generates high volume of flue gas at low pressure with a very diluted CO_2 concentration. Even if the CO_2 direct air capture is being proposed nowadays [21], the low partial pressure of CO_2 is the limiting parameter for the CCS process, so it is amplified with other means such as: pressurizing the feed gas, pulling a vacuum on the permeate side, or use a sweep gas on the permeate side. Another aspect to consider is the process temperature. Although H_2/CO_2 separation is favored with increasing temperature, it is not like that for CO_2/N_2 mixture because the CO_2 capture by the membrane is usually adsorption based, which decreases with increase in temperatures.

Regarding the CO_2/CH_4 mixture, some natural gas deposits are so depleted that they carry high concentrations of CO_2 and can not be fed into the distribution grid directly. Consequently, they become economically unapproachable, thanks to membrane technology, one of the economical and modest technology for recovering methane especially from higher CO_2 concentration. Additionally, membranes can withstand harsh conditions (such as moderate pressure and temperature and presence of minor components such as traces of H_2S) [22].

2.2. Membrane technology

In this section, the concept of membrane, types of membranes, methods of manufacturing, improvement procedures and the transport mechanisms will be discussed.

2.2.1. Introduction to membrane

Membrane is defined as a semi-permeable barrier capable of separating one or more components of a mixture by action of a driving force (difference in chemical potential, e.g. concentration or pressure, or difference in electrical potential) [23]. This mixture can be formed by components in the gaseous state (gas separation), components

in the liquid state that get transformed into gas phase in the permeate (pervaporation) side, or solute-liquid mixtures that are in the liquid phase. In this way, the flow passing through the membrane is called permeate, while the rest is called retentate or rejection (see **Figure 2.4**).

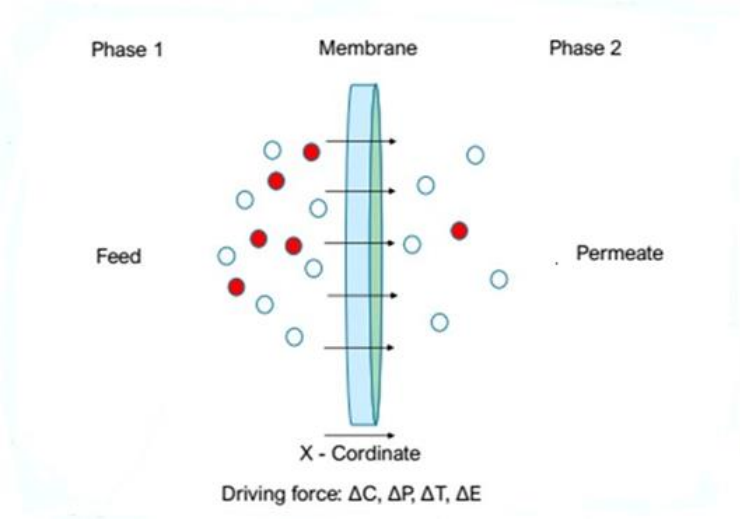

Figure 2.4. Schematic representation membrane separation [24]

2.2.2 Membrane types

Depending on their nature, membranes are classified as natural or synthetic. Natural ones are extracted from living species (such as: cellulose, lipids to name a few). Whereas, the synthetic membranes are man-made that can be organic, inorganic and mixed. Among these, the mixed is a combination of the first two. Geometrically, the membranes are classified as flat, tubular or hollow fiber. Tubular membranes feature higher permeation surface area per module volume than flat membranes, while for hollow fiber membranes this value is much higher than for the other two. That is why hollow fiber is commercially the most attractive configuration [25]. Structurally, membranes can be symmetrical or asymmetrical (see **Figure 2.5**) [26]. The asymmetrical membranes can be either composite or integral asymemtric which are characterized by their homogeneity irrespective to their volume. Again, composite membranes are classified as thin film composite (TFC) and thin film nanocomposite membranes (TFN; in fact, TFC membranes modified with typically porous fillers). Moreover, depending on the transport mechanism, membranes can be dense or porous. Dense are further classified as faciliated transport and solution- diffusion based membranes. On the other hand, porous membranes are classified as having a controlling transport mechanism based on Knudsen diffusion, molecular shieving etc. Another classification of membranes can be done depending on their applications as shown in **Table 2.1**: All these methods are carried out in the liquid phase, except those of pervaporation and separation of gases. The process of gas separation, specifically of CO_2-containing mixtures, is studied in this doctoral thesis.

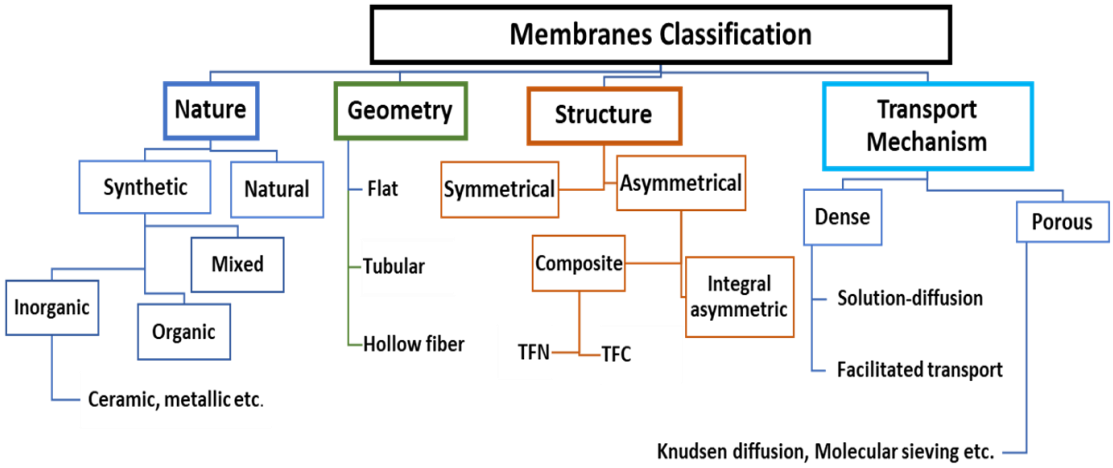

Figure 2.5. Schematic representation of classification of membranes[26] reproduced with permission from KeAi publishing communications Ltd.

2.2.2.1. Mixed matrix membranes (MMMs)

Mixed or hybrid membranes or mixed matrix membranes (MMMs), consist of an incorporated, typically porous (but there are may examples of non-porous fillers), inorganic or metal-organic filler within a polymeric matrix, as shown in the **Figure 2.6**. In such way, it is possible to enhance the permeo-selective capacity of the membrane. The effect of such fillers in the polymeric matrices depends on their chemical structure, surface chemistry and the type of particles (porous or non-porous) being used. The non-porous materials improve separation properties by increasing tortuosity and free volume. Moreover, they reduce the diffusion of large molecules [27]. Porous fillers on the other hand, having precise pore sizes, act as a molecular sieve in the MMMs (screening gas molecules according to their size) [28]. Therefore, pore size of the filling material should be in between those of the kinetic diameters of the gas molecules to be separated. Moreover, when these fillers are added to the polymeric matrix, not only the gas flow increases, since the filler materials are more permeable than polymers, but also selectivity rises due to aforementioned molecular sieving mechanism. Consequently, it is possible to have high permeabilities and superior selectivities to satisfy the so-called upper limit of Robeson plot [29].

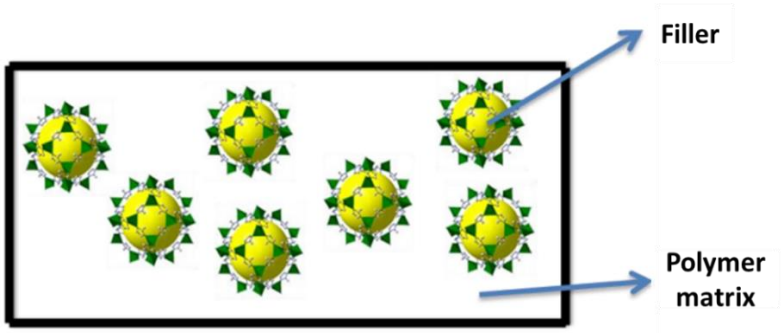

Figure 2.6. Schematic representation of MMM

In 1972, Paul and Kemp incorporated zeolite 5A into PDMS matrices and found an improvement in the separation performance (CO_2/CH_4) due to the phenomenon of preferential adsorption of CO_2 caused by the zeolite [30].Thus, zeolites were the first fillers used for MMMs in polymers, such as PDMS [31] or cellulose acetate [32] and later in different polysulfones [33]. Apart from zeolites, other materials that have been widely used in MMMs are metals, amorphous silcas, activated carbons and carbon nanotubes, among others. However, in the recent years, the use of metal-organic frameworks (MOFs) has been growing more and more [34]. The description of MOF materials, as well as their use in MMMs will be detailed in the following section.

2.2.3 Organo-metallic materials

2.2.3.1 Metal Organic Frameworks (MOFs)

Metal organic frameworks (MOFs), sometimes called porous coordination polymers (PCPs) [35,36], are a class of crystalline porous materials (porosity of around 90 %) combining the properties of inorganic (metal ion as cluster) and organic (linker) components with enormous internal surface area (some of them beyond 6000 m^2/g) [37]. MOFs pioonering works were published in the late 1990s [38,39]. They are formed by combination of coordinated metal ions or clusters with multidirectional organic ligands that act as linkers in 1-D, 2-D or 3-D lattice structures. One of the problems of MMMs with different inorganic linker than MOFs is the formation of voids at the interface because of the poor affinity between the inorganic and organic phase, thus lowering the selectivity of the membrane and therefore causing it to underperform. However, in the case of a MOF, the organic ligand may improve the filler-polymer interaction, avoiding the presence of non-selective micro-gaps. Design and synthesis of MOFs depend on their application, which is still aspiration of research for material scientists. MOFs can be synthesized by many routes including microwave, ultrasonic, electrochemical, mechanochemical and high-throughput syntheses.

MOFs are materials with large specific surface areas, for example, MOF-177 (4500 m^2/g) [40], MOF-210 (6240 m^2/g) [41], ZIF-8 (1250 – 1600 m^2/g) [42], MIL-101(Cr) (4230 m^2/g) [43]. Typically, MOFs can integrate multiple CO_2 adsorption sites, e.g. open metal sites, Lewis basic sites and covalently-bound polar functional groups, that enable to achieve preferential CO_2 adsorption over other gas molecules such as N_2, CH_4 and H_2O [44–46]. In addition, post-synthetic modification has been also employed to introduce novel CO_2 adsorption sites without altering or degrading the MOF structure [44,45,47]. Among different alternative MOFs, ZIF-94, the one most studied in this PhD thesis, also known as SIM-1 [48–50], possesses an SOD topology along with well distributed and defined 3D pore networks [51]. Undoubtedly the greatest advantage of MOFs compared to other porous materials is the possibility of adjusting size and shape of their pores, from the range of micropores to mesopores, which is beneficial for some specific applications. This is achieved by changing the organic ligand or its coordination sphere with the metal centers. For example, the appropriate choice of the organic ligand makes it possible to determine the size, shape, and chemical functionality of the cavities on the internal surface [52]. All these properties make

MOFs as interesting compounds for various potential applications [38]: gas-gas adsorption and separation [53], their use in membranes, and applications related to catalysis [54] and drug release [55]. The synthesis of any MOF consists of three different stages (**Figure 2.7**):

- Dissolution of the metal ions (generally a salt) and the organic ligand in a relevant solvent.

- Reaction: both solutions are mixed and the crystallization reaction takes place. Depending on the reaction media, the synthesis can be hydrothermal, solvothermal, microwave, electrochemical, ultrasonic, and solventless mechanochemical and at high pressure, etc.

- Activation: it consists of the elimination of the remains of ligand that have not reacted, as well as the solvent molecules that are trapped inside the pores of the MOFs. Activation is usually given thermally by washing and drying. The correct activation of the MOFs is what determines their specific surface area and the accessibility to their pores.

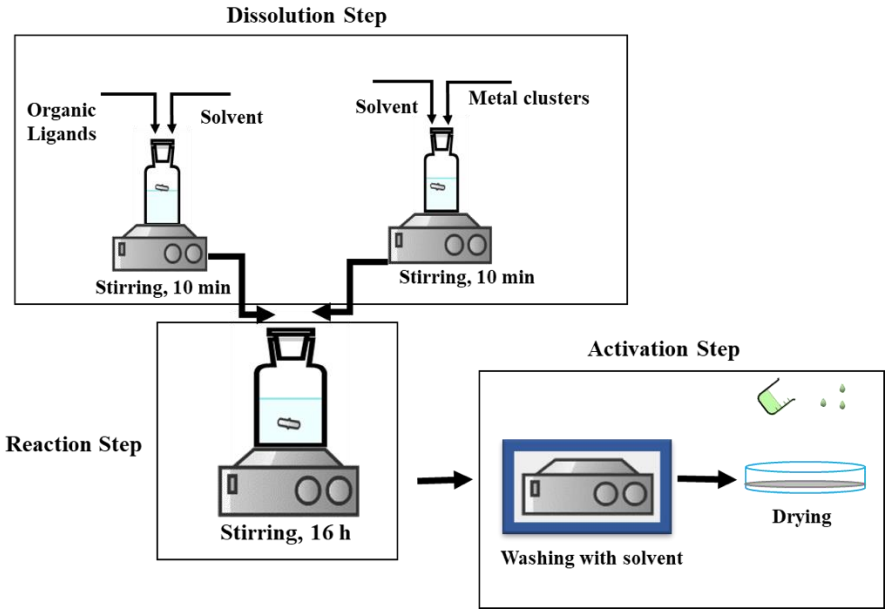

Figure 2.7. Schematic representation of three steps of synthesis of MOFs

This section describes the nature and properties of MOFs to explain their compatibility in gas separation membranes. Specifically, zeolitic imidazolate frameworks (ZIFs) will be studied in depth, which are a subfamily of these materials that are predominantly used in this doctoral thesis.

2.2.3.1.1 ***Zeolitic imidazolate frameworks (ZIFs)***

ZIFs are a subfamily of MOFs, often translated as "zeolite-type compounds based on imidazolates". These MOFs are formed by tetrahedral coordination bonding between Zn (II) or Co (II) ions and nitrogen atoms of imidazolate ligands [3]. They were discovered in parallel and independently by the groups of Yaghi [56] and Chen,

[57], where the metal-imidazolate-metal bond form an approximate angle of 145° (between metal cluster and organic linker), analogous to the O-Si-O bond in zeolites, [58] (**Figure 2.8**). The organic ligand used in ZIFs influences the topology of the crystals and the pore size. ZIFs are crystalline materials having similar topologies to those of zeolites (SOD, RHO, etc.). Such variation of topologies in ZIFs family is experienced due to different arrangement of inorganic and organic linkers in the structures, which results from either changing solvent or synthesis conditions (**Figure 2.9**). The microporosity of these fillers in the membranes serves as molecular sieving towards CO_2 separation [59] making them the ideal materials for CCS application. Next, different ZIFs used in fabrication of MMMs are detailed in this doctoral thesis:

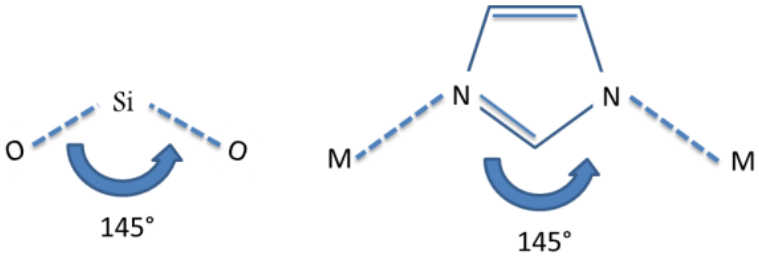

Figure 2.8. Approximate bond angle of zeolite and ZIF

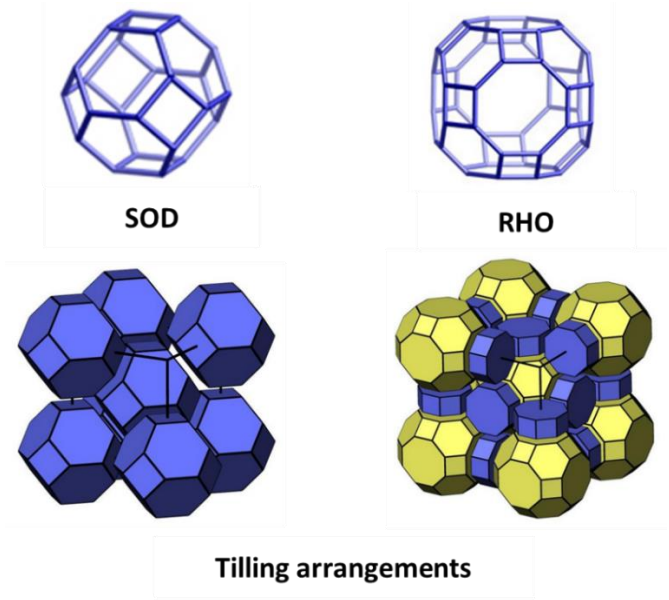

Figure 2.9. Schematic representation of SOD and RHO type framework structures and their tilling arrangements [60], adopted from Database of Zeolite Structures (www.iza-structure.org).

- ZIF-8

ZIF-8 (molecular formula is $C_8H_{10}N_4Zn$ and molar mass is 229.50 g/mol) displays a SOD topology consisting 1.16 nm cages connected through six-membered windows (0.34 nm in size), is presently the most investigated ZIF material for a range of applications. It is promoted under the commercial name Basolite® Z1200, formed by coordinating Zn (II) atoms with 2-methylimidazolate ligands, as shown in **Figure 2.10**. It is chemically stable in methanol, benzene or boiling water for 7 days or in

concentrated sodium hydroxide for 24 hours [56]. Although ZIF-8 was initially synthesized by solvothermal method [56,57], other synthesis routes are also available: microwave [61], ultrasonic, [42] electrochemical, [62] mechanics, [63] sol-gel conversion [64] and microfluidics [42]. Another outstanding feature of ZIF-8 is explained by "gate-opening" phenomenon which implies that, upon certain pressure, pore opening is extended due to elongation or breaking of certain bonds, allowing gas molecules whose kinetic diameter is slightly greater than the pore window [65]. This explains how ZIF-8 endures adsorption of N_2 whose kinetic diameter (0.36 nm) is slightly higher compared to the pore window of the ZIF-8 that is 0.34 nm.

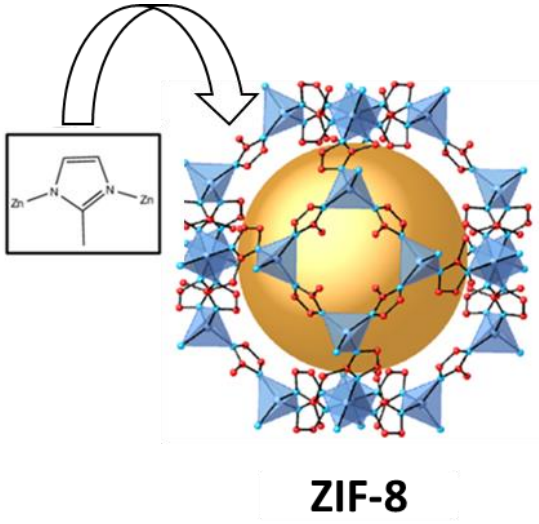

Figure 2.10. Structure of of ZIF-8 with organic linker [66] reproduced with permission from Springer Nature.

- ZIF-94

ZIF-94 (molecular formula $Zn(C_5H_5N_2O)_2$ and molar mass 284.3 g/mol), also named as SIM-1, with a specific surface area of around 591 $m^2 \cdot g^{-1}$[67]. It possesses a SOD type structure (analogous to that of ZIF-8) with well distributed and defined 3D pore network (**Figure 2.11**) [51] along with 0.26 nm of limiting pore diameter [68]. It can be synthesized with the Zn cluster coordinated to the organic linker imidazolate (ratio 1:1.7), with proper reaction and washing condition. It possesses high CO_2 adsorption ability: 2.4 mmol g^{-1}, with limiting pore diameter of 2.6 Å [69] compared to other ZIFs (ZIF-8 (0.7-0.8 mmol g^{-1}, 3.4 Å limiting pore diameter) [70], ZIF-7 (1.6 mmol g^{-1}, 2.9 Å limiting pore diameter) and ZIF-11 (0.8 mmol g^{-1}, 3.0 Å limiting pore diameter)) at 1 bar operating pressure [71–73].Moreover, it also facilitates gate-opening phenomenon, allowing gas molecules whose kinetic diameter is slightly greater than the pore window (such as CO_2 whose critical diameter is 0.33 nm).

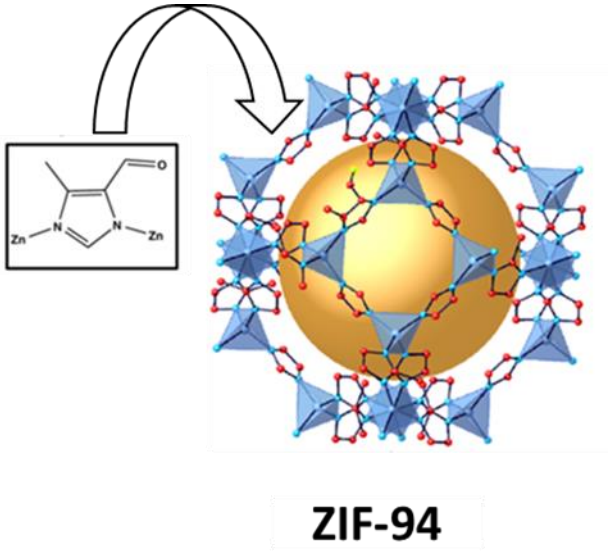

Figure 2.11. Structure of ZIF-94 with organic linker [66] reproduced with permission from Springer Nature.

2.2.3.1.2. ***MILs***

Materials Institute Lavoisier (MILs) are porous materials comprising of different trivalent metal cations and carboxylate type ligands, they possess micropores (and also mesopores, depending on the strucuture) and permanent porosity [74]. The synthesis routes and conditions of MILs determine the structure of the MOF. Such trivalent cation-based MILs are advantageous due to their microporous and mesoporous structure [75]. MILs possess high BET surface area (MIL-53(Al) – 1284 m^2/g, MIL-100(Fe) -1920 m^2/g, to name a few) [76,77], excellent hydrothermal stability, flexible frame structures [78], adjustable bond structure [78,79], permanent porosity which presides excellent mass transfer capacity [80], which favors them for applying in liquid phase catalysis. MIL-based materials are applied in the field of heterogenous catalysis [79,81] and as a solar energy converter [82]. Here in this study, MIL-178(Fe), a Fe (III) cation based 1-dimentional frame structure, is applied in MMMs for CO_2 separation application and biogas upgrade.

MIL-178(Fe)

PCP based on iron (III) and 1,2,4-benzene tricarboxylate, named MIL-178(Fe) that exhibits a 1D architecture delimiting ultra-micropores (ϕ < 4.5 Å) decorated with functional groups (- COOH, -OH) (**Figure 2.12**). The structural behavior of this PCP upon CO_2 pressure has been investigated by *in situ* powder X-ray diffraction and molecular modelling, thereby providing a detailed analysis of the preferential arrangement of the confined CO_2 molecules in the material porosity and the host/guest interactions [83].

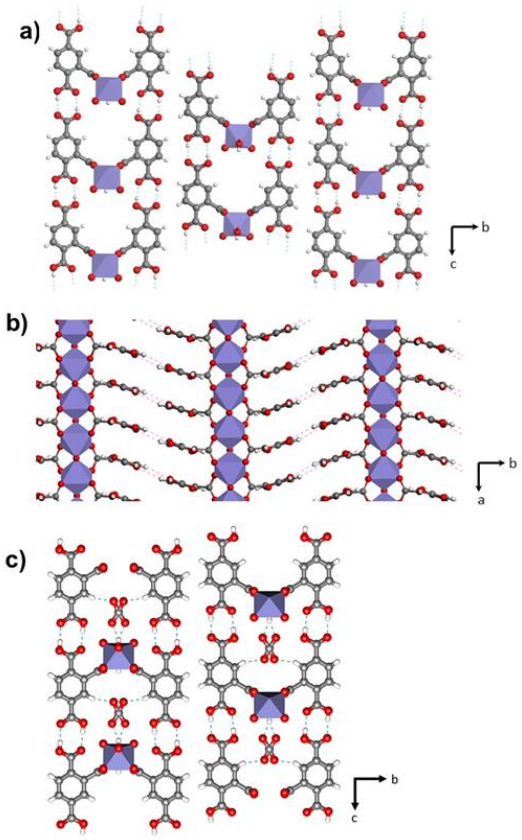

Figure 2.12. Crystal Structure of (a,b) MIL-178(Fe) along the (a) a axis and (b) c axis, (c) CO_2 loaded-MIL-78(Fe) along the c axis. Fe octahedral, carbon, oxygen and hydrogen are in purple, gray, red and white respectively. Hydrogen bonds are represented as dotted lines .Reproduced from [83] with permission from the Royal Society of Chemistry.

2.2.4. Polymeric membranes

Polymers are considered as matured materials for engineering commercial membranes due to their low cost, facile production and easy scale-up, they are limited due to their decreased chemical and mechanical stability and plasticization tendency [84]. On the other hand, inorganic membranes are characteristic of tunable pore size and adoptable to harsh condition, but they are brittle and expensive and difficult to scale-up [84]. However, polymers are classified into two large groups: thermoplastics and elastomers. Elastomers are rubbery in nature having large free volume whose glass transition temperature (T_g) is below the operating temperature. The separation mechanism of these membranes is mainly due to differences in the solubility of gases. Consequently, the most condensable gases, such as CO_2, permeate predominantly. Therefore, such polymers are suitable for CO_2 capture from CO_2/N_2 and CO_2/CH_4 mixtures. Thermoplastics, on the other hand, are polymers whose T_g (glass transition temperature) is above the operating temperature. Unlike elastomers, whose T_g is bellow operating temperature, the gas separation in thermoplastics follow diffusion mechanism due to their compact structures (glassy polymer) and for comparatively smaller free volume. Therefore, molecules with the smallest kinetic diameter are more permeable which is more favored with the increase in temperature. These polymers are ideal for

the separation of H_2 from a mixture of gases. Pebax® are a new family of coomercial copolymers, fabricated by the French company Arkema, with elastomeric behavior recently applied to gas separation membranes, the characteristic properties of the Pebax® are explained in the following section which is used in the fabrication of MMMs for the doctoral study.

2.2.4.1. Pebax® membranes

Co-polymers made of flexible polyether (PE) and rigid polyamide (PA) blocks are well-known under the trade name Pebax® (polyamide-b-ethylene oxide). They are semi-crystalline in nature comprising properties of both elastomer and thermoplastic polymers. The rigid PA block provides the mechanical resistance to the composite membrane, while gas transport mainly depends on the soft PE block [85]. Pebax® membranes show high CO_2/N_2 and CO_2/CH_4 selectivities, although permeability is limited. Specific codes of Pebax® are assigned depending on different polyamide/polyether ratio, which affects their properties, as shown in **Table 2.3**. These copolymers have two melting temperatures, which are correspond to the PE and PA segments respectively. One of the widely used Pebax® copolymers for gas separation is Pebax® MH 1657 [85].

Table 2.3. Properties of the Pebax® copolymers

Codes	PA content (wt. %)	T_m (PE) (°C)	T_m (PA) (°C)	Crystallinity of PA (vol. %)
3533	25	18	155	6
MH 1657	40	49	204	-
2533	20	10	126	3
4033	46	21	30	14

T_m: melting temperature

Pebax® MH 1657 is a commercial rubbery and thermoplastic polymer, which offers good thermal and mechanical property having melting point at 204 °C. Chemically, it is made of flexible polyether (60 wt.% polyethelene oxide (PEO)) and rigid polyamide (40 wt.% aliphatic polyamide (PA)), is very attractive especially for polar gas separation, such as CO_2, from nonpolar light gases, such as N_2. **Figure 2.13** represents molecular structure of commercial Pebax® MH 1657. Because of its higher melting point, it has found application in gas separation especially in MMMs as a matrix support at elevated temperature.

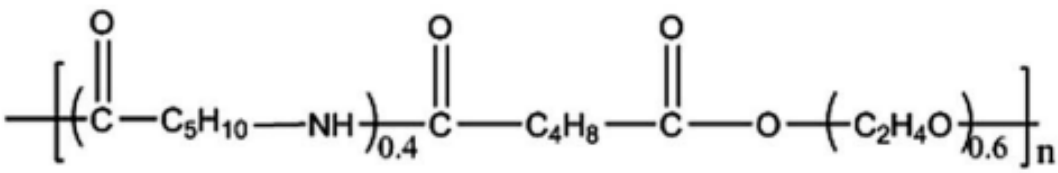

Figure 2.3. Molecular structure of Pebax® MH 1657 [86]. Reproduced from [86] with permission from the Royal Society of Chemistry

Pebax® 3533 is another interesting block copolymer composed of 75 wt.% of PE (poly (tetramethelene oxide) (PTMO)) and 25 wt.% of PA. Due to its high solubility in alcoholic solvents (less polar in nature than water), this polymer exhibits a long-term stability and durability under humid conditions and it has shown good performance in the separation of CO_2 containing mixtures [83,87].

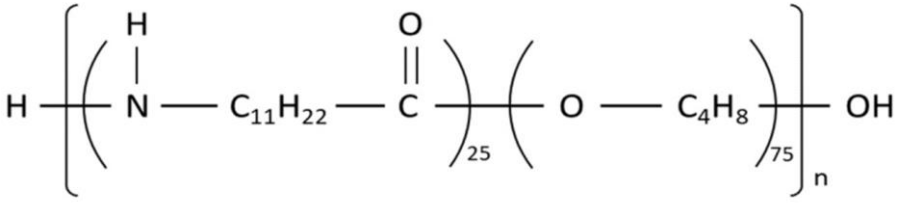

Figure 2.4. Molecular structure of Pebax® 3533 [87]. Reproduced from [87] with permission from the Elsevier Ltd.

2.2.4.2. Pebax® based MMMs

Even though pristine polymeric membranes are advantageous due to their low cost, facile production and easy scale-up, they are limited due to their decreased chemical and mechanical stability and plasticization tendency [84]. Lin and Freeman investigated different codes of pristine Pebax: 1657, 1878, 1074, 3000, 1041, 6100 and 1205 wherein, Pebax® 1657 was reported as the best based on its gas separation performance[88]. Additionally, Rezac et al. have reported that pristine Pebax 2533 shows promising permeation results among four different Pebax codes: 3522, 6333, 5533 and 2533 [89]. MMMs, combining both organic and inorganic components, become one of the best solutions to overcome existing limitations. However, a selection of the polymer matrix significantly influences the performance of an MMM towards gas separation performance. Polymer matrices having higher T_g and sufficient interchain spacing (compatible with target fillers) plays an important role in gas separation performance to satisfy Robeson upper bound limit. Li et al. reported mixed matrix composite membranes incorporating ZIF-7 (in 3 different loading 8, 22 and 34 wt.%) into Pebax® 1657 which was investigated towards CO_2 separation application [90]. Additionally, Nafisi and Hagg have incorporated ZIF-8 (35 wt.%) into Pebax 2533 to develop a self-supported and dual layer MMM, which resulted in a three times increase in permeability (from 351 Barrer to 1257 Barrer at 2 bar operating pressure) where a slight decrease in selectivity (CO_2/N_2) was observed compared to pristine Pebax 2533 [91]. Moreover, Zheng et al. synthesized ZIF-8 particles of 40, 60, 90 and 110 nm (by varying the ratio of Zn^{2+} ions to 2-methylimidazole), that were dispersed in Pebax® 1657 to evaluate their effect on CO_2 permeation [92]. Similarly, Ehsani and Pakizeh have reported better adhesion between ZIF-11 and Pebax 2533 in MMMs, which was used to study CO_2 separation from binary mixtures with H_2, CH_4 and N_2, where a decreasing tendency of CO_2/N_2 selectivities (from 53 to 29) was observed at high ZIF-11 loadings (10 – 70 wt.%) due to formation of defects [93]. Another MOF with Fe(III) and carboxylate group (benzene-1, 3, 5-tricarboxylate), called MIL-178(Fe), was fused with Pebax® 1657 to fabricate an MMM to separate CO_2 from a

binary mixture with CH_4 wherein both selectivity and permeability of the resulting membrane increased up to 17 % and 600 % as compared to pristine polymeric membrane [94].

Considering the effect of different fillers and Pebax codes (1657 and 3533) on CO_2 separation performance, this PhD study is focused on the recycling of fillers from either mother liquors and MMMs and to study their adaptability in MMMs. Moreover, applicability of 1-dimentional MIL-178(Fe) into MMMs has been investigated which is explained throughout the report. In the subsequent parts of the dissertation, membrane processes, fabrication and improvement techniques are discussed.

2.2.5. Membrane processes

In membrane processes, membrane characteristics (porosity, selectivity, electric charge etc.) play a significant role in the separation of the target species from the feed. Nature and magnititute of the driving forces being used and dimention of the components to be sepatared are considered to classify membrane processes (see **Table 2.1**). In osmosis process, spontaneous solvent transfer across the non-porus membrane takes place from a phase having a higher chemical potential: from pure solvent (due to concentration gradiant), whereas in reverse osmosis external applied force on the solution phase increases chemical potential and reverse the solvent transfer direction. In microfiltration, a microporous membrane (0.1 – 10 µm) replaces nonporous membrane of reverse osmosis process, where both solvent and micro level (0.1 – 10 µm) molecules are permeable under applied pressure. Both ultrafiltration and nanofiltration follow identical process, being addressed to particles of 0.1 µm – 5 nm and less than 5 nm, respectively. Membrane distillation is a thermal-driven water treatment process wherein only vapour molecules pass through a microporous hydrophibic membrane. In pervaporaion vacuum pressure is applied between feed and permeate sides, a vapour phase passing through the membrane. In gas separation, especially for dense membranes, transport mechanism follows solution-diffusion mechanism, which is described in the subsequent sections.

Table 2.1. Classification of the membranes depending on different driving forces

Pressure (ΔP)	Concentration (ΔC)	Temperature (ΔT)	Electric potential (ΔE)
Microfiltration	Dialysis	Thermal osmosis	
Ultrafiltration	Pervaporation	Membrane distillation	Electrodialysis
Nanofiltration	Osmosis		
Reverse osmosis			
Gas separation			

2.2.5.1 Gas transport mechanisms

Gas transport mechanisms are classified into four types: Poiseuille or viscous flow, Knudsen diffusion, molecular sieving and solution-diffusion. The first three explain the transport of gases in porous membranes, while the latter explains the transport in dense membranes. An explanatory scheme of these transport mechanisms is shown in **Figure 2.14**.

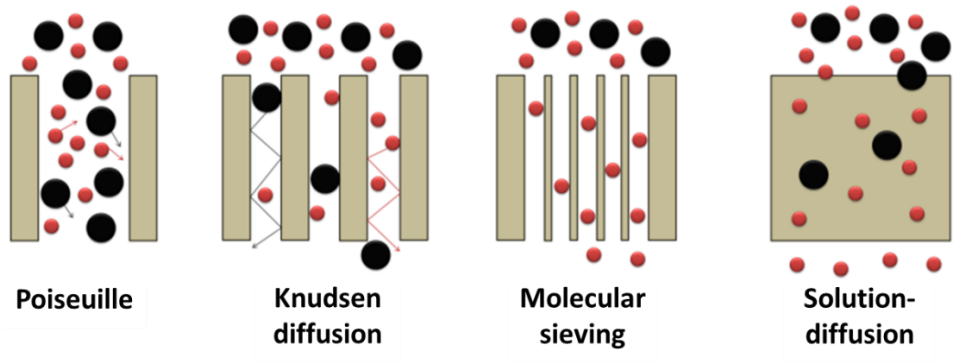

Figure 2.14. Different transport mechanisms

- Poiseuille type of flow

This type of transport is considered as an unwanted flow that is associated with defects, which occurs in membranes having large pores. When the pore diameter of the membranes (d) is higher than the mean free path (λ) of the penetrating gases, Poiseuille or viscous flow occurs. The mean free path refers to the distance that a gas molecule travels between collisions and is represented by Equation 2.2

$$\lambda = \frac{3\eta}{2P}\left(\frac{\pi RT}{2M}\right)^{0.5} \qquad Equation\ 2.2$$

where η is the viscosity of the gas, P is the pressure, T is the temperature in K, R is the universal constant for gas (8.314 J mol^{-1} K^{-1} at 298K) and M is the molecular mass of the gas.

- Knudsen Diffusion

Knudsen diffusion named after Martin Knudsen, occurs in membranes having pore sizes between 5 - 10 nm where each of the gases flows through the membrane independently. When an equimolar mixture is fed, the Knudsen selectivity is inversely proportional to the square root of the ratio of the molecular masses of each gas, as expressed by Equation 2.3

$$\alpha_{a/b} = \sqrt{\frac{M_b}{M_a}} \qquad Equation\ 2.3$$

where M_a and M_b are the molecular masses of each of the gases.

- Molecular sieving

The molecular sieving is defined as exclusion of one of the gases of the feed based on their molecular dimensions. It occurs in membranes having pores diameter less than 0.7 nm. Gases of smaller kinetic diameter and greater diffusivities permeate across the membrane, while larger molecules are retained. It is the typical transport mechanism of zeolites and porous metal-organic compounds.

- Solution-diffusion model

Such mechanism explains transport of gases through dense membranes which consists of three phases [95]: (1) gases are absorbed into the polymer in the feed side, (2) next they diffuse across the membrane due to concentration gradient and, (3) they are desorbed on the permeate side [96]. Fick's law of diffusion (Equation 2.4) is used to explain such separation mechanism where gas flow is defined as a function of concentration gradient:

$$J_i = -D\frac{dc}{dx} \qquad Equation\ 2.4$$

where J is gas flow rate through the membrane (mol cm^{-2} s^{-1}), D is diffusion coefficient (cm^2 s^{-1}), x is thickness of the membrane (cm) and c is the concentration (mol cm^{-3}). After integrating, Equation 2.5 is obtained:

$$J_i = -D\frac{C_2 - C_1}{l} \qquad Equation\ 2.5$$

where l corresponds to the thickness of the membrane (cm), C_2 and C_1 are the concentration of the gas at each side of the membrane (mol cm^{-3}). According to Henry's law, the gas concentration can be expressed as the product of solubility coefficient (S) and pressure (P), then Equation 2.6 becomes:

$$J_i = -D.S\frac{P_2 - P_1}{l} \qquad Equation\ 2.6$$

There are two key parameters that determine the intrinsic performance of a membrane for gas separation: permeability and selectivity. The first is related to the gas flow through the membrane, and the second is separation capacity. The permeability (P_i) is defined for each of the gases (i) according to Equation 2.7:

$$P_i = \frac{l.J_i}{\Delta P.A} \qquad Equation\ 2.7$$

where l is the thickness of the membrane, J_i is the gas flow rate, ΔP is the pressure difference between both sides of the membrane, and A is the effective membrane area. The most used unit for permeability is the Barrer (being 1 Barrer = 10^{-10} cm^3 (STP) cm^{-2} s^{-1} $cmHg^{-1}$), named after Professor Richard M. Barrer, who had a great influence in the field of zeolites [97]. For some membranes it is impossible to know the exact thickness of the selective layer responsible for the separation. In such cases, the flux across the membrane is defined as permeation, which does not account for thickness (Equation 2.8).

$$Q_i = \frac{J_i}{\Delta P.A} \qquad Equation\ 2.8$$

For membranes whose selective layer thickness is measurable, another most commonly used unit to define permeation is Gas Permeation Unit (GPU), where 1 GPU

= 10^{-6} cm^3 (STP) cm^{-2} s^{-1} $cmHg^{-1}$. This way, permeance and permeability are related according to Equation 2.9 (being the same for a thickness of 1 μm):

$$P_i\,(Barrer) = Q_i(GPU)\,.\;l_i(\mu m) \qquad Equation\ 2.9$$

The ideal selectivity (α_{ij}^*) is defined as the ratio of the permeabilities of two pure gases (Equation 2.10).

$$\alpha_{ij}^* = \frac{P_i}{P_j} \qquad Equation\ 2.10$$

where P_i and P_j are the permeabilities of pure gases i and j through the membrane. When this ratio is calculated from their mixture, it is called the real or separation selectivity. In general, the separation selectivity value is less than the ideal selectivity due to the existence of interactions, concentration polarization and competitions between the gases in the feeding. In some cases, it is preferred to use separation factor rather than selectivity. This is defined as the ratio between the composition of the feed stream to the permeate stream, which is expressed as shows Equation 2.11

$$\alpha_{ij}^* = \frac{y_i/x_i}{y_j/x_j} \qquad Equation\ 2.11$$

where y_i and y_j are the mole fractions of gaseous species i and j on the permeation side, while x_i and x_j, the mole fractions on the feed side. When the partial pressure difference of each gas between the feed and the permeate is very large, the separation factor approaches selectivity (see Equation 2.12). [79]

$$\alpha_{ij} = \frac{y_i/x_i}{y_j/x_j} = \frac{1}{x_i/x_j}\frac{P_i}{P_j}\frac{p_{f,i} - p_{p,i}}{p_{f,j} - p_{p,j}} \approx \frac{P_i}{P_j} = \alpha_{ij}^* \qquad Equation\ 2.12$$

According to the solution-diffusion model [95], the permeability of a gas i can be defined as the product of effective diffusion coefficient, D_i, and effective sorption coefficient, S_i: where, S_i indicates how much gas a membrane can retain in equilibrium with fugacity, and D_i is related to the mobility of penetrating molecules in the membrane. For a pair of gases, i and j, the selectivity, α_{ij}, is defined according to the Equation 2.13:

$$\alpha_{ij} = \left(\frac{D_i}{D_j}\right).\left(\frac{S_i}{S_j}\right) = \alpha_{ij}^D\ .\alpha_{ij}^S \qquad Equation\ 2.13$$

α_{ij}^D is called diffusivity selectivity, and D_i/D_j is related to the rate at which gases diffuse across the membrane due to differences in their kinetic diameters. On the other hand, α_{ij}^S is the selectivity by sorption S_i/S_j, the preferential adsorption of some gases over others. Solubility is a thermodynamic parameter that depends on both condensing capacity of the gas and its affinity with the polymer. On the contrary, diffusivity is a

kinetic parameter that depends on size and shape of the gaseous molecules, mobility of the gases and degree of packing in the polymer chains [98].

The gas transport through a MMM is a combination of both dissolution–diffusion mechanism in the polymeric phase and permeo-selective transport in the discrete phase. In the latter, there are two factors to consider: (i) adsorbate-surface interactions, relative to the physical and chemical interaction between gases and filler particles, and (ii) the size exclusion, related to the differences between the pore size of the filler particles and the size and shape of gas molecules [96].

2.2.5.2 Gas adsorption in polymers

The adsorption of gas molecules on polymers can be explained by the dual adsorption model [99,100], a combination of the Henry's law and Langmuir model. According to Henry's model, gas molecules follow an ordinary solution mechanism in the free volume of rubbery polymeric matrix. On the other hand, adsorption based on Langmuir model is applicable to glassy polymer, which contains excess free volume below their T_g [101]. According to Henry's laws and Langmuir model (Equation 2.14 and Equation 2.15), the concentrations of gases, C_D and C_H are, respectively (subscripts D and H stands for Henry laws and Langmuir model respectively):

$$C_D = k_D \,.\, p \qquad Equation\ 2.14$$

$$C_H = \frac{C'_H\, bp}{1 + bp} \qquad Equation\ 2.15$$

Summing up both equations, the overall concentration (sometimes called total sorption), C, is called the dual adsorption model (Equation 2.16):

$$C = C_D + C_H = k_D \,.\, p + \frac{C'_H\, bp}{1 + bp} \qquad Equation\ 2.16$$

where, k_D is the Henry's law coefficient, and C'_H and b are the saturation constant and the Langmuir affinity parameter, respectively. k_D parameter represents the amount of penetrating gas dissolved in the polymeric matrix in equilibrium conditions. The solubility parameter is obtained following Equation 2.17:

$$S = \frac{C}{P} = S_D + S_H = k_D \,.\, p + \frac{C'_H\, bp}{1 + bp} \qquad Equation\ 2.17$$

where S is the solubility of the penetrating gas, and S_D and S_H, the solubilities based on the Henry's and Langmuir's laws, respectively.

The solubility in the polymer is related to its free volume fraction [102]. Langmuir adsorption of gas molecules on polymers occur below their glass transition temperature due to the presence of non-equilibrium states and excess free volume. On the other hand, the Henry's law coefficient constants and the Langmuir affinity constants increase with the condensability of the permeate gas.

2.2.5.3 Factors affecting gas transport in a membrane

- Size of gas molecules

The size of the gas molecules affects the diffusion coefficients, since the smaller molecules can diffuse faster. Additionally, the diffusion coefficient is proportional to the average velocity and the average free path of the gaseous molecules. Consequently, gaseous molecules having kinetic diameters compatible with the gaps between polymer chains have better diffusivity. Thermoplastic polymers typically have the highest selectivities due to high diffusion selectivity. Another factor that influences diffusion, is molecular form. For example, having the same molecular mass, linear molecules have higher diffusion coefficients than spherical structures [103]. **Table 2.2** shows kinetic diameters and critical temperatures of common gases of pre or post combustion fuel production [86].

Table 2.2. Critical temperatures and kinetic diameters of common gases of membrane process

	H_2	CO_2	O_2	N_2	CH_4
Kinetic diameter (nm)	0.289	0.330	0.346	0.364	0.380
Critical temperature T_c (K)	33	304	155	126	191

- Condensability of gases

The condensability of gases affects their solubility in the polymer. The solubility is proportional to the condensability of the gases, at its critical temperature. In the separation of CO_2/N_2 and CO_2/CH_4 mixtures, CO_2 diffuses faster and shows higher solubility than other gases. Consequently, both the selectivity by diffusivity and by solubility are favored. However, the separation of gases becomes complicated when there is a competing effect between diffusion and solubility. This is the case of the H_2/CO_2 mixture, typical in the capture processes in pre-combustion. H_2 diffuses faster due to its smaller kinetic diameter, but CO_2 is a more condensable gas, and its solubility in the polymer is greater. In such cases, high temperatures favor selectivity by diffusion but penalize the dissolution selectivity, and vice versa. This means that, for some polymers, such as polybenzimidazole, an intermediate operating temperature is important to achieve a better selectivity value [104].

- Operating pressure

The feed pressure influences the adsorption of gases in the MMMs. The pressure effect on diffusion is different for condensable gases than the rest of the gases. For non-condensable gases the pressure increase has little effect on permeability. However, for condensable gases, an increase in supplied pressure leads to an increased permeability. In fact, when the pressure increases up to a value determined, the phenomenon of plasticization may occur. Plasticization is a phenomenon that occurs due to the dissolution of condensable gases such as: CO_2, H_2O, H_2S in a polymeric membrane, preventing the correct packing of polymer chains and thus increasing fractional free

volume (FFV) in the membranes [105]. Therefore, plasticization leads to an increase in mobility of all the gas species in the polymer that usually causes increase in permeability but decreases separation selectivity.

- Operating temperature

Temperature is a factor that affects both diffusion and solubility of the gases. Diffusion is a kinetic phenomenon related to the speed with which gas molecules cross the membrane. Relation of diffusion coefficient with temperature is given by the Arrhenius equation (Equation 2.19):

$$D = D_0 \exp(-\frac{E_D}{RT}) \qquad Equation\ 2.19$$

where D_0 is a pre-exponential factor, E_D the diffusion activation energy, R the universal gas constant and T the temperature in K. On the other hand, the solubility is a thermodynamic parameter and its variation with temperature follows van't Hoff's laws (Equation 2.20).

$$S = S_0 \exp(-\frac{\Delta H_S}{RT}) \qquad Equation\ 2.20$$

where S_0 is a constant and ΔH_S, the enthalpy of adsorption. Since the permeability is the product of diffusion and solubility, the two equations can be encompassed as Equation 2.21 shows:

$$P = P_0 \exp(-\frac{E_P}{RT}) \qquad Equation\ 2.21$$

where $P_0 = D_0$. S_0 is a constant and $E_P = E_D + \Delta H_S$ is the activation energy of permeation. Normally, an increase in temperature leads to an increase in diffusion coefficient and a decrease in solubility. Since the absolute value of E_P is usually greater than that of ΔH_S, the permeation of the membranes increases with temperature for most of the polymers.

- Free volume

FFV is defined as open space between crosslinked polymer chains in the polymer matrix, provides enough scope towards gas molecules to diffuse, influences the diffusion of gases. The higher is the free volume, the greater is diffusion coefficient, and therefore, the greater the permeability of the gases in the polymer. FFV of polymer matrix is measured through the estimation of bulk density and permeability of helium. Helium is small enough to pass through the interstitial space among polymer chains.

- Mobility of polymeric chains

The mobility of the polymeric chains affects the diffusion coefficient of the penetrating gases. This mobility is important as there must be enough space between the polymer segments to allow the passage of gas molecules. For example, the presence of rigid aromatic groups in polymer reduces the mobility of their chains, consequently decreasing the permeability of the gases in the membrane [106].

2.2.5.4 Permeation models for MMMs having porous fillers: ideal models

This permeation model is used to predict the permeability of gases in mixedmatrix membranes containing a porous filler. It considers three parameters: 1) the permeability of the continuous phase (polymer), Pc, 2) the permeability of the dispersed phase (filler), Pd, and 3) the volumetric fraction of each phase, Φ. The minimum P_{eff} (effective permeability) occurs when the mechanism of transport across the membrane follows a resistance in series model (Equation 2.23) [107]

$$P_{eff} = \frac{P_c\, P_d}{\Phi_c\, P_d + \Phi_d\, P_c} \qquad Equation\ 2.23$$

When the two phases work in parallel to the direction of the gas flow, the maximum P_{eff} is obtained (Equation 2.24):

$$P_{eff} = \Phi_c\, P_d + \Phi_d\, P_c \qquad Equation\ 2.24$$

Maxwell theory of a heterogeneous medium that describes the flow of gas through a mixed matrix membrane composed of a homogeneous distribution of non-contacting spherical particles (Equation 2.25): [108]

$$P_{eff} = P_c . \frac{P_d + 2P_c - 2\Phi_d\,(P_c - P_d)}{P_d + 2P_c + \Phi_d\,(P_c - P_d)} \qquad Equation\ 2.25$$

This Maxwell model is only applicable to mixed matrix membranes whose filler is spherical and for low loads (up to 20% by vol.).

2.2.5.5 Permeation models for MMMs with Porous Filler: Deviation from Theoretical Predictions

There are several factors that influence the satisfactory separation performance of a mixed matrix membrane: a proper interaction between the filler material and the polymer matrix, non-selective gaps between both phases and access to the pores of continuous phase for gas flow (filler should not block the pores). Additionally, fillers must be evenly distributed throughout the membrane so that its effect is maximum. However, there are several cases of imperfections occurring in composite materials that deviate from the predictions of the ideal models. Those cases are explained below: [109]

- Case 1: poor interaction between the filler and the polymer matrix

If the filler-polymer interaction is poor, the polymer chains do not fully adhere to the surface of the filler materials, giving rise to the formation of preferential channels between both phases. In such case, the permeability of the gas in the dispersed phase and around the particles is much greater than in the continuous phase ($P_d >> P_c$) and then P_{eff} is obtained as per equation 2.26.

$$P_{eff} = P_c \left[\frac{1 + 2\Phi_d}{1 - \Phi_d}\right] \qquad Equation\ 2.26$$

Such imperfections at the filler-polymer interface allows gases non-selectively, consequently permeability in increased. Generally, at low loads this leads to an increase in permeability while the selectivity remains constant. However, higher loads decrease the selectivity of the membrane [110].

- Case 2: blockage of the pores of the filler

Blocking of porosity (either partial or total) of the filler particles by polymeric phase causes the permeability of the dispersed phase to be much smaller than that of the continuous phase (Pd<<Pc). This means, the filler particles are impermeable to the gas and their addition to the polymer phase doesn't bring change in the transport properties of the membrane. Sometimes, filler particles may affect packing of the polymer chains, which would indirectly influence the permeability [100], then Maxwell's equation changes to the following expression:

$$P_{eff} = P_c \left(\frac{P_c - \Phi_d \, P_c}{P_c + 0.5 \, \Phi_d \, P_c} \right) \qquad Equation\ 2.27$$

- Case 3: equivalent permeability of both continuous and dispersed phases

If the permeability of the continuous phase is exactly same as of the dispersed phase (P_c=P_d), Equation 2.29 simplifies to the following expression:

$$P_{eff} = P_c \qquad Equation\ 2.28$$

This means that the presence of the filler material has no influence on the transport properties of a membrane for a particular gas. In this case, the mixed matrix membrane will show identical permeability as a pure polymer membrane, although the selectivity might be different as different gases may be affected differently by the presence of the filler particles.

- Case 4: rigidification of the polymer

Sometimes, rigidification of the MMM occurs, when the polymer chains lose their mobility with respect to the rest of the crosslinked polymer chains or due to their strong interaction with the fillers. This decreases the permeability of the membrane for both of the gases (of a certain binary mixture). Since it affects both gases that permeate, in some cases, an increase in the selectivity is observed [111].

2.2.6. Fabrication of flat sheet polymeric membranes

- Casting

Casting method is widely used for a fabrication of symmetrical (dense or porous) membranes (see **Figure 2.15**) as per aforementioned steps. The process begins with a "dissolution of casting": polymer is dissolved in a suitable solvent to obtain a homogenous solution. Then polymer solution is poured onto a completely flat surface or into a petri dish and placed onto a flat surface, afterward allowing the solvent to evaporate. Finally, after drying, flat polymeric surface is obtained whose structure can be either dense or porous depending on the employed conditions and polymer being

used. These flat sheets can be used either as a membrane or as a support depending on their properties and on the purpose of the project.

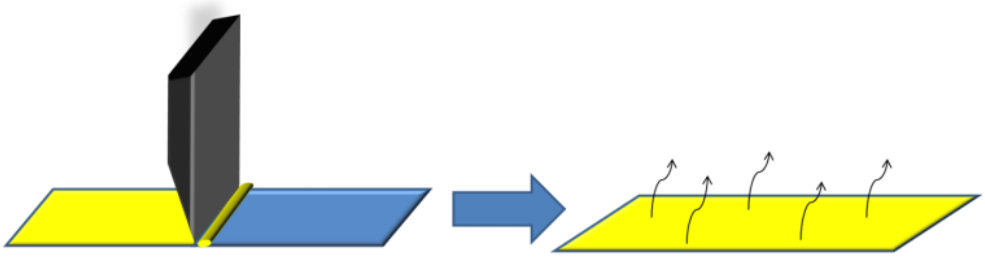

Figure 2.15. Fabrication of flat membranes by casting method

- Phase inversion

Phase inversion method, developed in the 1960s by Loeb and Sourirajan, is widely applied for fabrication of asymmetric membranes [112]. Similarly, to the casting method, the technique also begins with dissolving the polymer and spreading it on a flat surface to form a sheet, but instead of drying by solvent evaporation, the membrane is immersed in a non-solvent bath (usually water bath) to initiate coagulation. This results in rapid precipitation of the polymer forming a dense upper layer which acts as a barrier to water for the subsequent innermost polymer layers, which leads to formation of the porous substructure. Such phase inversion process can be easily explained using a ternary diagram (**Figure 2.16**) which consists of an equilateral triangle where each vertex corresponds to the pure state of one of the three compounds; the sides (1 and 4), to bicomponent mixtures and the interior points (2 and 3) are mixtures of the three components. The interior of the diagram has two zones separated by the binodal curve. The left zone signifies one phase in the system, where three components are completely miscible. On the other hand, in the right zone the solid phase (rich in polymer) is in equilibrium with a liquid phase (low in polymer).

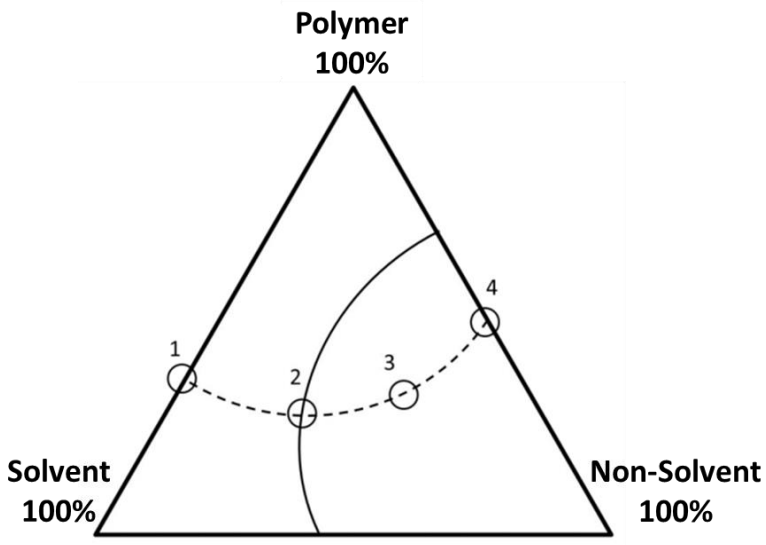

Figure 2.16. Ternary diagram of phase inversion process

- Coating by immersion: dip-coating

The dip-coating or immersion coating method is one of the simplest means of multilayer membrane fabrication. The method consists of immersing a support in a polymeric solution and then withdrawing it. Thus, the support gets soaked with polymer solution. After drying, a polymeric membrane is formed on the support. Concentration of the polymer in the casting solution, immersion rate, immersion time and drying condition control the thickness of the multilayered membrane [113]. However, the affinity of the support towards the coating solution determines the efficiency of coating process, eventually membrane performance.

- Coating by turning: spin-coating

Spin coating is an interesting technique for fabrication of supported membranes. It consists of fixing the support on a horizontal substrate and pouring of the certain amount of polymer solution on it. The support is then rotated at a certain speed so that the solution spreads uniformly due to centrifugal force. Finally, after drying, a selective layer is generated on the support which acts as a membrane [114]. Concentration of the spreading solution and rotation speed controls the thickness of the resulted membranes.

- Interfacial polymerization

Interfacial polymerization involves step-growth polymerization between two immiscible liquid phases containing dissolved multifunctional monomers. It begins by soaking the support with the aqueous solution of the first monomer, afterword adding the organic solution. Upon contacting the solutions, a rapid polymerization reaction occurs at their interface causing the polymer to precipitate forming a very thin dense sheet, typically of aromatic polyamide [115].

2.2.7. Improvement strategies in polymeric membranes fabrication

In general, polymeric membranes are commercially limited due to their poor gas separation efficiency. Highly permeable membranes tend to be less selective and vice-versa which reduces their commercial attraction. In 1991, Lloyd M. Robeson defined such compromise between permeability and selectivity using more than 300 bibliographic references of polymeric membranes, which is known as “Robeson upper limit” [116]. In 2008, Robeson upper limit was updated by incorporating new gas mixtures of industrial interest, such as CO_2/N_2 [29]. The upper bound is an expression of $P_i = k\,\alpha_{ij}^{n}$, where P_i is the permeability of the most permeable gas, k is called front factor, α is the separation factor (P_i / P_j) and n is the slop of the log-log plot [29]. Robeson limits are frequently used by researchers to compare their experimental results. **Figure 2.6** represents the 2008 Robeson upper limit for the CO_2/N_2 separation (black lines), where the points in red are the bibliographical experimental results of membranes. A latter update of these limits for certain pairs (CO_2/N_2 and CO_2/CH_4)of gases has been published by Comesaña-Gándara et al. [117].

The challenge of polymeric membranes is to surpass the upper limit of Robeson plot. Such membranes can be improved to have better gas separation performance in a number of ways: by controlling its microstructure, by post-treatments (thermal

annealing), using mixture of polymers or incorporating inorganic or metal-organic materials to form hybrid membranes (which are called mixed matrix membranes). Improvement strategies of polymeric membranes are described in the following section:

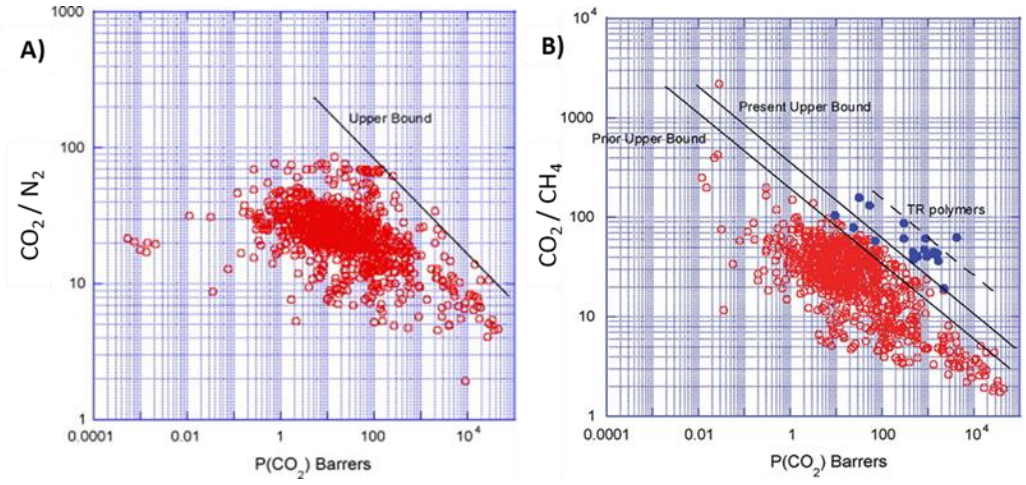

***Figure 2.17**. Robeson upper bound limit: A) for the CO_2/N_2 and B) for the CO_2/CH_4 separation* [29] *reproduced with permission from Elsevier Ltd.*

- Thermal annealing

In thermal annealing process, a membrane is exposed to high temperatures (below their glass transition) for a certain time. As a result, polymeric chains rearrange themselves into a new equilibrium state wherein packing of the material increases and the free volume decreases. Consequently, such post-treatment for polymeric membranes usually leads to an increase in the selectivity, but decreases its permeability. Literature demonstrates, post-treatment of polyimides such as Matrimid® [118–120], 6FDA-based copolyimides [121] or P84® [122] to avoid plasticization of the membranes.

- Crosslinking

Crosslinking is usually defined as formation of chemical bonds between polymer chains either by physical or chemical means, thus altering gas separation performance. Physical crosslinking can be produced by heat treatment at high temperature [115] or with ultraviolet radiation [123]. However, in chemical crosslinking, a reagent is used which carries some functional group that can interact with polymer chains. Chemical crosslinking has been widely used with different polyamides [124] or polyethylene [125] to reduce plasticization and improve capacity of membrane separation. There are several impacts of crosslinking in the polymeric membranes such that: (1) reduction of the degree of crystallinity of the polymer by disrupting the regular polymer chains [126], (2) an increase of the mechanical resistance of the polymer, (3) prevention of plasticization [127], (4) improvement of the selectivity of the membranes by increasing packing between polymer chains [126] and (5) reduction in permeability.

- Repairing with polydimethylsiloxane (PDMS)

PDMS is an organosilicate compound having versatility in properties (easy processability, gas permeability, easy adhesion and bonding to different substrates, biocompatibility, transparency, low cost processing) [128,129] and applications (membrane separation, microfluidic devices, biomedical applications to name a few) [129–131]. PDMS can be used as a membrane support or as a covering on defected surface due to its rubbery nature at solid state. One face of the imperfect membranes is immersed in a diluted solution of PDMS for a certain time and then removed (usually, such process is called dip coating, already explained in section 2.2.6.), so that a layer of elastomer is formed on its surface. The PDMS solution is capable of filling all the intricacies of the membrane, thus covering all defects responsible for the viscous flow that penalize gas selectivity (see diagram in the **Figure 2.18**). This method is especially adopted for asymmetric membranes (such as: thin film composite membranes). Such repairing increases selectivity but a decrease in permeability is also observed due to an addition of a new layer.

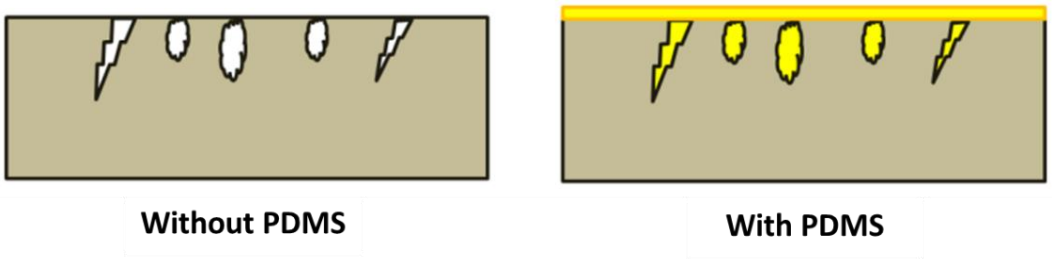

Figure 2.18. Schematic representation of repairing of membranes

- Blending of polymers

Blending process can be homogenous or heterogenous mixing of two polymers without forming any covalent bond between their chains [132]. When mixing of two polymers is complete at the molecular level, it is called homogeneous blending. On the contrary, when this is not the case, the blending is called heterogeneous. The homogeneous blending is interesting for the gas separation application, since the inhomogeneities tend to decrease the mechanical resistance and continuity of the membranes, which cause imperfections in the matrix. The polymer obtained from homogenous blending presents a single T_g value which can be estimated using Equation 2.1. Beyond the Tg, polymers become rubbery since secondary links between the segments of the polymers become weaker. It is an intermediate point between the molten state and the rigid state of a polymer material as per Equation 2.1.

$$\frac{1}{T_g} = \frac{W_1}{T_{g1}} + \frac{W_2}{T_{g2}} \qquad Equation\ 2.1$$

where T_{g1} and T_{g2} are the glass transition temperatures in K and W_1 and W_2 are the mass fractions of the polymers in the blend. Hereby, Pebax can be mentioned as a example of blended polymer, which is obtained by mixing of PA and PE segments (having disimiliar properties: one is glassy and the rest is rubbery) in different

compositions (also marked different codes depending on their compositions). These Pebax polymers represent a combined property of the ingredients, which are explained in section 2.2.4.

Chapter 3: Experimental and Characterization Techniques

3.1. Synthesis of MOFs

Synthesis procedures of MOFs being used in this doctoral study are detailed in the subsequent sections:

3.1.1. Synthesis of ZIF-94

ZIF-94 was synthesized by a two-step process [126], following an activation step. Chemicals being used and their respective molar ratio is presented in **Table 3.1**. Initially, 1.584 g (7.2 mmol) of zinc acetate dihydrate was dissolved in 6 mL of methanol (99.8% purity). On the other hand, 1.584 g (14.4 mmol) of 4-methyl-5-imidazole carboxaldehyde was dissolved in 15 mL of tetrahydrofuran (THF). Next, the methanol solution was added to the THF solution under vigorous mixing. Afterwards, the mixture was stirred for 16 h at room temperature (RT). The product was collected by centrifugation with MeOH at 10000 rpm for 10 min (the process was repeated three times). The resulting ZIF-94 was dried in air overnight under RT. Finally, ZIF-94 was ready for characterization and application for MMM preparation and subsequent gas separation performance testing. Schematic representation of the synthesis of ZIF-94 is shown in **Figure 3.1.**

Table 3.1: List of chemicals being used and their respective molar ratio.

Chemicals	Quantity	No. of mmol	Molar ratio (metal: ligand: NaOH: MeOH: THF)
Zinc acetate dihydrate	1.584 g	7.2	**1: 2: 2: 20: 25**
4-methyl-5-imidazole carboxaldehyde	1.584 g	14.4	
NaOH	0.578 g	14.4	
MeOH	6 mL	148	
THF	15 mL	185	

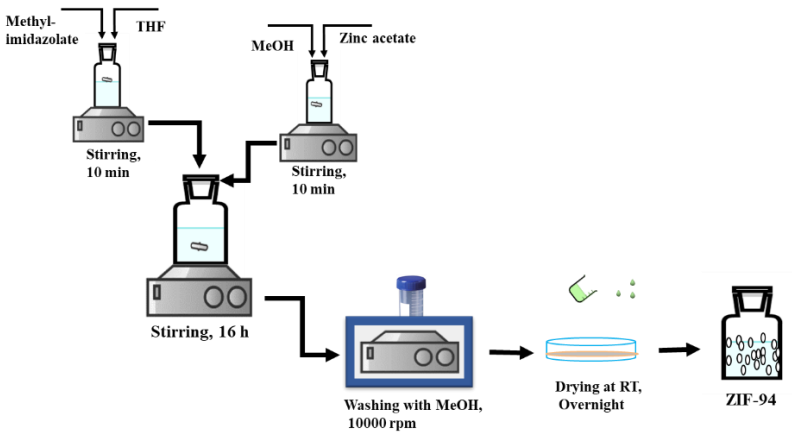

Figure 3.1. Schematic representation of synthesis of ZIF-94

The representative reaction for the synthesis of ZIF-94 is shown below in Equation 3.1 ($C_5H_6N_2O$ being 4-methyl-5-imidazolecarboxaldehyde). Two moles of acetic acid are produced per mol of ZIF-94, justifying the need of the addition of base as a means to control the pH of the reaction.

$$Zn(CH_3CO_2)_2 \cdot 2H_2O + 2C_5H_6N_2O \rightarrow Zn(C_5H_5N_2O)_2 + 2H^+ + 2CH_3CO_2^- + 2H_2O \qquad Equation\ 3.1$$

The Scherrer equation (Equation 3.2) was used to calculate primary ZIF-94 particle sizes from X-ray diffraction (XRD) patterns.

$$L = \frac{K \cdot \lambda}{B \cdot \cos\theta} \qquad Equation\ 3.2$$

where L is the crystallite size (nm), K is a constant (0.96), λ - X-ray wavelength (λ = 0.154 nm), B the peak width and θ the diffraction angle.

Moreover, the yield of the reaction was defined as the ratio of the amount of solid ZIF-94 obtained from 100 g of synthesis mixture to the maximum possible amount of ZIF-94 that can be produced from 100 g of synthesis mixture if all limiting reactants (Zn^{2+} or ligand, both in stoichiometric quantity) are consumed according to equation 3.3:

$$Yield\ (\%) = \frac{Exp.\ ZIF{-}94}{Theor.\ ZIF{-}94} \cdot 100 \qquad \text{Equation 3.3}$$

where Exp. ZIF-94 is the mass of dry ZIF-94 collected after the synthesis and Theor. ZIF-94 is the theoretic yield considering the limiting reagent and the empirical formula of ZIF-94, Zn $(C_5H_5N_2O)_2$.

3.1.2. Synthesis of ZIF-94 from recycled mother liquors

After the synthesis of ZIF-94, the mother liquor was separated by centrifugation from the nanocrystals to be used in the subsequent synthesis of ZIF-94. The main purpose was to reduce chemical waste discharge to environment by their reuse and to keep the size and the morphology of the nanocrystals as similar as possible to the original ZIF-94 reproducing the exact same synthesis. To do that, once synthetized the nanocrystals were recovered by centrifugation, and thermogravimetry was used to estimate the percentage of pure ZIF-94 synthesized (i.e. excluding trapped solvent and ligand). Knowing this percentage, the quantities of the unreacted reagents in the mother liquor were calculated by mass balance and the lacking amounts of those reagents were added together with the volume of the solvent that was lost. The reaction produces acetic acid (see Equation 3.1), therefore the pH of the medium decreases with the crystallization. In order to restore the pH of the mother liquor and to favor the deprotonation of the organic ligand, a procedure of adding NaOH as a base was conducted [133]. Besides, some experiments were carried out changing the pH or the temperature of the original synthesis to observe how these parameters affect the crystallinity, morphology and particle size of ZIF-94. Such procedure (see **Figure 3.2**),

resulted in the formation of products A.1 – A.5 for the pH control and product B for the temperature control.

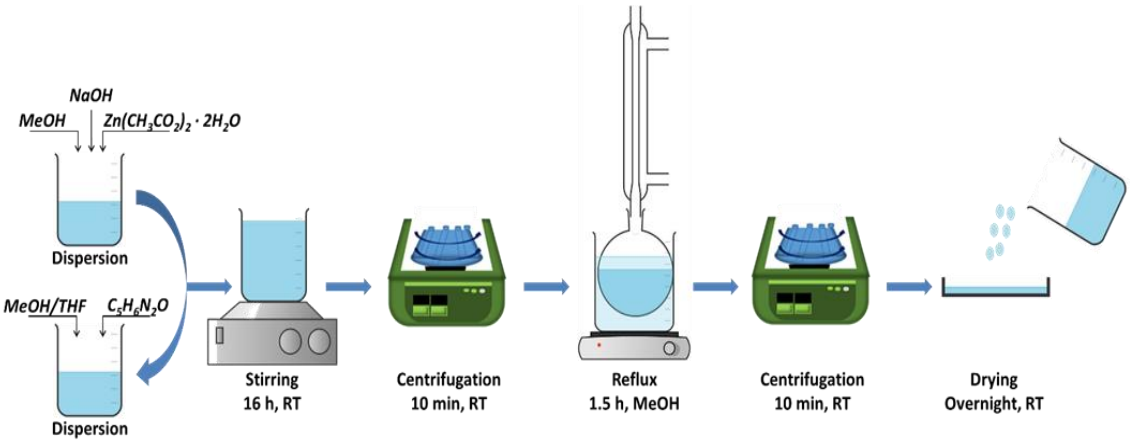

Figure 3.2. Schematic representation of synthesis of ZIF-94 from mother liquor

3.1.3. Synthesis of ZIF-8

Synthesis of ZIF-8 was performed according to [134] wherein 0.47g of zinc nitrate hexahydrate (Zn (NO3)2·6H2O > 98%, Sigma Aldrich) was dissolved in 10 mL of MeOH (Scharlau) and 10 mL of water. Besides, 1.0 g of 2-methylimidazole (mIm, $C_4H_6N_2$, >99%, Sigma Aldrich), was dissolved in 10 mL of MeOH, and the two solutions were mixed and stirred for 2 h. The final product was collected by centrifugation, washed once with MeOH, and dried at 110 ºC overnight.

3.1.4. Synthesis of MIL-178(Fe)

3.1.4.1 Hydrothermal synthesis of MIL-178(Fe)-hyd

Single crystals of MIL-178(Fe)-hyd were synthesized via a hydrothermal route. 1,2,4-BTC (1.15 g, 5.5 mmol) was poured into a 125 mL Teflon-lined steel autoclave with anhydrous $FeCl_3$ (1.29 g, 8 mmol) and 10 mL of deionized H_2O. The mixture was stirred for10 min and heated to 200°C for 72 h under autogenous pressure. The resulting solution was then filtered and a yellow powder was obtained after extensive centrifugation with water and ethanol to remove the unreacted ligand.

3.1.4.3 Room temperature synthesis of MIL-178(Fe)-RT

1,2,4-BTC (1.05 g, 5 mmol) and anhydrous $FeCl_3$ (0.81 g, 5 mmol) were poured into a 100 mL beaker with 50 mL of deionized H_2O and stirred at RT for 5 days. A bright yellow powder was then recovered by filtration after extensive centrifugation (H_2O and ethanol). These two syntheses were carried out by Profs. Serre and Steunou's Group from CNRS.

3.2. Membrane fabrication

3.2.1. Fabrication of mixed matrix membranes (MMMs)

The general procedure of the membrane fabrication by the solution casting method can be seen in **Figure 3.3** and consists of four steps: (i) Filler dispersion in specific solvent, (ii) polymer dissolution, (iii) mixing of fillers and polymer solution, followed by a priming step (small amount of polymer solution added, left it for stirring, added the rest) and (iv) Casting and solvent evaporation. Pure polymeric membranes were prepared analogously but just skipping the first step, since they contain no filler. First, different concentrations of polymer matrices were dissolved in an appropriate solvent (EtOH/water (30/70 (v/v)) for Pebax® MH 1657 and 1-propanol/1-butanol (75/25 (v/v)) for Pebax® 3533) by stirring under reflux at 80 °C for approximately 1 h. In the meantime, the required dose of filler was dissolved in 1.5 mL same solvent by repeated sonication and stirring at RT. Next, both solutions were mixed and kept for overnight stirring at RT. The solution was poured on a Petri dish (PDC) and dried in a top-drilled box under a solvent-saturated atmosphere (overnight drying at RT for Pebax® MH 1657 whereas, 24 h drying for Pebax® 3533 based membranes). Schematic representation of fabrication of MMMs is shown in **Figure 3.3**.

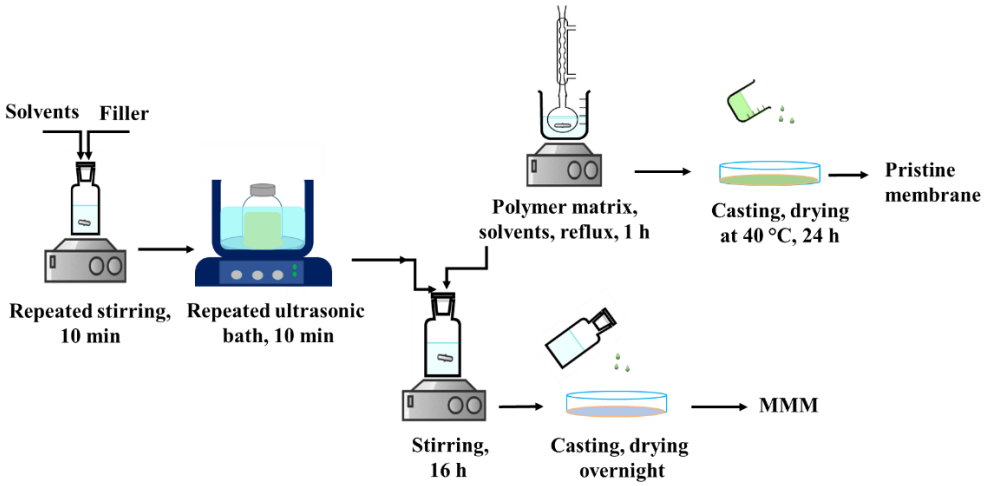

Figure 3.3. Schematic representation of fabrication of pristine membrane and MMM

3.2.2. Fabrication of mixed matrix membranes (MMMs) from the recycled reagents

In order to fabricate the MMM from the recycled reagents (the recycling procedure is explained in the following section (section 3.3)), the required amount of recycled polymer was dissolved (3 wt.% polymer in solvent) in a specific solvent by stirring under reflux for 1 h. Next, 10 wt.% of recycled ZIF-94 was dispersed in the same solvent by repeated sonication and stirring for three times, which was later mixed with dissolved polymer and stirred overnight before casting on a Petri dish dried in a top-drilled box under a solvent-saturated atmosphere at environmental conditions.

3.3. Recycling of MOFs and polymer matrix

Due to the growing interest in the development and use of MOF and an increasing amount of waste generated, especially in research centers, an easy and effective method to recycle the mentioned was developed. In this case, ZIF-94 has been used as a starting material for recycling from their MMMs due to its high price, and sometimes low availability of the required organic ligand in the market. The recycling method developed in this thesis attains a high rate recovery of the ZIF-94 and re-incorporation of the MOF in the membranes, which were investigated for the separation of CO_2/N_2. Membranes with such recycled ZIF-94 were found comparable to the fresh components based MMMs.

Additionally, the proposed method was repeated for ZIF-8 and Pebax® MH 1657 based MMMs, where, both ZIF-8 and polymer matrix were successfully isolated and reincorporated in their MMMs. Such repetitions justified validation of the proposed recycling method for alike MOFs.

3.3.1. Recycling of ZIF-94 and a polymeric matrix from MMMs

ZIF-94 was recovered from MMM by a two-step method and then scalled-up: 1) initially, 3.9 ± 0.4 g of MMM sample was dissolved in 25 mL of EtOH/water (70/30 (v/v)) by stirring under reflux for 1 h, and 2) the obtained mixture was centrifuged at 9000 rpm for 20 min in order to collect ZIF-94. Next, collected ZIF-94 was washed with EtOH/water (70/30 (v/v)) under the same conditions (25 mL EtOH/H_2O, stirring with reflux for 1 h and centrifugation at 9000 rpm for 20 min) to ensure the removal of remaining polymer traces (the process was repeated three times) and facilitate the subsequent characterization. The resulting ZIF-94 was dried overnight at RT. To recover a polymer matrix (Pebax® MH 1657) from MMM, dissolved polymer (supernatant) was collected from the very first centrifugation of the MMM solution. Next, centrifugation of the supernatant (polymer without MOF) was repeated for three times at 9000 rpm for 20 min to remove remaining ZIF-94. Finally, the polymer solution was cast on a Petri dish and dried at 40 ºC to be later re-included into MMMs following the fabrication procedure discussed in section 3.2.2. Recovery efficiency of the process was calculated following Equation 3.4:

$$Recovery\ (\%) = \frac{Experimentaly\ \ recycled\ amount}{Theoretical\ amount} \cdot 100 \qquad \text{Equation 3.4}$$

where “Theoretical amount” signifies amount of polymer matrix or filler present in the fresh membrane (used for recycling) as per their composition, whereas “Experimentally recycled amount” signifies recovered amount of the polymer and ZIF-94. Similarly, “Recovery (%)” stands for the ratio of the total amount of the material recovered to the total amount of the membrane being recycled. Schematic representation of recycling of MMMs is shown in **Figure 3.4** and identification names of the fabricated membranes are given in**.**

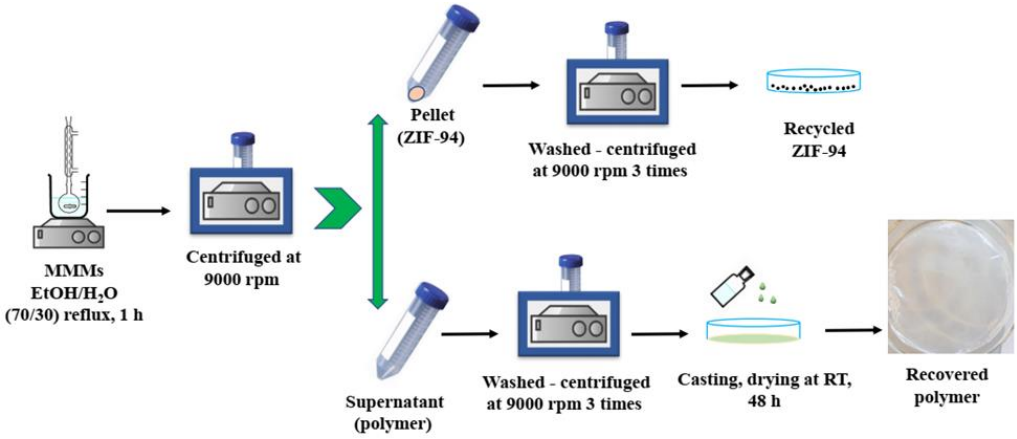

Figure 3.4. Schematic representation of recycling of ZIF-94 from MMM

3.3.2. Recycling of ZIF-8 and a polymeric matrix from MMMs

To study the applicability of the prescribed recycling methodology for other MOF based MMMs, the present study also investigated ZIF-8 (synthesized according to [134]) and Pebax® MH 1657 based MMMs of the same composition (10 wt.% filler in 3 wt.% polymer matrix). Recovery (%) of both polymer and ZIF-8 was calculated using Equation 3.4. The recycling procedure was maintained the same as in the case of ZIF-94 and it is shown in **Figure 3.4**.

3.4 Gas separation analysis

Gas chromatography (GC) is a quantitative analysis where relative concentration of the gas components of a mixture can be determined. An inert carrier gas (e.g., Helium, Argon etc.) is used to bring those mixture components to the detector which produces a corresponding chromatograph. GC may also be used to separate and purify components of a mixture. The separation of the CO_2/N_2 mixture through the membrane was performed in the experimental system that is schematically presented in **Figure 3.5**. The membranes were cut and placed in a module consisting of two stainless steel pieces and a 316LSS macroporous disc support (Mott Co.) with a 20 μm nominal pore size. Membranes, 2.12 cm^2 in area, were gripped inside with Viton O-rings. To control the temperature of the experiment, which influences gas separation, the permeation module was placed in an UNE 200 Memmert oven. Gas separation measurements were carried out by feeding the gaseous mixtures of CO_2/N_2 (15/85, both cm^3(STP) min^{-1}) or CO_2/CH_4 (50/50, both cm^3(STP) min^{-1}) at an operating pressure of 3 bar and 35 °C) to the feed side, controlled by two mass-flow controllers (Alicat Scientific, MC-100CCM-D). The permeate side of the membrane was swept with 2 cm^3(STP) min^{-1} of He, at atmospheric pressure (approx. 1 bar) (Alicat Scientific, MC-5CCM-D). Concentrations of CH_4, N_2 and CO_2 in the outgoing streams were analyzed online by an Agilent 3000A micro-gas chromatograph. Permeability was calculated in Barrer (10^{-10} cm^3 (STP) cm cm^{-2} s^{-1} cm Hg^{-1}) once the steady state of the exit stream was reached (at least after 3 h). The separation selectivity was calculated as the ratio of permeabilities of CO_2 over permeabilities of N_2.

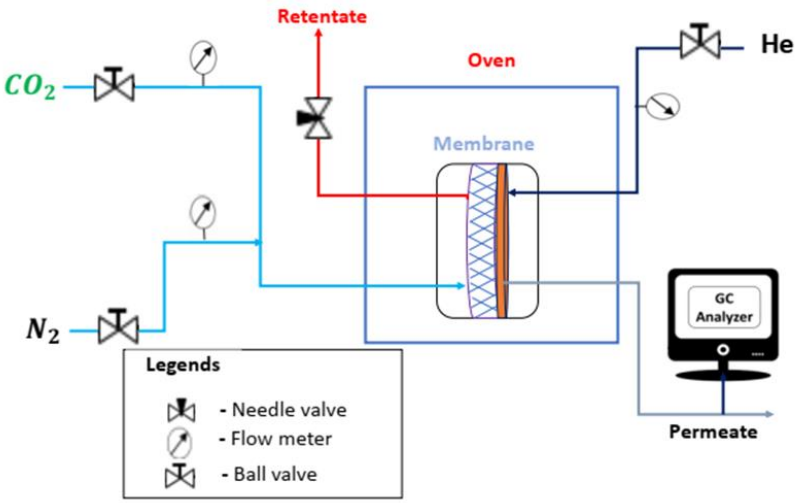

Figure 3.5. Schematic representation of experimental set-up used for gas separation analysis

3.4.1. Time lag permeation experiments

Experimental set-up used for time-lag measurement is shown in **Figure 3.6**. The membranes were cut into 3.2 cm^2 in area, placed in a module, consisting of two stainless steel pieces and a 316LSS macroporous disc support (Mott Co.) with a 20 μm nominal pore size, gripped with Viton O-rings. To control the temperature of the experiment, which influences gas separation, the permeation module was placed in a Memmert oven (Model: 30-1060). Single gas separation measurements were carried out by feeding N_2 first and then CO_2 at an operating pressure (3 bar upstream pressure and vacuumed at the downstream) and 35 °C. Corresponding upstream and downstream pressure was measured which was used to calculate concentrations of N_2 and CO_2 in the downstream. Permeability was calculated in Barrer (10^{-10} cm^3 (STP) cm cm^{-2} s^{-1} cm Hg^{-1}), diffusivity in cm^2/s, and solubility in (cm^3(STP)/(cm^3 cm Hg)) once the steady state of the exit stream was reached. The separation selectivity was calculated as the ratio of permeability of CO_2 over permeability of N_2.

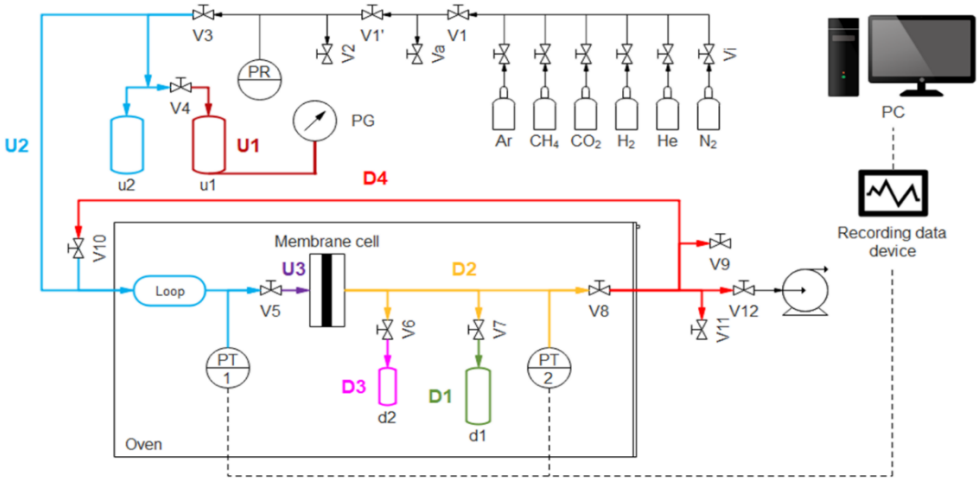

Figure 3.6. Schematic representation of the experimental set-up used for time-lag analysis

3.5. Characterization techniques

3.5.1. X-ray diffraction (XRD)

XRD diffraction analytically allows the phase identification of a crystalline material including its unit cell characteristics. In an X-ray diffractometer, monochromatic X-rays are directed onto the sample while the sample and the detector rotate within a certain range of angles (θ). The intensity of the reflected X-rays is recorded and the detector converts those signals into a count rate. When the angle of the incident X-rays impinging on the sample satisfies the Bragg´s law (Equation 3.5), a constructive interference occurs and an intensity peak appears. Membranes and nanoparticles were characterized by using a Panalytical Empyrean equipment with CuK_α radiation (λ = 0.154 nm), over the range of 5º- 40º at a scan rate of 0.03º s^{-1}, to examine the *d*-spacing of the nanoparticles and membranes. Moreover, the d-spacing can explain the packing density of a material since it is related to the distance among the central atoms of close planes.

$$2d.sin\theta = n.\lambda \qquad Equation\ 3.5$$

Where, d refers to the distance between crystallographic planes, n is a positive integer number and λ is the wavelength of the XRD radiation.

3.5.1.1. Pressure-dependent PXRD under CO_2

The sample was activated overnight at 70°C with a turbomolecular pump (~10^{-7} mbar) and then transferred to an argon-filled glovebox (0.1 ppm H_2O, 0.4 ppm O_2), were it was loaded into a sapphire capillary. The capillary, embedded in a sample holder was removed from the glovebox and immediately connected to the gas loading system, followed by immediate exposure to vacuum for one hour, before running the diffraction experiment. Two adsorption/desorption cycles were measured from vacuum to 45 bar CO_2 (CO_2 N50, Air Liquide, purity >99.999%), using a Rigaku Mo rotating anode (λ = 0.71073Å), XENOCS focusing mirror and a MAR345 image plate detector.

3.5.2. Thermal analysis

- Thermogravimetric analysis (TGA)

TGA reveals the amount of weight change of a material as a function of increasing temperature and time, in an inert (N_2, Ar, He…) or air. This technique determines weight change of the material under investigation due to the decomposition reaction over temperature and it makes a possible quantitative composition analysis. It can also indicate the presence of water and other residual solvents in the sample, allowing verifying the right activation of MOFs and membranes.

Thermogravimetric analysis was carried out using a Mettler Toledo TGA/STDA 851e. Small amount of the materials (approx. 5 mg) placed in 70 μL alumina pans was heated under an air flow (40 mL min^{-1}) from 35 to 700 ºC at a heating rate of 10 ºC min^{-1}. Loss of wt. % as a function of temperature was revealed which is characteristic of removal of solvents and thermal degradation of the sample under

investigation. This information is very helpful for the selection of the materials for industrial application, especially in aggressive environmental condition of flue gas.

- Differential scanning calorimetry (DSC)

Differential scanning calorimetry (DSC) measures the amount of energy absorbed or released by a sample while it is heated or cooled, providing quantitative data on endothermic and exothermic processes. DSC can be used to measure the melting temperature, the heat of fusion or the T_g of a sample.

DSC analysis was performed using a Mettler Toledo DSC822e. Approximately 5 mg of a sample was deposited and sealed at ambient temperature (25 °C) in 40 µL aluminum crucible with a perforated lid. The reference was an empty crucible (i.e. air) and the heat exchange was calibrated with indium. The thermal protocol was identical for all samples: samples were (1) introduced at room temperature, (2) cooled down to -30 °C in 30 min, (3) equilibrated for 2 min at -30 °C and (4) finally heated up to 250 °C at 20 °C/min. To quantitatively analyze the degree of crystallinity of the PTMO phase (one copolymer of Pebax® 3533), the enthalpy of fusion of the PTMO phase was determined by integration of the endothermic peak attributed to the fusion of the PTMO crystalline fraction ($i.e.\ T_{melting}\ (PTMO) \approx 9\ °C$). The degree of crystallinity (X_c) was then calculated as:

$$X_c = \frac{\Delta H_f}{\Delta H_f^*} \times 100 \qquad Equation\ 3.6$$

where ΔH_f (J/g) is the enthalpy of fusion of the PTMO phase and ΔH_f^* (J/g) is the enthalpy of fusion when the polymer phase is purely crystalline as obtained from the literature ($\Delta H_f^* \approx 200\ J/g$) [135].

3.5.3. Electron microscopy

Electron microscopy is used to generate high-resolution images of objects whose size is too small to be seen with an optical microscope. Electron microscope is widely used to understand morphology of the membranes, homogenous distribution MOFs in the polymer matrix and to see possible defects in the membranes.

- Scanning electron microscopy (SEM)

Scanning electron microscope (SEM) impinges a high-energy electron beam on the surface of solid samples. This way, the signals deriving from the electron-sample interactions reveal information about the external morphology of the sample. The SEM is also capable of performing elemental analyses of selected point locations on the sample, quantifying its chemical compositions (EDX, energy-dispersive X-ray spectroscopy). The accelerated electron beams are focused onto the solid sample which produces secondary electrons, backscattered electrons, diffracted backscattered electrons and photons (characteristic X-rays used for the EDX analysis). Secondary electrons and backscattered electrons are commonly used for the sample imaging. The secondary electrons are useful for morphology and topography analysis of the samples, while the backscattered electrons are advantageous for contrast of the images of multiphase samples.

SEM images of MOFs and membranes were obtained using a FEI Inspect F50 model scanning electron microscope, operated at 20 kV. Cross-sections of membranes were prepared by freeze-fracturing after immersion in liquid N_2 and subsequently coated with a conductive metal: Pt. Such conductive coating reduces thermal damage to the sample and improves secondary electron signals required for topographic imaging

- Transmission electron microscopy (TEM)

Transmission electron microscope (TEM) also uses a high-energy electron beam (100-400 kV). In this case, the beam passes through the sample and the interactions between the electrons and the atoms form the image. The sample must be thin enough (<100 nm) to transmit sufficient electrons to form an image with minimum energy loss. Elemental analysis is also possible with this microscopy and the characterization of crystalline samples by electron diffraction.

TEM images of the MOFs were obtained using a FEI Tecnai F30 microscope, operated at 300 kV. This particular TEM, fitted with a SuperTwin® lens allowing a point resolution of 1.9 Å, is equipped for spectroscopy experiments performed in EDS (X-Ray Microanalysis). The samples were prepared by dispersion of the powder in ethanol before placing a few drops of the suspension onto the copper carbon coated microgrid.

3.5.4. Spectroscopy

- Fourier transform infrared spectroscopy (FTIR)

In this kind of spectroscopy, infrared radiation passes through a sample. Some of the radiation is absorbed by this sample and the rest is transmitted. The resulting spectrum represents the molecular absorption and transmission, creating a one-of-a-kind molecular fingerprint of the sample. The term “Fourier-transform” stands for the use of Fourier transformation to convert the raw data into the actual spectrum. Infrared spectroscopy can be useful for the qualitative analysis of a material. Besides, the size of the peaks in the spectrum is related to the amount of material present.

FTIR was performed on a Bruker Vertex 70 FTIR spectrometer equipped with a deuterated triglycine sulfate (DTGS) detector and a Golden Gate diamond ATR accessory. Powder samples and membranes were measured in a diffuse reflectance module. Both spectra were recorded by averaging 40 scans in the 4000-600 cm^{-1} wavenumber range at a resolution of 4 cm^{-1}.

3.5.5. Brunauer-Emmett-Teller (BET) analysis

BET analysis is interesting for revealing specific surface area (m^2/g), pore volume and pore size distribution of the solid materials. BET analysis deals with the physisorption of an inert gas, typically nitrogen, argon, or krypton (whose selection depends on the sample properties), at the sample surface at constant temperature (isothermal). The appropriate temperature depends on the inert gas used (e.g. 77 K for liquid nitrogen). Before performing a gas sorption analysis, the solid must be degassed

to remove contaminants (other adsorbed gases and humidity) that would interfere with the analysis. The sample degassing is carried out heating it under vacuum or a flow of dry inert gas. After that, the test is performed under isothermal conditions where small amounts of gas are injected into the evacuated sample chamber as the gas pressure increases. The adsorption process starts when small gas molecules are attracted to the pores and surface of the solid sample forming a monolayer of adsorbed gas. Desorption process is initiated once the gaseous monolayer of molecules is formed, where the sample is placed into a non-nitrogen atmosphere and heated. This allows the release of the adsorbed nitrogen gas molecules from the surface of the sample. The released gas molecules can then be quantified and the surface area and porosity of the sample calculated following Equation 3.7 (wherein, X_m represents number of molecules needed for a monolayer formation, X is the number of molecule adsorbed at a given relative pressure, P/P_0, and C is related to heat of adsorption. The N_2 adsorption-desorption isotherms are helpful to confirm type of porous materials (microporous or macro-porous). Adsorption isotherms can be classified in six different types according to IUPAC and when fitted to a certain adsorption model (see **Figure 3.7**) [136].

$$\frac{1}{X\left[\left(\frac{P_0}{P}\right)-1\right]} = \frac{1}{X_m.C} + \frac{C-1}{X_m.C}\left(\frac{P}{P_0}\right) \qquad Equation\ 3.7$$

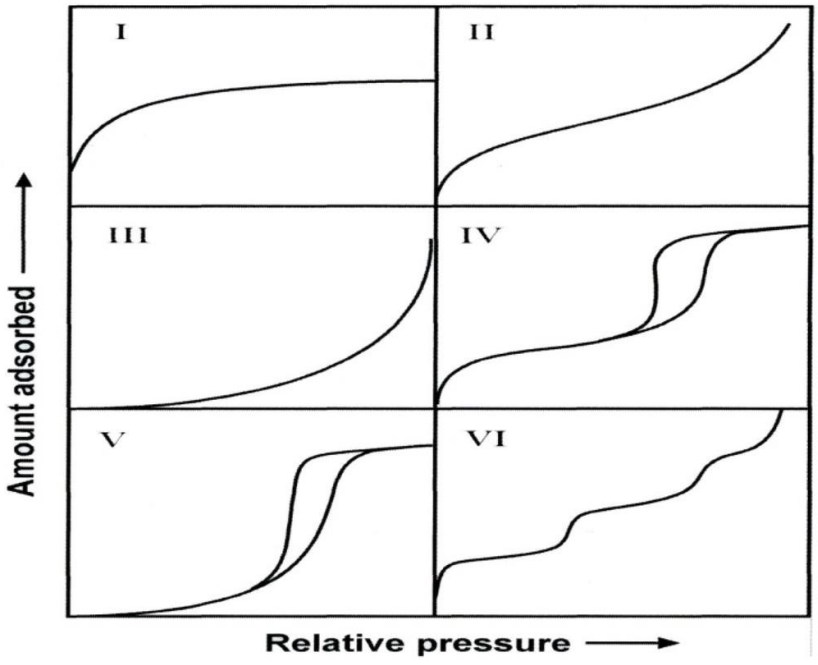

Figure 3.7. IUPAC classification of adsorption isotherms: microporous (type I, the most interesting in this PhD thesis dealing with microporous MOFs), mesoporous (type II and IV), nonporous (type III and V) and quite rare type VI [120]. Besides, types IV and V present hysteresis [adopted from Advances in Mesoporous materials, MPDI, as per their permission policy]

The N_2 adsorption-desorption isotherms were obtained using Micrometrics Tristar 3000 at 77 K. Before these measurements, the samples were degassed for 8 h under vacuum at 200 ºC using a heating rate of 10 ºC min^{-1}.

3.5.6. Tensile tests until failure

The mechanical tests were carried out at ambient (T ≈ 25 °C and reltive humidity (HR) ≈ 40 %) on a tensile testing machine (Zwick-Roell, Model Z0.5TN), using a 0.5 kN load cell. Hexahedral-shaped specimens, having a calibrated dimension 20 mm x 6 mm x 0.05 mm were cut from the films with a stamp. These samples were held on the machine between pneumatic clamps. Tensile measurements were performed at a constant crosshead displacement rate of 10 mm min^{-1}. Data acquisition was started as soon as a preload of 0.5 N was reached. The Young's moduli were calculated using Equation 3.8. (wherein, E, Young moduli in Pascal (Pa), σ is uniaxial stress in Pa, σ is proportional deformation or strain), in the initial elastic segment (i.e. 0 ≤ e (%) ≤ 10).

$$E = \frac{\sigma}{\varepsilon} \qquad Equation\ 3.8$$

5.3.7 Molecular weight measurement

Molecular weights of both fresh and recycled polymers were measured to study if there were any changes between the recycled and fresh products using mass spectrometer Bruker Autoflex III Smartbeam MALDI-TOF/TOF.

5.3.8 Polydispersity and Zeta potential measurement

Dynamic light scattering (DLS) was carried out using Brookhaven 90 plus to study polydispersity of recycled and fresh polymer solution and zeta potential of fresh and recycled MOF.

Chapter 4: Synthesis of ZIF-94 from recycled mother liquors: study of the influence of its loading on post-combustion CO_2 capture with Pebax® based mixed matrix membranes

Outlines

Reproduced from "M.R. Hasan, L. Paseta, M. Malankowska, C. Téllez, J. Coronas, Synthesis of ZIF-94 from Recycled Mother Liquors: Study of the Influence of Its Loading on Postcombustion CO_2 Capture with Pebax Based Mixed Matrix Membranes, Adv. Sustain. Syst. 6 (2022) 2100317. https://doi.org/10.1002/adsu.202100317".

4.1 Introduction

Fossil fuels are considered as the primary energy sources in anthropogenic activities whose consumption will be substantially increased by the year 2030 [137]. Burning fossil fuels produces huge CO_2 emission to the environment with 6 % increment every year [138] causing global warming and unpredictable climatic changes such as rising sea levels, melting of glaciers throughout the entire planet [138] and affecting agriculture [139], to name a few. As a result, searching of green energy sources or filtering post-combustion gases is must to limit the global temperature rise below 2 °C (as per Paris conference in 2015) [140]. CCS technologies (solvent based absorption, solid adsorbents (adsorption), cryogenic process or membrane-based approach to name a few), are one of the straightforward solutions to avoid concerned challenges.

Among these alternatives, membrane-based technology, a fast growing and environmental-friendly separation process provides reliable solutions for CCS due to the low energy consumption linked to membranes, operation flexibility and simplicity, good stability, easy control and scale-up. Typically, polymeric membranes are used for gas separation, thanks to a solution-diffusion mechanism, are bounded by their stability at the operating conditions and separation performance, known as the Robeson upper bound [29]. However, MMMs with specific fillers (such as MOFs), are considered as a possible solution due to their improved stability and decent separation performance. [37]. In fact, the incorporated fillers favor permeability of the desired component in the mixture, through the modification of the diffusivity and solubility properties of the membranes. In consequence, permeability of gases through MMMs depends on intrinsic compatibility between polymer-filler pair. As a result, interest on MMMs with various MOFs increasing over years, towards CO_2 separation application. Now a days, ZIFs have been widely been used as additives in MMMs to improve their separation properties [141,142], examples include, with ZIF-94 [69,71], ZIF-8 [92,143] , ZIF-67 [144], ZIF-300 [142] as fillers. Unfortunately, synthesis of different MOFs are associated with discharge of lots of chemical. It is worthy to mention that, searching a solution for grean-house effect is supposed to become a reason for chemical hazard to the environment.

For instance, in a typical ZIF-94 synthesis, if the crystallization yield is below 100 %, the mother liquor contains unreacted metal and ligand, together with the solvent (e.g. MeOH). All these reagents are expensive to replace and usually are discarded after the synthesis. Hence, it is important to investigate a reagent recycling on the synthesis of MOFs considering environmental and economic reasons [145,146]. Few works have been developed dealing with this issue with the example of ZIF-8 [146–149]. In these research articles, the attempts to synthesize ZIF-8 from recycled mother liquors are related to the use of sodium hydroxide and potassium hydroxide as well as ammonia as deprotonators to initiate the nucleation and to favor the crystal growth [150,151].

The objective of this chapter is to synthesize ZIF-94 from recycled mother liquors emphasizing the influence of different parameters (such as pH or temperature)

on the final MOF structure, and to use it as a filler to be incorporated in Pebax® MH 1657 for post-combustion CO_2 capture. The effects of recycled MOF loading and polymer concentration in the casting solution were investigated, as well as the influence of using a filler synthesized from the mother liquor and by the original method.

4.2 Experimental procedure

4.2.1 Materials

Zinc acetate dihydrate and 4-methyl-5-imidazolecarboxaldehyde were purchased from Acros Chemicals (98% and 99% purity, respectively). Methanol (99.8%) was obtained from Honeywell, and anhydrous tetrahydrofuran (THF, ≥99.9%) was obtained from Sigma-Aldrich. Sodium hydroxide (NaOH pellets, ACS grade) was purchased from Carlo Erba. Absolute ethanol was purchased from Gilca, Spain. For the membrane fabrication, commercially available Pebax® MH 1657 was kindly provided by Arkema, France.

4.2.2 Methodology

4.2.2.1. Synthesis of ZIF-94 crystals from recycled mother liquors

After the synthesis of ZIF-94, the mother liquor was separated by centrifugation from the nanocrystals to be used in the subsequent synthesis of ZIF-94. The recycling procedure is illustrated in section 3.1.2 in chapter 3. Such procedure resulted in the formation of products A.1 – A.5 for the pH control and product B for the temperature control. **Figure 4.1** shows a scheme of different synthesis procedures aiming at ZIF-94 pure phase conducted in this study.

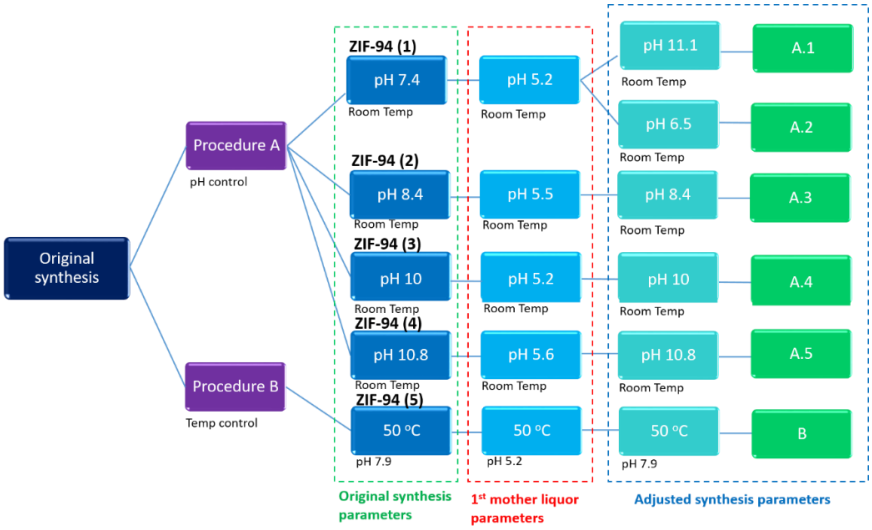

Figure 4.1. Schematic representation of all syntheses carried out. The washing was performed in refluxing MeOH followed by drying at room temperature.

4.2.2.2 Fabrication of mixed matrix membranes (MMMs)

MMMs were fabricated with two different polymer concentrations: 6 wt.% and 9 wt.% Pebax® MH 1657 as a matrix (i.e. the polymer concentration in the solvent as a casting solution) and various ZIF-94 doses (5 - 20 wt.%). The MMMs were prepared following a two-step process [152]. First, 6 wt.% and 9 wt.% Pebax® MH 1657 (of total

weight of 3 g (polymer + solvent)) was dissolved in EtOH/water (70/30 (v/v)) by stirring under reflux for 1 h. Afterwards, the dissolved polymer was used to cast pristine polymeric membranes. In case of MMMs fabrication process, ZIF-94 was dispersed in the dissolved polymer. The required amount of filler (5 - 25 wt.%) which was calculated against the amount of Pebax® MH 1657 being used, was dispersed in 1.5 mL of EtOH/water (70/30) by repeated sonication and stirring at RT for 1 h. Next, both dispersions were mixed and kept stirred at RT overnight. In the extension of the fabrication process, the solution was poured on a Petri dish. At the end of the process, the membranes were dried for overnight in a top-drilled box under a solvent-saturated atmosphere at environmental conditions.

4.3 Results and discussion

4.3.1 Characterization of ZIF-94 from the original synthesis

TEM analysis confirmed homogeneous distribution of the synthesized ZIF-94 (1) particles represented in **Figure 4.2 (A)**, which was synthesized following prescribed method by Johnson et al [153]**.** The reaction (reaction 3.1) yield was approximately 76% (following equation Equation 3.3) BET specific surface area (SSA) is 317 m^2/g (**Table 4.1**).

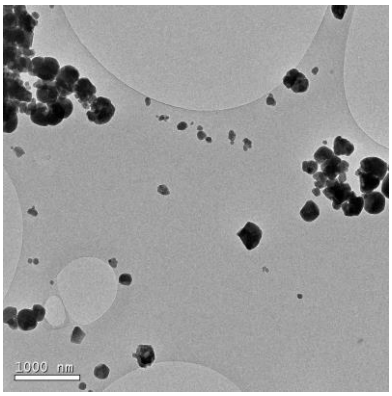

Figure 4.2. TEM image of synthesized ZIF-94 (1)

Table 4.1. Yield, BET surface area and average particle size of the ZIF-94 synthesized by the original synthesis according to Johnson et al.

Material	Yield (%)	BET SSA (m^2/g)	Average particle size (nm)
ZIF-94 (1)	76	317	173 ± 68

X-ray diffraction pattern allowed to determine the crystallinity, purity of the product and its crystal phases. **Figure 4.3** represents the XRD pattern of the synthesized ZIF-94 where relative intensities and peak positions match well with published crystallographic data corresponding to ZIF-8 (since the two MOFs share the same SOD structure)[50,71,154]. The N_2 adsorption-desorption analysis provides BET specific surface area (SSA) that lies in between 424 - 480 m^2/g for ZIF-94, according to the literature [50,66]. Synthesized ZIF-94 produced BET SSA of 464 m^2/g (see Table 4.2).

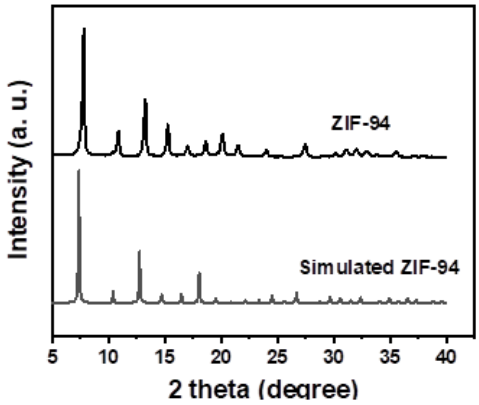

Figure 4.3. Comparison of XRD pattern of synthesized ZIF-94 with simulated ZIF-94

4.3.2. Characterization of ZIF-94 synthesized from recycled mother liquors

4.3.2.1. pH control and modification (Procedure A)

Five different syntheses were conducted in procedure A where the pH was monitored and controlled (see **Figure 4.4** for details of each procedure). In the first case, the initial pH of the original synthesis was equal to 7.4 (ZIF-94 (1) – see **Figure 4.1**), which decreased down to 5.2 after 16 h of the reaction due to the formation of acetic acid according to Equation 3.1. All the reactions were carried out a room temperature. As it was mentioned above, NaOH was added to control the influence of pH on the ZIF-94 nanocrystals morphology and size. Two pH values were obtained: 11.1 resulting in product A.1 and 6.5 resulting in product A.2. The obtained products were washed in MeOH under reflux during 1.5 h and dried at RT.

As it can be observed in **Figure 4.4 (A)**, XRD patterns of products A.1 and A.2 match well with the XRD pattern of the ZIF-94 obtained in the original synthesis. On the other hand, thermogravimetric analysis (**Figure 4.4 (B)**) shows two weight losses between 35 °C and 180 °C corresponding to the removal of MeOH and THF used in the synthesis. Besides, neither the ZIF-94 obtained from the original synthesis nor products A.1 and A.2 have organic ligand trapped in the structural pores. The yield of the reactions was calculated according to Equation 3.3 being higher for product A.2 (53.8 %) than for product A.1 (41.5 %), although in both cases, the yield was lower compared to the ZIF-94 from the original synthesis (71.4 %). Moreover, the BET SSA decreased slightly for both products being equal to 417 m^2/g and 428 m^2/g for product A.1 and A.2, respectively (see **Table 4.2**), in comparison to that of the original synthesis (464 m^2/g). Nevertheless, the values are still within those reported in literature (415 - 480 m^2/g) [50,66]. The average particle sizes of both products were determined from TEM images by measuring approximately 80 particles of each sample and calculating the average value. In case of product A.1, its particle size was 49 ± 11 nm, whereas for product A.2 it was equal to 34 ± 16 nm. In addition, product A.1 was characterized by higher particle agglomeration than product A.2, and large particles coexisted with typical nanoparticles. The calculations done with Scherrer equation (Equation 3.2) revealed that the particle sizes should be in the range of 40-42 nm which reinforced the

idea about the small formation of ZIF-94 agglomerates in the case of product A.1 in line with the hysteresis loops observed in the adsorption and desorption isotherms.

Next, the reactions with pH equal to 8.4, 10 and 10.8 of the original syntheses (labelled as ZIF-94 (2), ZIF-94 (3) and ZIF-94 (4)) were conducted to obtain their corresponding products (A.3, A.4 and A.5, respectively). The washing and drying procedures were the same as it was described in case of products A.1 and A.2. As **Figure 4.4 (C)** shows, the XRD patterns of all synthesized materials are consisted with the ZIF-94 simulated pattern. The decomposition temperature of all materials agrees with that of ZIF-94 (~270 °C) and no weight loss due to the organic ligand trapped in the pores is observed (**Figure 4.4 (D)**). Nonetheless, two weight losses appear between 35 °C and 180 °C due to the removal of MeOH and THF used in the synthesis as it was in case of products A.1 and A.2.

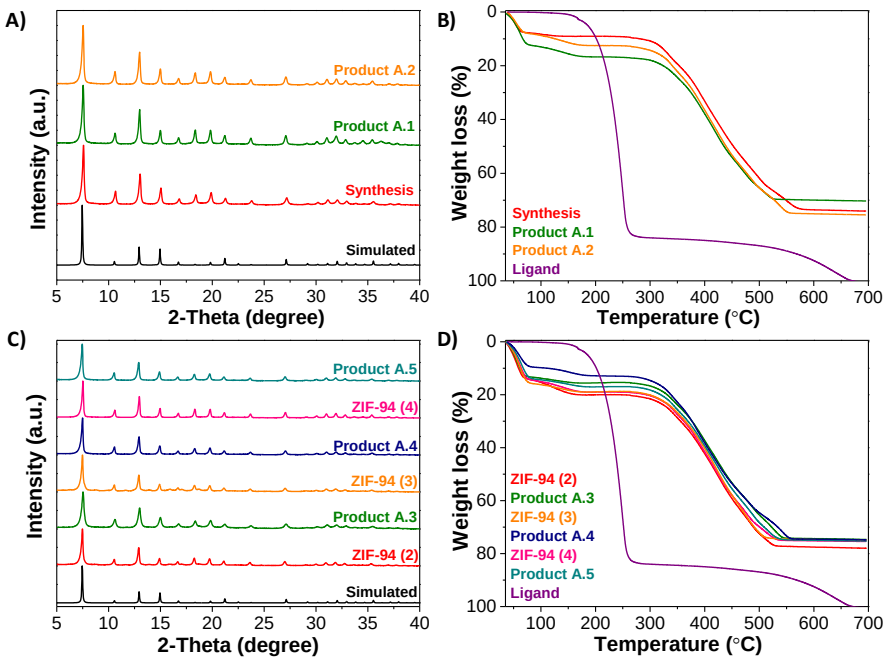

Figure 4.4. ZIF-94 and products A.1 and A.2: A) XRD patterns, and B) TGA curves. ZIF-94 (2), product A.3, ZIF-94 (3), product A.4, ZIF-94 (4) and product A.5: A) XRD pattern; B) TGA curves.

As it is shown in **Table 4.2**, the highest yield was obtained when the initial synthesis and the synthesis from recycled mother liquor were performed at pH=8.4 (67.5 %, Product A.3). However, their BET SSA values were the smallest compared to those of the other samples, these values being still in the range of those published in the literature (415-480 m^2/g). Regarding the samples obtained at pH=10 (product A.4) and 10.8 (product A.5), their yields (60.5 % and 61.8 %, respectively) were slightly lower than the one obtained in the original synthesis (71.4 %). The same happens with their corresponding BET SSA values. **Figure 4.5** shows the TEM images of the materials obtained at different pH values and their corresponding products from the recycled mother liquors (products A.3-A.5). As can be observed, ZIF-94 synthesized at pH=10.8 has larger particle size in comparison to the previous samples. Moreover, it can also be

seen that agglomerates of particles appear in all cases, in line with the calculations done with the Scherrer equation (30-50 nm).

Table 4.2. Synthesis pH, yield, BET SSA and average particle size of ZIF-94 obtained from electronic microscopy images, product A.1, product A.2, ZIF-94 (2), product A.3, ZIF-94 (3), product A.4, ZIF-94 (4) and product A.5 obtained at room temperature. ZIF-94 and ZIF-94 (2) to (4) correspond to fresh reagents syntheses, while Products A.1 to A.5 used recycled mother liquors.

Sample code	**Synthesis pH**	**Yield (%)**	**BET specific surface area (m^2/g)**	**Average particle diameter (nm)**
ZIF-94	7.4	71.4	464	53±14
Product A.1	11.1	41.5	417	49±11
Product A.2	6.5	53.8	428	34±16
ZIF-94 (2)	8.4	84.6	405	37±8
Product A.3		67.5	423	44±34
ZIF-94 (3)	10	77.4	463	43±10
Product A.4		60.5	483	34±14
ZIF-94 (4)	10.8	77.0	442	199±84
Product A.5		61.8	506	36±8

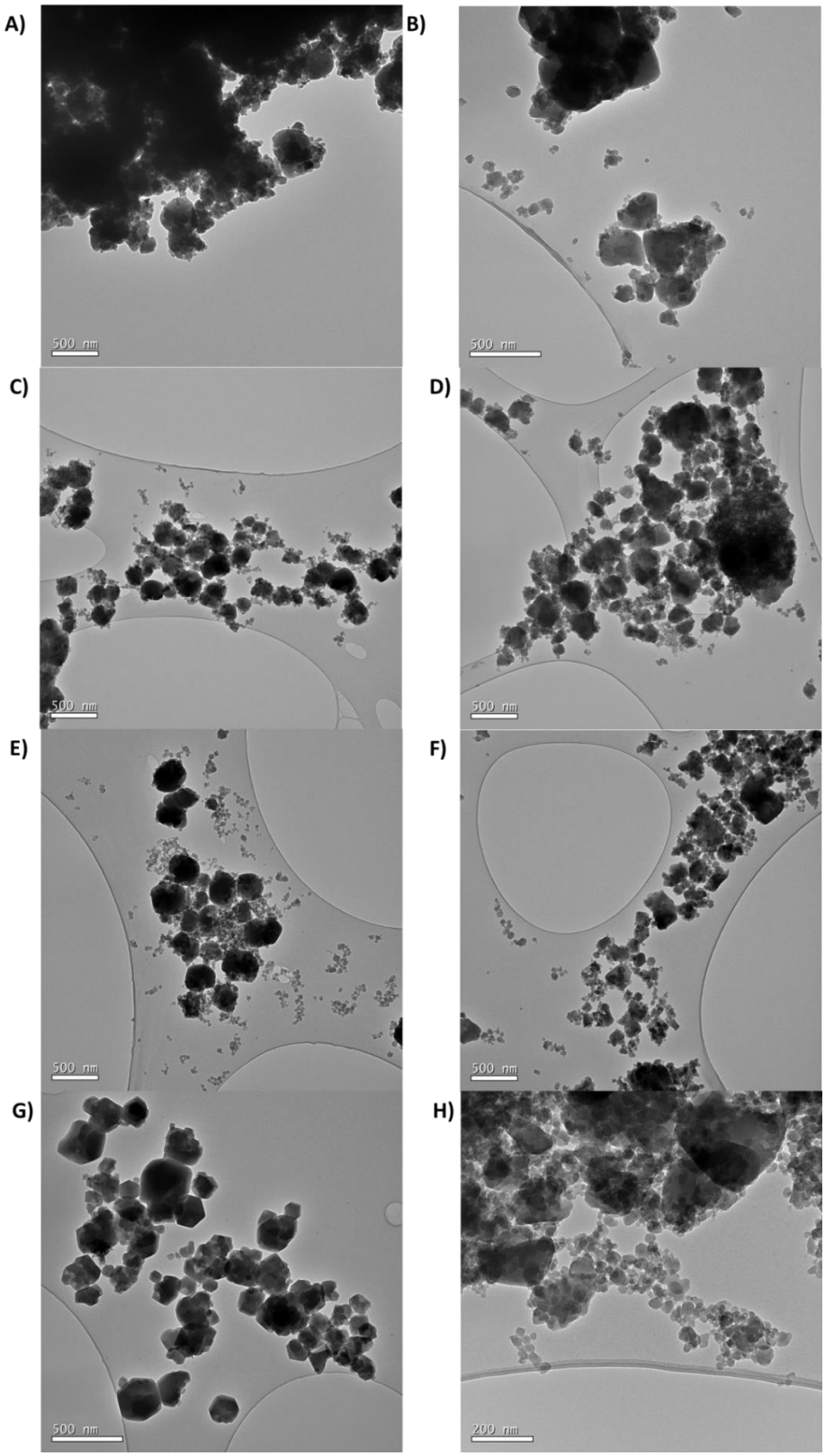

Figure 4.5. TEM image of A) Product A.1, B) Product A.2, C) ZIF-94 (2), D) Product A.3, E) ZIF-94 (3), F) Product A.4, G) ZIF-94 (4) and H) Product A.5

4.3.3.2. Temperature control at 50 °C (Procedure B)

As has been said above, one synthesis (ZIF-94 (5)) and its recycling were carried out at 50 °C as a way to investigate the effect of the temperature on the properties of ZIF-94 obtained (Product B). The initial pH of the original synthesis was equal to 7.9 and after 16 h of the reaction it decreased down to 5.2 due to the formation of acetic acid. Next, the pH of the mother liquor after the addition of the consumed reactants was increased up to 7.9. **Figure 4.6** shows the XRD pattern and the TGA curves of the ZIF-94 synthesized at 50 °C and the product B obtained from the recycled mother liquor of this synthesis. As can be seen, the peak positions and the intensities of both materials match well with those of the simulated pattern of ZIF-94. Besides, TGA curves do not present any weight loss due to the presence of organic ligand trapped in the pores indicating that the material is well activated.

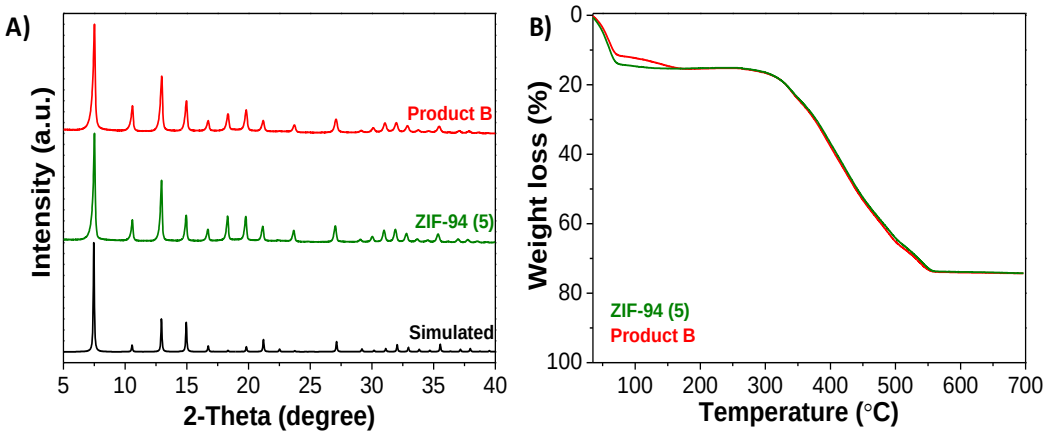

Figure 4.6. ZIF-94 (5) and product B: A) XRD patterns; B) TGA curves.

Table 4.3 shows the characteristics of the materials obtained when both the initial synthesis and the recycled mother liquor were carried out at 50 °C. The yield obtained was higher than the one obtained in the original synthesis (see Table 4.1), whereas BET surface area was closer to the original ZIF-94 (464 m^2/g). This allows to think that this reaction is favored with temperature. The average particle size (180 ± 73 nm) of the original synthesis (ZIF-94 (5)) is much larger than in case of the recycled Product B (41±8 nm) shown in **Table 4.3** and **Figure 4.7**. According to the Scherrer equation, the crystal size of these samples should be in the 41-49 nm range, suggesting the existence of ZIF-94 agglomerates. However, in both cases the yield is higher than in the synthesis of ZIF-94 and it's recycle.

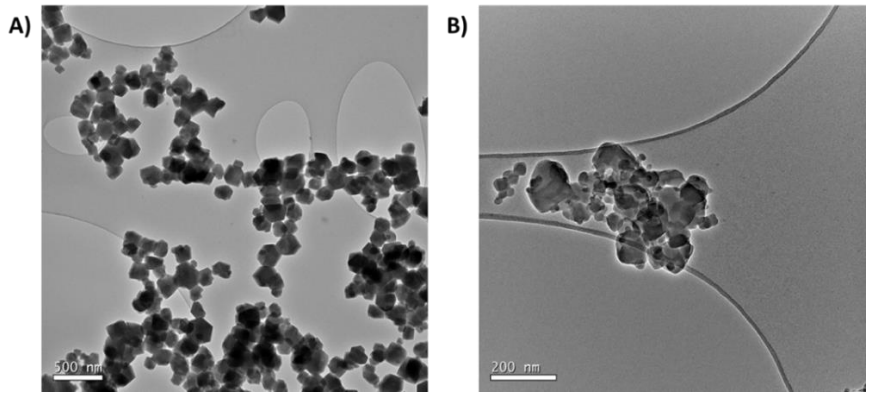

Figure 4.7. TEM image of A) ZIF-94 (5) and B) Product B

Table 4.3. Yield, BET SSA and average particle size of ZIF-94 (5) and product B obtained at 50 ºC.

Sample code	Synthesis pH	Yield (%)	BET specific surface area (SSA) (m^2/g)	Average particle diameter (nm)
ZIF-94 (5)	7.9	78.9	457	180 ± 73
Product B	7.9	62.7	468	41 ± 8

For the testing of the synthesized MOFs and the improvement in membrane performance for gas separation after their incorporation in MMMs, four samples were selected: i) freshly synthesized ZIF-94 according to Johnson et al. [153] and particle size of 173 ± 78 nm, ii) ZIF-94 (3) at pH 10, RT and particle size of 41 ± 8 nm, iii) ZIF-94 (5) at pH 7.9, 50 ºC and particle size of 180 ± 73 nm, and iv) Product B synthesized from the recycled ZIF-94 (5) with particle size of 41 ± 8 nm. The reason for such selection was to examine the effect of different particle size, the influence of the recycled or freshly synthesized MOF and the effect of the particles synthesized either at higher pH or higher temperature on the final performance of the membrane. All the details of the samples chosen for the incorporation in the MMMs are presented in **Table 4.4**.

Table 4.4. Different types of fillers used in MMMs for the gas separation analysis

Sample code	Properties of MOF	BET SSA (m^2/g)	Average particle diameter (nm)
ZIF-94 (1)	Original 1st synthesis	317	173 ± 68
ZIF-94 (3)	Fresh synthesis	463	43 ± 10
ZIF-94 (5)	Fresh synthesis	457	180 ±73
Product B	Recycled from ZIF-94 (5)	468	41 ± 8

4.3.3 Characterization of MMMs

The fabricated membranes were thoroughly characterized for homogenous MOF distribution (**Figure 4.8 (A-C)**), lack of defects, cracks and non-selective gaps. **Figures 4.8 (A)** shows, as an example, an SEM image of one the MMMs: 9 wt. % Pebax® MH 1657 with 15 wt. % ZIF-94 (1) (i.e. the MOF obtained from fresh reactants,

see **Table 4.3**). ZIF-94 was homogenously distributed across the polymeric matrix, no visible defects can be appreciated ensuring well fabricated membranes. TGA analysis of three different MMMs was also investigated and compared to a bare polymeric membrane (shown in **Figure 4.8 (B)**. As it is shown in **Figure 4.8 (B)**, it is clearly observed that thermal behavior of MMM is different compared to that of bare polymeric membrane. Interaction between MOF and polymer matrix is the reason for such change in behavior. MMMs are quite stable up to 270 ^{o}C with no significant weight loss. Next, they start initial degradation, which continues up to 380 ^{o}C where they undergo sharp degradation of polymer matrix which continues until 410 ^{o}C resulting in a total loss of 70 % of the initial weight. Afterwards, they undergo comparative slow weight loss resulted from degradation of incorporated ZIF-94. Finally, weight loss ends at 570 ^{o}C with a residue of 5 % of its initial weight. This residue corresponds to ZnO generated upon the thermal oxidation of the MOF embedded in the MMM.

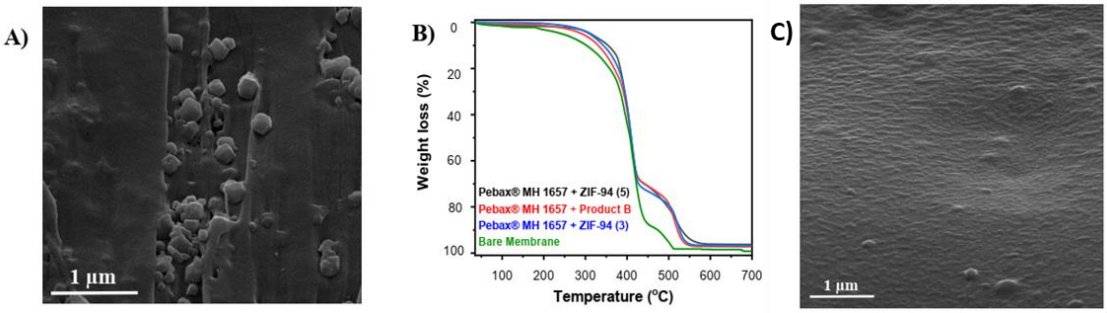

Figure 4.8. A) SEM imaging of a MMM 9 wt.% Pebax® MH 1657 with 15 wt% ZIF-94 (1) as a filler cross section, B) TGA analysis of the bare Pebax® MH 1657 membrane and a comparison to MMMs with different types of fillers and C) cross section image of bare membrane

4.3.4 CO_2 separation performance of MMMs

For membrane performance analysis, we focused on the four different types of fillers described in **Table 4.4**. Filler types ZIF-94 (1) and ZIF-94 (5) have very similar particle size but differing in BET SSA, hence the comparison of these two fillers will reveal the effect of BET SSA on membrane performance for CO_2 capture. ZIF-94 (product B) is a filler synthesized from the waste mother liquor of ZIF-94 (5). In this case, gas separation performance comparison between ZIF-94 (5) and Product B will reveal applicability of recycled ZIF-94 and potential differences in membrane performance. ZIF-94 (3) was MOF synthesized at higher pH (10) which will reveal information of the influence of the pH on membrane performance.

4.3.4.1 Polymer-matrix optimization: ZIF-94 original synthesis

MMMs were fabricated with two different polymer concentrations: 6 wt.% and 9 wt.% Pebax® MH 1657 as a matrix (i.e. the polymer concentration in the solvent as a casting solution) and various ZIF-94 (1) doses (5 - 20 wt.%). These MMMs were analyzed for their performance over CO_2/N_2 mixture separation and compared with bare polymer membrane where error was calculated for two consecutive measurements with different membrane samples. The membrane thickness was between 33 – 45 µm, and the CO_2 permeability as well as CO_2/N_2 selectivity for both polymer concentrations and different ZIF-94 loadings are presented in **Table 4.5** and **Figure 4.9**. Focusing firstly

on the 6 wt. % Pebax® MH 1657, we have noticed that permeability increased by 200 % (for MMM with 10 wt.% fillers) compared to bare membrane due to the addition of ZIF-94 (1) filler (increment was calculated from Equation 4.1). However, CO_2/N_2 selectivity was slightly lower compared to bare membrane for all compositions of 6 wt. % Pebax® MH 1657 MMMs which implies there is a trade-off between both parameters.

$$Improvement\ (\%) = \frac{\text{performance of a membrane} - \text{performance of bare membrane}}{\text{performance of bare membrane}} \times 100 \quad (Equation\ 4.1)$$

Moving to 9 wt. % Pebax® MH 1657, it was found that selectivity of this bare membrane decreased significantly compared to 6 wt. % bare membrane (see **Figure 4.9** and **Table 4.5**). This trend is also reported by Martínez-Izquierdo et al. The highest CO_2/N_2 selectivity of 36 ± 7 and the permeability of 137 ± 31 Barrer was obtained for 9 wt. % Pebax® MH 1657 based MMMs and 10 wt. % loading of ZIF-94 (1) (highlighted in a red frame). Comparison with bare membrane indicates that 10 wt. % ZIF-94 (1) dose in the MMM increases selectivity and permeability by 71 % and 80 %, respectively. Further increase in MOF dose was found to decrease selectivity (CO_2/N_2) down to 26 ± 7 for 20 wt. % filler content whereas the permeance did not change significantly (128 ± 27 Barrer). 15 wt. % filler in 9 wt. % polymer is another interesting composition which yields a mean permeability of 96 ± 11 Barrer with a CO_2/N_2 selectivity of 31 ± 2. It is also indicated that, inclusion of fillers (for all compositions) in the polymer matrix has produced considerable increase of both permeability and CO_2/N_2 selectivity by 120 % and 105 %, respectively. This justifies that 9 wt. % polymer matrix can be considered optimum composition to investigate the other 3 different types of ZIF-94. ZIF-94 improved the MMM performance due to its microporosity with limiting pore diameter of ca. 0.26 nm [155], favoring the diffusion of the smallest CO_2 molecule (0.33 nm of kinetic diameter versus 0.364 nm for N_2) in the mixture [156]. This is complemented with the improved CO_2 affinity of the MOF due to its aldehyde functionalized ligand [122,157].

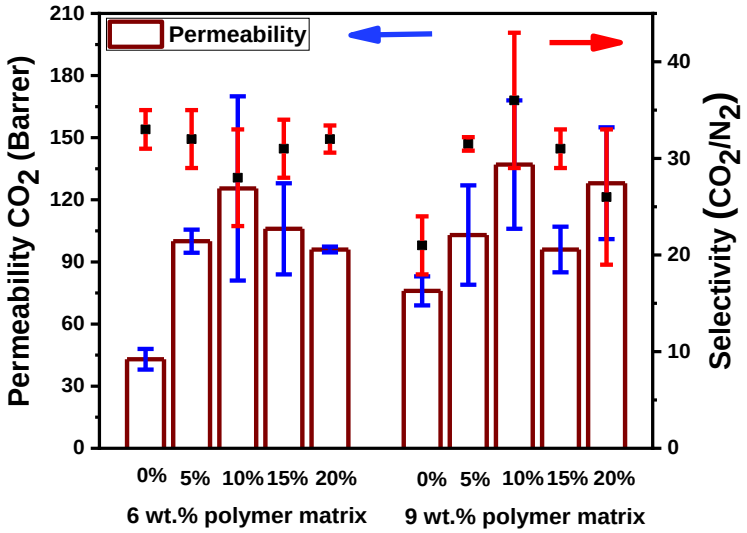

Figure 4.9. Performance of MMMs (6 wt.% and 9 wt.% Pebax® MH 1657 + various ZIF-94 (1) loadings).

Table 4.5. Summary of the CO_2 capture performance of 6 wt.% matrix based MMMs with ZIF-94 (1)

Polymer (wt.%)	MOFs loading (wt.%)	Average Membrane thickness (µm)	Permeability (Barrer)	Selectivity (CO_2/N_2)
	0	33 ± 7	43 ± 5	33 ± 2
	5	36 ± 5	100 ± 6	32 ± 3
6	10	38 ± 8	126 ± 44	28 ± 5
	15	41 ± 7	106 ± 22	31 ± 3
	20	45 ± 3	96 ± 2	32 ± 2
	0	40 ± 5	76 ± 7	21 ± 2
	5	42 ± 3	103 ± 24	32 ± 1
9	10	45 ± 4	137 ± 31	36 ± 7
	15	46 ± 8	96 ± 11	31 ± 2
	20	46 ± 6	128 ± 27	26 ± 7

4.3.4.2 Effect of different ZIF-94 fillers on the membrane performance

Further investigation on the optimum matrix composition (9 wt. % polymer matrix) was carried out for other three different types of MOFs: (ZIF-94 (5), Product B and ZIF-94 (3)), with loadings variation of 5, 10 and 15 wt.% which are represented in **Figure 4.10**. Investigation on ZIF-94 in 9 wt. % polymer based MMMs represents that CO_2 permeability increases for all compositions of MMMs (for all 4 different ZIF-94 fillers) compared to bare polymeric membrane. As expected, 10 wt. % of ZIF-94 (5) loading resulted in the highest selectivity of 32 ± 2 and permeability of 125 ± 12 Barrer

which represent 52 % and 65 % increments, respectively, when compared with bare membrane. Moreover, the conducted measurements showed a decreasing tendency for both selectivity and permeability on further increase of the filler in MMMs. The investigation on Product B, which was recycled from waste mother liquor of ZIF-94 (5), revealed that permeability can be improved compared to bare membrane for all composition filler dose being used but CO_2/N_2 selectivity surpassed the bare membrane only in case of 10 wt. % filler dose. A similar response was found for ZIF-94 (3) when it was incorporated inside MMMs and examined for CO_2 analysis. From the discussion so far, it can be considered that 10 wt. % filler is the optimum loading for 9 wt. % Pebax® MH 1657 based MMMs. Robeson upper bound plot is presented in **Figure 4.11** with performance of the MMMs under investigation. Additionally, gas separation performances of the membranes are listed in **Table 4.6**

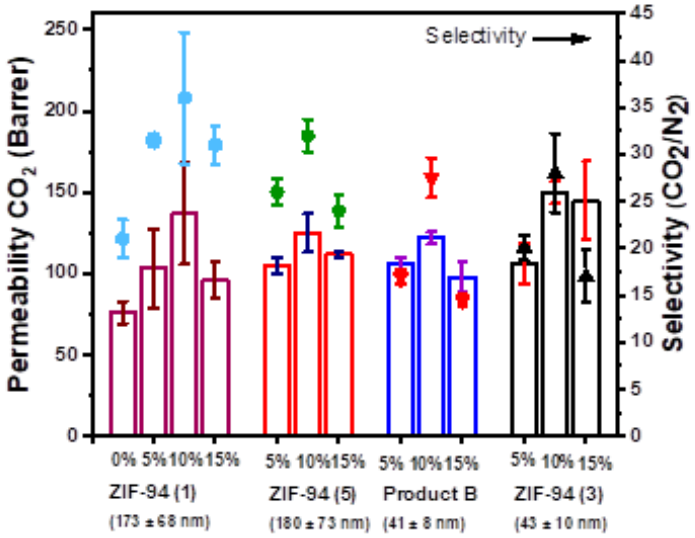

Figure 4.10. Performance of MMMs at 9 wt.% of Pebax® MH 1657 with different types of ZIF-94.

Table 4.6: Performance of fabricated MMMs with 9% polymer matrix in different conditions

ZIF-94 used	ZIF-94 dose in 9 wt.% Pebax® MH 1657	Membrane thickness (µm)	P_{CO2} (Barrer)	Selectivity (CO_2/N_2)
	0	40	76 ± 7	21 ± 2
	5	42	103 ± 24	32 ± 1
ZIF-94 (1)	10	45	137 ± 31	36 ± 7
	15	46	96 ± 11	31 ± 2
	5	38	108 ± 5	26 ± 1.4
ZIF-94 (5)	10	42	125 ± 12	32 ± 1.7
	15	45	112 ± 2	24 ± 1.7
	5	36	106 ± 3.5	17 ± 0.7
Product B	10	37	122 ± 3.5	28 ± 2
	15	39	98 ± 9	15 ± 0.7
	5	34	106 ± 12	20 ± 1
ZIF-94 (3)	10	47	150 ± 4	28 ± 2
	15	44	145 ± 24	17 ± 3

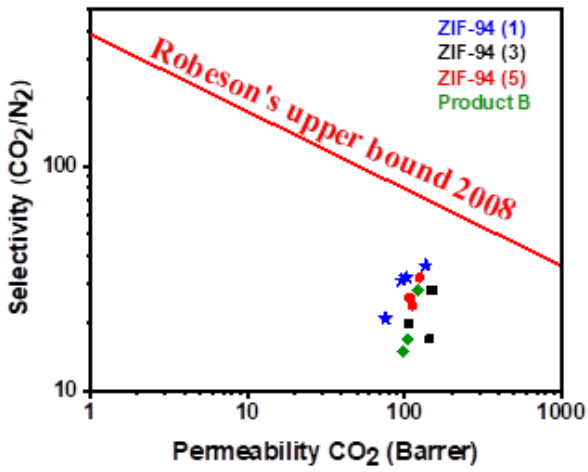

Figure 4.11. Robeson plot and findings of this research

Comparison of two different fillers (ZIF-94 (1) and ZIF-94 (5)) possessing similar average particle sizes but different BET SSA (317 m^2/g and 457 m^2/g, respectively, see **Table 4.4**) demonstrated the effect of this textural parameter on the CO_2 capture. It is clearly evidenced that both fillers produced different responses when incorporated into MMMs at optimum concentration (i.e. 10 wt.%). More importantly,

there were improvements by 10 % and 11 % for permeability and selectivity, respectively, due to higher BET SSA. In the further observation, recycled ZIF-94 (i.e. Product B) with mean particle size of 41 ± 8 nm and fresh ZIF-94 (5) possessing an average particle size of 180 ± 73 nm produced different performance on CO_2 separation (see **Figure 4.12**). Best CO_2/N_2 selectivity of freshly synthesized filler at 10 wt. % filler loading is 32 ± 2 which is 14 % higher than in case of recycled Product B, being equal to 28 ± 2. Whereas selectivity for 5 wt. % and 15 wt. % loadings are significantly lower than that of the bare polymer membrane. This allows one to partially conclude that the recycled mother liquor filler may improve, at the best optimum loading, the MMM performance of the bare polymer. Nonetheless, the particle size shows an important effect on the MMM performance which has been already reported for MMMs containing ZIF-8 where it was explained that, fillers agglomeration tendency may prevent the smallest MOFs nanoparticles to constitute the best MMMs [134]. In addition, this suggests that additional synthesis work is needed to control the particle size of ZIF-94 when prepared from recycled mother liquors.

A comparison between recycled and fresh MOF pairs: Product B and ZIF-94 (3) with almost identical particle size (41 ± 8 nm nm and 43 ± 10, respectively) was conducted (see **Figure 4.10**). Only optimum filler composition (that is 10 wt. %) surpasses the limit of bare membranes in terms of both selectivity and permeability. Confirming the suitability of mother liquor recycle to obtain ZIF-94 as filler for MMMs, both fillers produce similar selectivity of 28, whereas freshly synthesized ZIF-94 (3) showed 23 % additional increase in permeability (that is 150 ± 6 Barrer) compared to recycled Product B which resulted in 122 ± 4 Barrer. Comparison of all the fillers at the optimum concentration of 10 wt. % is represented in **Figure 4.12**. It is evidenced that higher selectivity is attainable for fillers having bigger particle size. Whereas smaller particles produce higher permeability with some extend of sacrificial selectivity. A maximum increase in permeability (100 % increase) has been found for ZIF-94 (3) which has particle size of 43 ± 10 nm. **Figure 4.12** also suggests better reproducibility in the separation performance for the MMM prepared from the pH-controlled synthesis as compared to the parent ZIF-94 synthesis. On the other hand, highest increment in average selectivity (71 %) was obtained for ZIF-94 (1) which possesses average particle size of 173 ± 68 nm. Recycled Product B also comply with the performance of freshly synthesized ZIF-94 (3). This confirms the reuse of waste mother liquor as a green practice to reduce the chemical loss in the MOF synthesis and thus minimize the impact of the MMM preparation on the environment.

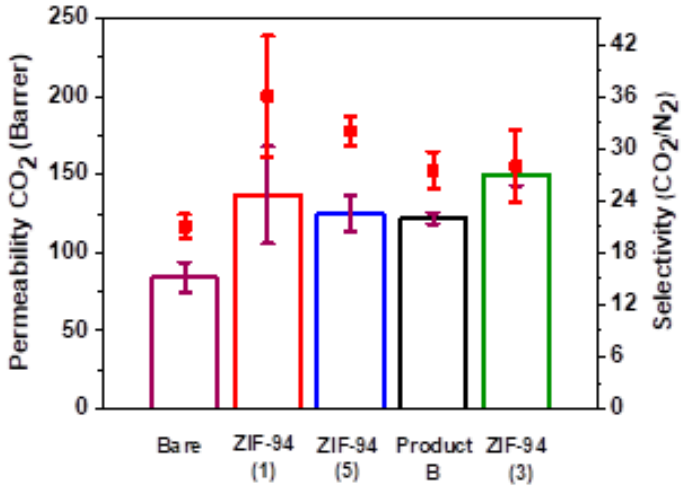

Figure 4.12. Effect of different ZIF-94 fillers for MMMs 9 wt.% Pebax® MH 1657 on CO_2 capture at the optimum filler composition (10 wt.%).

Moreover, it was noticed that there is a correlation between membrane thickness and permeability. Permeability through MMMs is linearly proportional to the membrane thickness. Produced results also found to be reproducible with some error. According to the literature, Selyanchin et. al has reported that CO_2 permeability through bare Pebax® MH 1657 membrane increases up to 140 Barrer at 80 µm membrane thickness. It was reported by the authors that further increase of membrane thickness reduces CO_2 permeability down to 110 Barrer for 128 µm thickness [158]. In this research, MMMs with thickness of 37 µm and 47 µm results CO_2 permeability of 122 Barrer and 150 Barrer respectively.

4.4 Conclusions

In this work, the initial synthesis and methodology developed to produce ZIF-94 nanocrystals from the recycling of its mother liquors was carried out. Two main synthesis parameters were modified: pH and temperature. In all the conditions investigated pure, crystalline ZIF-94 was obtained. The most promising results, considering crystallinity, yield of the reaction and BET specific surface area, were obtained when both, the initial synthesis (BET: 463 m^2/g, particle size: 43 nm) and the mother liquor (Product A.4; BET: 483 m^2/g; particle size: 34 nm), were carried out at pH = 10.

After the successful synthesis of ZIF-94 from the recycled mother liquors, the fabrication of a defect-free mixed matrix membrane with Pebax® MH 1657 as a continues phase and synthesized ZIF-94 as a dispersed phase was successfully conducted. ZIF-94 fillers obtained at different conditions with different particle sizes and slightly different BET specific surface area values were incorporated inside the polymeric membrane and the resulted MMMs were applied for the CO_2/N_2 separation. The optimum composition of MMMs was found to be 9 wt. % Pebax® MH 1657 and 10 wt. % ZIF-94 loading. ZIF-94 of ca. 180 nm in particle size was found to be the best filler in terms of selectivity 36 ± 7 and permeability 137 ± 31 Barrer, whereas ZIF-94 of ca. 40 nm produced maximum permeability of 150 ± 7 Barrer (with selectivity of 28 ± 4). This suggests that particle agglomeration of the filler may affect the separation performance, in line with previous reports with analogous ZIFs. In conclusion, additional synthesis improvement is needed to control the particle size of ZIF-94 when preparing it from recycled mother liquors, and fabricated membranes were found to be stable at the operating condition since no damage, cracks or non-selective gaps in the membrane was observed.

Chapter 5: Study on the recycling of zeolitic imidazolate frameworks and polymer Pebax® MH 1657 from their mixed matrix membranes applied to CO_2 capture

Outlines

Reproduced from "M. Rafiul Hasan, A. Moriones, M. Malankowska, J. Coronas, Study on the recycling of zeolitic imidazolate frameworks and polymer Pebax® MH 1657 from their mixed matrix membranes applied to CO_2 capture, Sep. Purif. Technol. 304 (2023). https://doi.org/10.1016/j.seppur.2022.122355".

5.1 Introduction

Energy demands of the current world is mostly satisfied with fossil fuels, which results in global warming and other unpredictable climatic changes [138]. Therefore, it was agreed to search for either green energy sources or capturing CO_2 from pre or post-combustion gases or from industry exhaust (such as those related to cement and stainless-steel plants) to limit the global temperature rise below 2 °C (as per Paris conference in 2015 [140] and confirmed at the Glasgow COP26 in 2021) [159]. Green hydrogen fuel, hydrothermal, wind, solar and uranium based atomic energy are the possible alternative solutions to fossil fuels for power generation but they are constrained by either affordability or geographical location. Alternatively, CCS from flue gas is a feasible and straightforward solution over persisting concern risen from burning of fossil fuels.

Membrane separation especially with MMMs is expected to replace conventional energy-intensive CO_2 separation technologies, since they are characterized by high cost of operation [125,146]. In general, CO_2 permeability and selectivity of a MMMs higher than that of pristine polymers. However, the CO_2 separation performance depends on the intrinsic compatibility between polymer and filler. Since ZIFs are interesting for the fabrication of MMMs for CO_2 separation application, the facile and scalable production of different ZIFs (ZIF-8, ZIF-67, ZIF-71 and ZIF-94) has been reported to make them cost effective and available for MMMs [119,131,147–149]. Pan et al. reported a green synthesis of ZIF-8 from aqueous solvent [148], whereas others have recycled mother liquors from the syntheses of ZIF-7 [136], ZIF-8 [37,136], ZIF-67 [136], ZIF-L [136], ZIF-94 [150], etc. to make the process sustainable. Moreover, Hasan et al. have reported a sustainable synthesis of ZIF-94 from mother liquor applied to fabricate MMMs with Pebax® MH 1657 polymer matrix which shows good CO_2 separation performance [150].

Although many attempts have been found in the literature to make the synthesis of MOFs sustainable, yet none have reported the recycling of MMMs to extract MOFs and polymer matrix to study their reusability. Recycling of MMMs shows many advantages, such as: i) making membranes economically feasible, since extracted materials can be reused (either in membrane or in other purposes), which leads to ii) reducing loss and cost of chemicals, and finally iii) ensuring environmentally sustainable membranes, due to less waste disposition. Waste membrane can be defined as: if the membrane significantly loses its selectivity and permeability over time, or it is contaminated by H_2S or other impurities while purifying flue gas streams or in any other application, or it is incompatible with the working condition over time of using. Major component of MMM is a polymer, which is another environmental concern over CO_2 release, due to its adverse effect on soil (reducing soil fertility, crop productivity, water penetration etc.) and water (causing nano, micro and macro plastic pollution, it enters into the food chain and reduces aqueous animals reproductivity, etc.) [151,152]. Understanding all the consequences of polymer waste to the earth, more emphasis should be given to study the recyclability of polymer-based membranes before they are adopted for large scale CO_2 separation application. The objectives of this study are

firstly to recycle ZIF-94 and polymer Pebax® MH 1657 matrix from their corresponding MMMs, and secondly to re-incorporate them into MMMs demonstrating efficient CO_2/N_2 separation performance. Finally, to validate the approach, the procedure was repeated with ZIF-8-Pebax® MH 1657 MMMs.

5.2 Experimental procedure

5.2.1 Materials

Zinc acetate dihydrate and 4-methyl-5-imidazolecarboxaldehyde were purchased from Acros Chemicals (98% and 99% purity, respectively). Methanol (99.8%) was purchased from Honeywell, and anhydrous tetrahydrofuran (THF, ≥99.9%) was attained from Sigma-Aldrich. Absolute ethanol was purchased from Gilca, Spain. For the membrane fabrication, commercially available Pebax® MH 1657 was kindly provided by Arkema, France.

5.2.2 Methodology

5.2.2.1 Fabrication of MMMs with recycled reagents

Recycled MOFs and polymer matrix are obtained following experimental procedures explained in section 3.3 in chapter 3. The MMMs from the recycled reagents are discussed in section 3.2.2 in chapter 2. Identification names of the fabricated membranes are given in **Table 5.1**.

Table 5.1: Names of the membranes fabricated for this study and their definition (applied in gas separation)

Name	***Membrane type***	***Description***	***Thickness (µm)***
M1	Bare polymer	Fabricated with fresh polymer matrix	46 ± 2
M1.1	Bare polymer	Fabricated by re-dissolving and re-casting of fresh bare membrane	43 ± 5
M1.2	Bare polymer	Fabricated with polymers recovered from MMMs	45 ± 3
M2	MMM	Fresh polymer matrix + fresh ZIF-94	56 ± 4
M2.1	MMM	Recycled polymer + recycled ZIF-94	58 ± 3
M2.2	MMM	Fresh polymer + recycled ZIF-94	55 ± 4

5.3 Results and discussion

5.3.1. Recovery and reuse of MMM components

The current study focuses on 10 wt% ZIF/polymer based MMMs since in chapter 4 (related with ZIF-94/Pebax® MH 1657 MMMs), reported it as an optimum loading considering both CO_2 permeability and CO_2/N_2 selectivity [160]. The total amount of MMMs (3.9 ± 0.4 g) used for the recycling process produced a total recovery of 95 ± 0.5 % (**Table 5.2**). In fact, the recycling was repeated for three batches corresponding to about 12-14 membranes of 70 mm in diameter per batch, that is 3.8 ±

0.3 g (wt. of recovered polymer + wt. of recovered ZIF-94). This means an overall process loss of 5 ± 0.5 % (as per Eq. 3.3). The prescribed process yielded 97.8 ± 0.5 % recovery of the polymer from MMMs, whereas ZIF-94 recovery was 76 ± 2.5 %.

Table 5.2: Mass balance of recovery polymer and ZIF-94 by recycling of MMMs

Parameters	***Total***	***Pebax® MH 1657***	***ZIF-94***
Initial weight (g)	3.9 ± 0.4	3.5 ± 0.3	0.40 ± 0.02
Recovered weight (g)	3.8 ± 0.3	3.4 ± 0.3	0.30 ± 0.04
Recovery (%)	95.5 ± 0.5	97.8 ± 0.5	76.0 ± 2.5

Moreover, due to the fact that, the recovered ZIF-94 was purified by repeated washing-centrifugation, the major loss of ZIF-94 was observed in this step. In fact, the recycled ZIF-94 obtained from first centrifugation showed a BET SSA of 270 m^2/g, whereas second and third-time washing by reflux and centrifugation increased SSA to 387 m^2/g and 412 m^2/g, respectively (**Table 5.3**).

Table 5.3. Effect of washing cycle on the BET SSA of recycled MOFs

Centrifugation cycle for washing of recycled MOFs	**BET SSA (m^2/g)**	
	ZIF-94	***ZIF-8***
1st washing	270	1087
2nd washing	387	1260
3rd washing	412	1325

However, a little fraction of the dissolved polymer was stuck on the bottom of the round flask which resulted in loss of some polymer as well (reflux was only once for polymer, and sonication was repeated three times in one bottle, hence loss was minimum). Recycling of MMMs was repeated 3 times to confirm the recovery efficiency of the method. Similarly, ZIF-8 was also recovered following the same method where the overall recovery (polymer + MOFs) was 91 ± 0.8 % and ZIF-8 recovery was 74 ± 4 %. Mass balance for ZIF-8 recovery and change in SSA with centrifugation cycle are presented in **Tables 5.3** and **5.4**, respectively. This demonstrates the generalization of the methodology for at least two different MOFs.

Table 5.4. Mass balance of recovered polymer matrix and ZIF-8 by recycling of MMMs

	Total	***Pebax® MH 1657***	***ZIF-8***	***Loss (%)***
Initial weight (g)	2.354 ± 0.5	2.12 ± 0.4	0.115 ± 0.05	
Recovered weight (g)	2.146 ± 0.39	2.06 ± 0.37	0.086 ± 0.02	9 ± 1
Recovery (%)	91.2 ± 0.8	97.1 ± 0.7	74.8 ± 4.0	

5.3.2 Characterization of MOFs and membranes

SEM images of fresh and recycled ZIF-94 are presented in **Figure 5.1 (A)** and **(B)**, respectively. No significant difference in terms of particle shape between this couple of MOFs is observed. Cross section images of MMMs containing both fresh and recycled ZIF-94 within the polymer matrix are shown in **Figure 5.1 (C)** and **(D)**, correspondingly. The fabricated membranes show homogenous distribution of both MOFs. Membranes are also found without apparent defects and cracks, which justifies the reusability of recycled ZIF-94 in imperfection free MMMs.

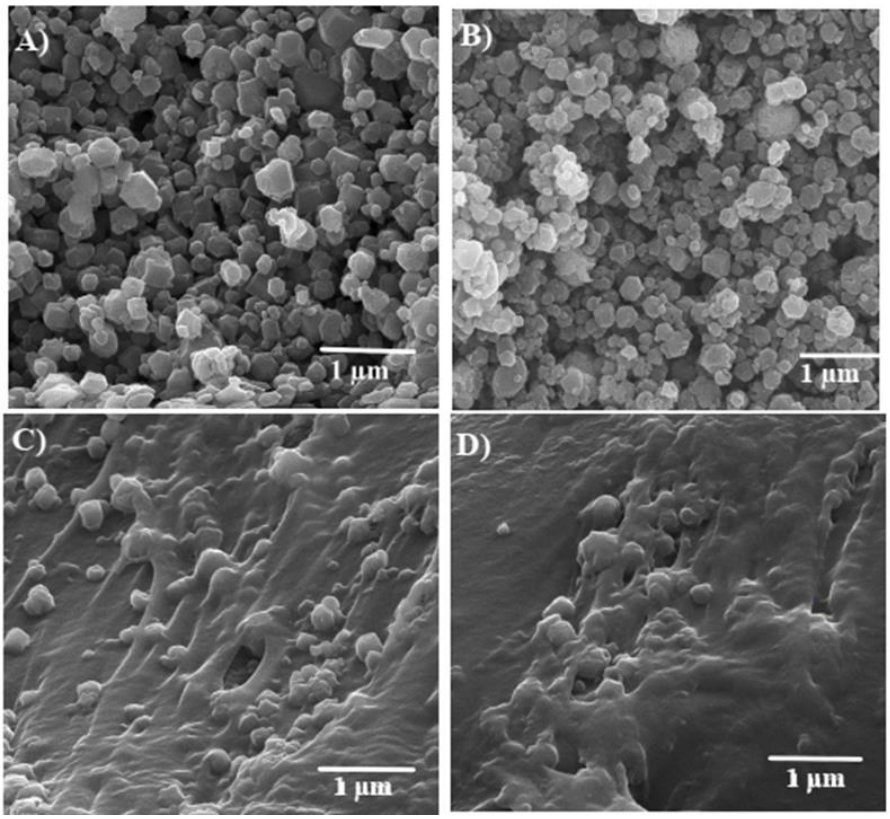

Figure 5.1: SEM images: (A) fresh ZIF-94, (B) recycled ZIF-94 from MMM, (C) cross section image of MMM (M2) incorporated with fresh ZIF-94, (D) cross section image of MMM (M2.1) incorporated with recycled ZIF-94.

Similarly, fresh and recycled ZIF-8 were analyzed with SEM, which is represented in **Figure 5.2**. ImageJ was used to calculate particle size from SEM images for both fresh and recycled ZIF-94. Counts of the particle diameter was taken arbitrarily from different part of the same image. SEM image analysis of fresh ZIF-94 with ImageJ resulted in MOF particle size in the range of 74 – 258 nm with mean value of 148 ± 44 nm, as shown in the Gaussian distribution in **Figure 5.3 (A)**. Whereas particle size of recycled ZIF-94 was found in the range of 97 – 246 nm with a mean value of 164 ± 32 nm (**Figure 5.3 (B)**).

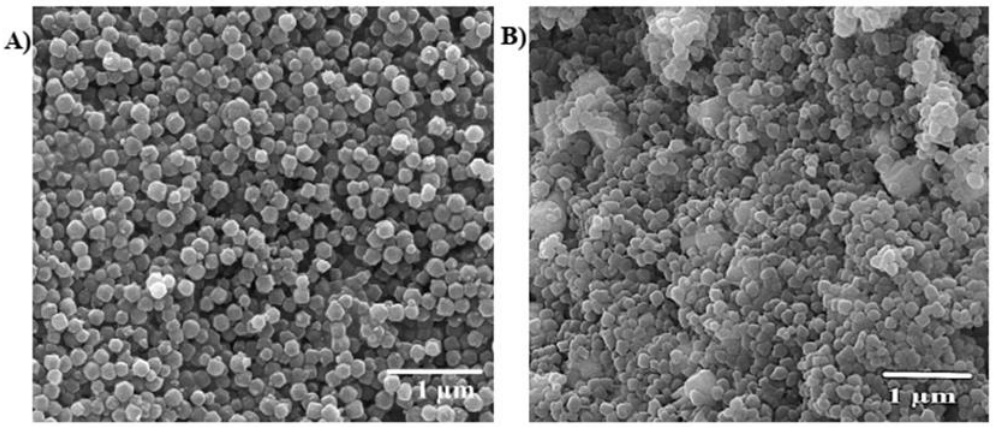

Figure 5.2. SEM image of fresh ZIF-8 (A) and recovered ZIF-8 (B)

Gaussian distributions of ZIF-8 and recycled ZIF-8 are presented in **Figure 5.3 (C)** and **(D)**. Analysis of SEM images of both MOFs with ImageJ shows that mean particle sizes of the fresh and recycled ZIF-8 correspond to 120 ± 30 nm and 110 ± 20 nm (**Table 5.5**), respectively. In general, ZIF-94 is hydrophilic, whereas, ZIF-8 is hydrophobic. Consequently, ZIF-94 is less interactive to the polymer (especially, when there are traces of polymer on it), which causes agglomeration of recycled ZIF-94 particles due to interparticle chemical interaction (i.e., hydrogen bond), hence an increase in the particle size is observed. On the other hand, hydrophobic ZIF-8 may interact with polymer, which causes shielding of the ligand charges, causing disaggregation of the MOFs particle, resulting in a decrease in the particle size.

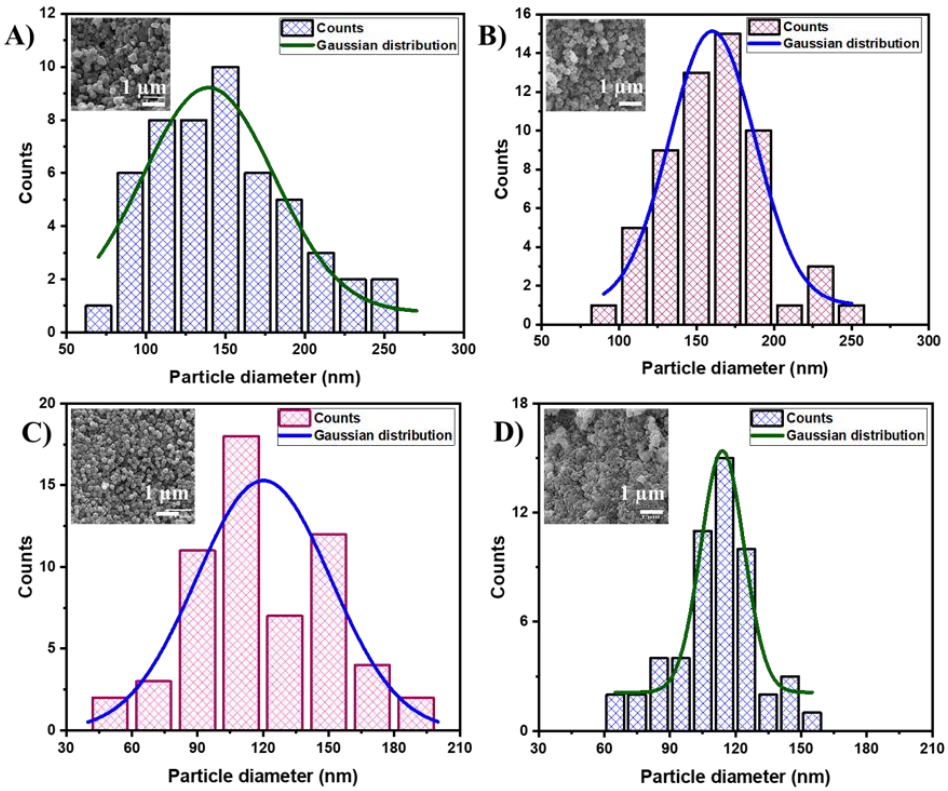

Figure 5.3: Particle size distributions: (A) fresh ZIF-94, (B) recycled ZIF-94, (C) fresh ZIF-8 and (D) recycled ZIF-8.

Additionally, N_2 adsorption – desorption mediated BET analysis added another analogous information between this set of MOFs: BET SSA values for fresh ZIF-94 and recycled ZIF-94 are 427 ± 7 m²/g and 412 ± 6 m²/g, respectively. These values are comparable and in the range of those published in the literature (415 - 480 m^2/g) [50,66,160]. N_2 adsorption – desorption isotherms are shown in **Figure A.1** which corresponds to hybrid of type I / type IV isotherm, which justifies that both MOFs are microporous having some extend of mesopores [161,162]. Additionally, zeta potential analysis confirmed some remaining polymer coating on recycled ZIF-94. Fresh ZIF-94 produced a zeta potential response of 16.8 ± 0.5 mV whereas recycled ZIF-94 showed 6.6 ± 1.1 mV which are presented in **Table 5.5.** This descending trend of zeta potential justifies polymer coating (which reduces surface charge on fillers) on the recycled ZIF-94. This argument agrees with Herynek et al. results who reported that polymer coating on iron oxide (maghemite) nanoparticles reduced zeta potential score as compared to that of the uncoated [163]. To justify the applicability of this methodology for other MOFs, ZIF-8 was also recycled from its Pebax® MH 1657 matrix based MMM (10 wt.% loading as well). Zeta potential response of recovered ZIF-8 was expectedly lower than that of fresh ZIF-8, whereas BET SSAs of both recycled (1325 ± 26 m^2/g) and fresh (1507 ± 30 m^2/g) ZIF-8 are comparable and are presented in **Table 5.5**. ZIF-8 has been reported with a wide range of BET SSA (700 -1946 m^2/g) [164–167] which agrees with the BET SSA values of fresh and recycled ZIF-8. Additionally, SEM images and N_2 adsorption – desorption isotherms of fresh and recycled ZIF-8 are presented in **Figure 5.2** and **Figure A.2**, respectively.

Table 5.5: Zeta potential, BET specific surface area (SSA) and particle size of fresh and recycled ZIF-94.

Parameters	***Zeta potential (mV)***	***BET SSA (m^2/g)***	***Mean particle size (nm)***
Fresh ZIF-94	16.8 ± 0.5	427 ± 7	148 ± 44
Recycled ZIF-94	6.6 ± 1.1	412 ± 6	164 ± 32
Fresh ZIF-8	19.7 ± 0.3	1507 ± 30	120 ± 30
Recycled ZIF-8	7.6 ± 0.7	1325 ± 26	110 ± 19

In addition to the MOFs, polymer matrix was also recovered from MMMs by the recycling process. Cross-section images of both fresh bare membrane and recycled bare membrane are presented in **Figure A.3 (A)** and **(B)**, respectively. Presence of ZIF-94 was not found in the membrane (**Figure A.3 (B)**), while the cross-section is defect free and identical to that of the fresh bare membrane. Further confirmation of removal of MOFs was obtained by EDX analysis of polymers (obtained by recycling of ZIF-94 and ZIF-8 based MMMs), as presented in **Figures A.4** and **A.5** EDX analyses confirmed the removal of Zn below its detection limit, while a certain Pd percentage appeared since samples were made conductive by coating them with it. DSC analyses of both fresh and recycled polymeric membranes are presented in **Figure 5.4 (A)** which reveal that fresh (M.1), re-cast (M1.1) and recycled polymer (M1.2) produced similar

response to calorimetry analysis. Those measurements confirm identical melting temperature for the polyamide segment of fresh, re-cast and recycled membranes, that is T_m = 205 °C which was already justified by Martinez-Izquierdo et al. [152]. Moreover, no significant difference was observed in terms of DLS polydispersity between this set of polymers. Polydispersity is an important index for nanomaterial research, which suggests heterogeneity of the sample based on their particle size. Polydispersity can arise due to agglomeration or aggregation of the particles under investigation during their isolation or analysis [168]. Although mean particle diameter of dissolved recycled polymer was higher (580 ± 30 nm) compared to that of fresh polymer (464 ± 41 nm), both of them showed identical polydispersity (0.22 and 0.21, respectively), which suggests that both polymers agree in terms of heterogeneity (**Table 5.6**).

Table 5.6. DLS analyses of fresh (M1) and recycled (M1.2) Pebax® MH 1657 polymer.

	DLS particle diameter (nm)	***Polydispersity***
Polymer M1	464 ± 41	0.21 ± 0.04
Polymer M1.2	580 ± 30	0.22 ± 0.03

Moreover, it is clear that polymer chains are much smaller than the aggregates that the DLS detects [169]. In any event, the larger DLS particle diameter suggests lower solubility of the recycled polymer. This can be due to the remains of MOF (i.e. small MOF nanoparticles from the relatively wider particle size distribution harder to remove) or MOF components creating chemical interaction (i.e., hydrogen bonding, Van der Walls interaction etc.) within primary polymer constituents. XRD analysis outcomes are presented in **Figure 5.4 (B)** where fresh and recycled ZIF-94 show identical response, which justifies similarity in crystalline structure of both MOFs. This confirms that the complex process carried out of MOF recycling did not alter its crystallinity. Correspondingly, fresh and recycled MMMs also produced similar peaks, whereas peaks of ZIF-94 are not observed for recycled polymer from MMMs, which suggests complete removal of MOFs from the membranes.

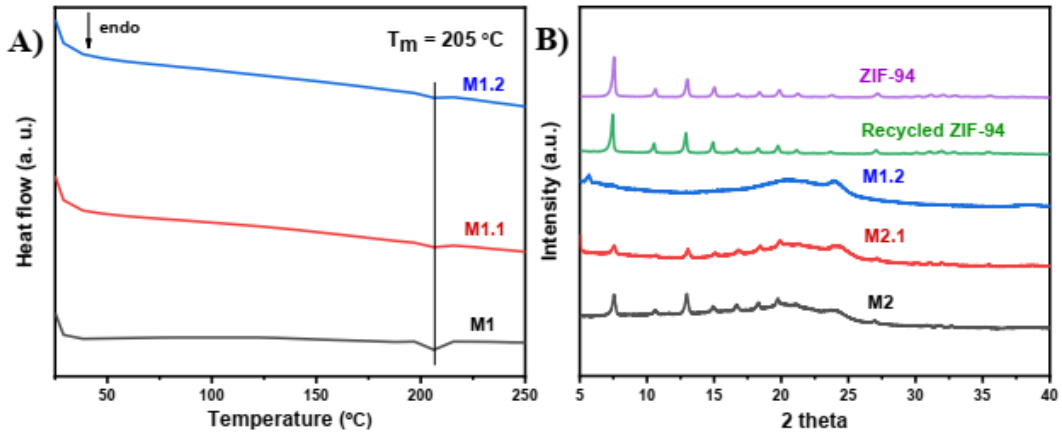

Figure 5.4. (A) DSC analyses of fresh and recycled and re-cast bare polymer membrane, (B) XRD patterns of fresh ZIF-94, recycled ZIF-94, fresh MMM (M2), recycled MMM (M2.1) and recycled polymer matrix from MMM (M1.2).

Additionally, FTIR was performed for pure polymer, recycled polymer and MMMs, both ZIF-94 and ZIF-8 which are shown in **Figures 5.5**, demonstrating absence of fillers in the recycled polymer and vice-versa. Molecular weight analysis of both fresh and recycled polymers dissolved in the same 70/30 ethanol/water mixture used to prepare the membranes was performed with the results presented in **Figure A.6 (A)** and **(B)**, respectively. No significant difference was observed between them, showing the expected molecular weight distribution corresponding to polyethylene oxide with 44 as repeated unit (m/z). All these compared characterizations justify the possibility of recovered polymers for reuse in MMMs if they satisfy the gas separation performance expectations.

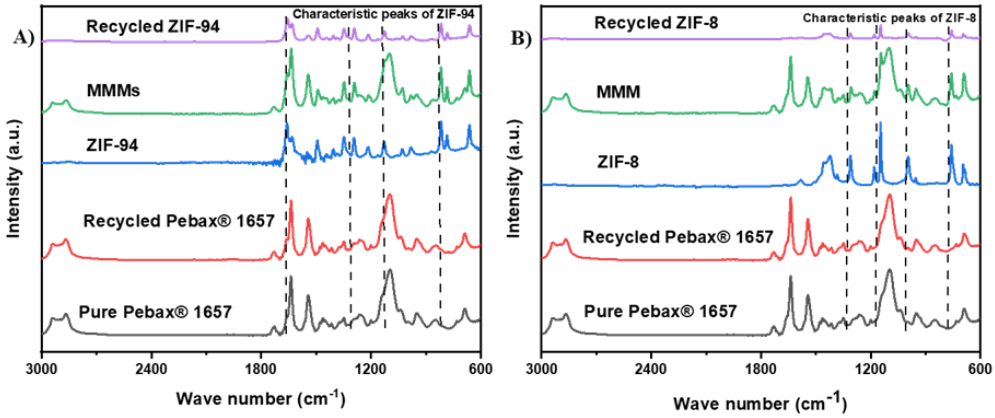

Figure 5.5. FTIR analyses: A) of pure polymer, fresh ZIF-94, fresh MMM with ZIF-94 and recycled products from ZIF-94 based MMM, B) of pure polymer, fresh ZIF-8, fresh MMM with ZIF-8 and recycled products from ZIF-8 based MMM.

TGA analysis outcomes of the materials under investigation are represented in **Figure 5.6**. Fresh bare membrane (M1) and recycled bare membrane (M1.2) show identical response on thermal degradation analysis. Both of them are stable up to 250 °C, then they start to undergo a first weight loss. Weight loss of these two membrane samples become intense after 400 °C due to thermal decomposition which, through a

second step, continues up to 530 °C with a residual lower than 2 % of an initial weight. Similarly, fresh MMM (M2) and recycled MMM (M2.1) showed analogous response on TGA. They also exhibit a rapid thermal degradation after 400 °C, which continue until 550 °C with residues of 3.5 % and 4 %, respectively, due to the ZnO generated from the MOF since TGA was carried out in air [170]. Fresh and recycled ZIF-94 were also studied with TGA to compare their thermal behavior. Both of them start losing weight before 100 °C, which is due to the loss of moisture and solvents from inside of the micropores which ends at ca. 300 °C. Rapid thermal degradation of both fresh and recycled MOFs starts after 300 °C, which continues up to 600 °C generating ZnO. Recycled ZIF-94 shows comparatively small amount of extra weight loss than the fresh MOF and finally gives a 0.7% less residue. This tendency agrees with the presence of traces of polymer coating on the MOF surface (since this polymer decomposes between 400 and 530 °C as seen above), also responsible for the small loss of BET SSA quoted above for the two MOFs ZIF-94 and ZIF-8.

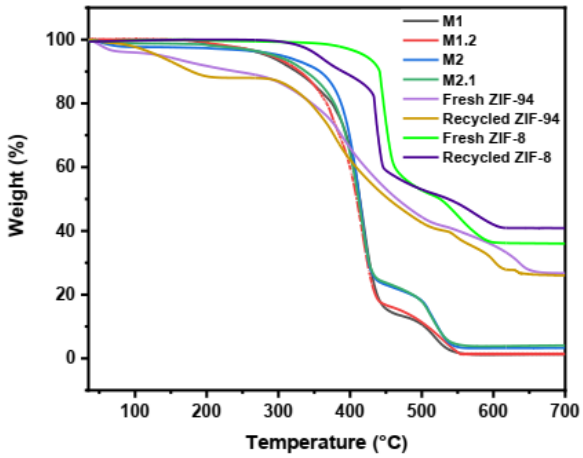

Figure 5.6: TGA analyses in air of fresh and recycled ZIF-94, their membranes and fresh and recycled ZIF-8 (see Table 1).

5.3.3. CO_2 separation performance

Due to its higher CO_2 adsorption capacity, already discussed in the introduction section, ZIF-94 was chosen for the MMM fabrication. As shown in **Figure 5.7**, gas permeation analysis reveals that the re-cast bare membrane (M1.1) and fresh bare membrane (M1) produced similar CO_2 permeabilities which are 94 ± 2 Barrer and 90 ± 3 Barrer, respectively. However, the re-cast membrane (M1.1) sacrificed 21 % of CO_2/N_2 selectivity compared to fresh bare membrane (M1) with values of 18 ± 1 and 23 ± 2, respectively. Analogously, the bare membrane made with polymer recycled from 10 wt. % ZIF-94 MMM (M1.2) performed lower in terms of selectivity (18.5 ± 0.8) but outperformed in terms of permeability (106 ± 2 Barrer) than the fresh bare membrane (M1, 90 ± 3 Barrer). Such improvement of CO_2 permeability can be due to the existence of traces of MOFs in the recovered polymer (below the detection limits of FTIR, XRD and TGA) and in any event agrees with the larger DLS particle size, which may produce an increase of free volume (responsible in turn of the CO_2/N_2 selectivity decrease). However, recovered polymer can be reused in MMMs, which is

evidenced from the gas separation performance of MMM M2.1 presented in **Figure 5.7**. This recycled MMM improved fresh MMM M2 in terms of permeability with a trade-off in selectivity. The permeability and selectivity values corresponding to M2.1 are 174 ± 3 Barrer and 25.6 ± 0.6, respectively, whereas M2, which is called fresh MMM, produced a permeability of 137 ± 3 Barrer with a selectivity of 29.0 ± 1.8. Such performance of M2.1 follows the general phenomena, increase in the permeability at the cost of selectivity and vise-versa. In addition, M2.1 prepared with reused materials still outperformed the fresh bare membrane (M1) in terms of both permeability and selectivity. Similar performance of pure polymer and MMM containing fresh ZIF-94 and Pebax® MH 1657 matrix has been reported by several authors [160,171]. Moreover, when recycled ZIF-94 was incorporated into fresh polymer matrix (MMM M2.2) the selectivity of the membrane went down to 27.5 ± 1.4 (5 % lower than M2) but the permeability increased to 157 ± 6.5 Barrer which is still 67 % higher than that of fresh bare polymer (M1) and 15 % higher than that of M2. The separation performances and thicknesses of all the membranes are shortlisted in **Table 5.7**.

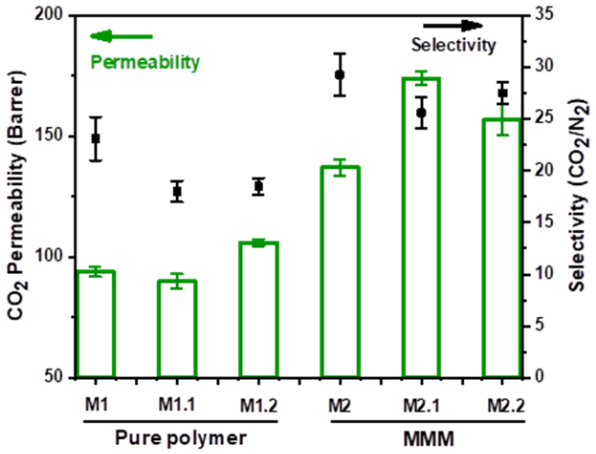

Figure 5.7. Gas permeation results of the membranes when applied to the separation of the CO_2/N_2 mixture at 35 °C. At least 3 different membrane samples were tested for each membrane type.

Table 5.7. Performance of fabricated MMMs with 3 wt.% polymer matrix in different conditions

Membranes	***Membrane thickness (μm)***	***Permeability CO_2 (Barrer)***	***Selectivity CO_2/N_2***
M1	46 ± 2	94 ± 2	23.0 ± 2.1
M1.1	43 ± 5	90 ± 3	18.0 ± 1.0
M1.2	45 ± 3	106 ± 2	18.5 ± 0.8
M2	56 ± 4	137 ± 3	29.0 ± 1.8
M2.1	58 ± 3	174 ± 3	25.6 ± 1.6
M2.2	55 ± 4	157 ± 7	27.5 ± 1.3

5.4 Conclusions

In this chapter, a methodology was developed to recycle ZIF-94 and Pebax® MH 1657 polymer components from their MMM which was also applicable for the recycling of ZIF-8. The recycled nanocrystals were undistorted in terms of size, shape and crystallinity. The reported methodology is excellent in terms of recovery yield for both polymer (97.8 ± 0.5 %) and MOF ZIF-94 (76 ± 2.5 %). Fresh and recycled ZIF-94 have quite similar BET SSA values which are of 427 ± 7 m^2/g and 412 ± 6 m^2/g, whereas respective particle diameters of 148 ± 44 nm and 164 ± 32 nm seem to be within the experimental error. Similarly, fresh ZIF-8 and recycled ZIF-8 show BET specific surface areas of 1507 ± 30 m^2/g and 1325 ± 26 m^2/g, respectively, and their mean particle sizes correspond to 120 ± 30 nm and 110 ± 20 nm, corroborating the applied method with two different MOFs.

Additionally, the recovered polymer was found highly selective to the CO_2/N_2 mixture with a comparable CO_2 permeability to that of the fresh bare membrane. All these remarks validate the reported approach for the recycling of MMMs to obtain ZIF-94 and polymer matrix. The MMMs containing recovered MOFs and fresh polymer matrix produced an acceptable gas separation performance with CO_2 permeability and CO_2/N_2 selectivity of 174 ± 3 Barrer and 25.6 ± 0.6, respectively. These values are comparable to those achieved with MMMs obtained from totally fresh MOF and polymer materials (permeability of 134 ± 6 Barrer and selectivity 29 ± 0.8).

These parameters suggest successful recovery of precious components (MOFs) from MMMs. Additionally, recovered polymer matrices are still selective, suggesting that they could be used in other applications (i.e. plastic bags). Finally, this work reinforces the environment friendly industrial application of MMMs establishing the principles for the recovery and reuse of their individual components. Although, recycled materials are found compatible for the CO_2 separation application, still, estimation of energy consumption, recycling of the solvents and life cycle assessment are considered as future objective of the project, which will reveal complete insight of the recycling of MMMs. Moreover, this new approach suggests a way for membrane and MMM researchers to make their investigations cheaper and more sustainable.

Chapter 6: Mixed matrix membranes for CO_2 capture from Microporous Iron Coordination Polymer MIL-178(Fe) and Pebax® 3533

Outlines

Reproduced from "M. Benzaqui, M. Wahiduzzaman, H. Zhao, M.R. Hasan, T. Steenhaut, A. Saad, J. Marrot, P. Normand, J.M. Grenèche, N. Heymans, G. de Weireld, A. Tissot, W. Shepard, Y. Filinchuk, S. Hermans, F. Carn, M. Manlankowska, C. Téllez, J. Coronas, G. Maurin, N. Steunou, C. Serre, A robust eco-compatible microporous iron coordination polymer for CO_2 capture, J. Mater. Chem. A 10 (2022). https://doi.org/10.1039/d1ta10385g" with permission from the Royal Society of Chemistry.

6.1 Introduction

Metal organic frameworks and porous coordination polymers are a class of porous crystalline hybrid materials [159,160], which have gained widespread interest toward CO_2 capture and separation [44,45,47]. Indeed, numerous MOFs reported so far for CO_2 capture, still lack the requisite chemical stability. Note that moisture is a major concern in industrial gas separation as it is not economically feasible to use completely dry feed-gas streams. Therefore, only hydrothermally stable MOFs can be considered for real practical applications.

In this context, Fe (III) carboxylates - denoted here "Fe-MOFs"- are considered, since the association of Fe^{3+} cation with strong Lewis acid property and carboxylate ligands can produce, although not systematically, water stable MOFs [172,173]. The natural abundance of iron and its low toxicity have promoted the development of Fe-MOFs, not only for gas separation but also for (photo)catalysis [174], heat reallocation, (bio)sensing or biomedicine due to their good chemical stability[175], high porosity and biocompatibility [174,176,177]. So far, Fe (III) MOFs of different architectures, such as the MIL-n (MIL-53, MIL-59, MIL-88, MIL-100, MIL-101) series have been designed by assembling either di-, tri-, tetranuclear clusters as SBUs and polycarboxylate aromatic moieties as organic linkers [174,178] [179–181]. However, not all of these MOFs exhibit a high hydrolytic stability that is not only driven by the type of SBUs but also the connectivity as well as the size and hydrophobic character of the organic linker[182]. As an example, the good hydrothermal stability of MIL-53(Fe) is certainly due to its 1D micropore channel structure based on $[Fe(OH)(COO)_2]_n$ chains while the mesoporous MIL-101(Fe) and PCN-333(Fe) based on the oxotrimers SBU present a limited water stability. Due to the presence of CO_2 adsorption sites, such as Lewis acid Fe^{3+} sites or polar functions (OH, F) and a high pore volume, a few Fe-MOFs, such as MIL-100(Fe), MIL-88A(Fe), soc MOF(Fe), Fe-BTB and Fe-BTC have been considered for CO_2 capture and some of them have shown attractive CO_2 uptake at low pressure (> 2 $mmol.g^{-1}$ at 1 bar, 298 K) [183,184]. Recently, an Fe-MOF ($Fe_4(\mu_3\text{-}O)_2(BTB)8/3(DMF)_2(H_2O)_2$), whose structure consists of two interpenetrating 3D skeletons, has shown a greater CO_2 uptake than that of several known MOFs with larger pore volume as a result of its small pore and the presence of multiple CO_2 adsorption sites induced by the framework interpenetration [179]. Another property of MOFs and PCP that was exploited for CO_2 capture is their propensity for structural flexibility.

In spite of these interesting results, the number of Fe-MOFs and Fe-PCPs that combine all the properties required for CO_2 separation (high CO_2 adsorption capacity and selectivity, high chemical and thermal stability) is still limited. Moreover, many challenges regarding their synthesis remain unaddressed. Numerous Fe-MOFs are often prepared in the presence of toxic organic solvents and reactants, which restricts their applications to a great extent. Therefore, the development of Fe (III)-MOFs using safer synthetic conditions allowing both the control of the crystal size and their large-scale production is still an open challenge for their future practical applications [185].

Considering all these limitations, our French collaborator (research group of Profs. Nathalie Steunou and Christian Serre) synthesized MIL-178(Fe) microcrystals

through a hydrothermal route, using the 1,2,4-BTC ligand and $FeCl_3$ as iron precursor [83]. Adsorption properties of this material were investigated by the research group of Profs. Nathalie Steunou and Christian Serre, and then compared with molecular silulation. Wherein, this porous material was found as a prospective filler for CO_2 seperation. According to single gas absorption experiment of N_2 at 77 K (**Figure 6.1**), MIL-178(Fe)-*RT* presents very small N_2 uptake which is consistent with the theoretically calculated small pore volume of 0.18 cm^3/g and pore dimensions (< 4.5 Å) of the cavities vs the kinetic diameter of N_2 (3.64 Å).

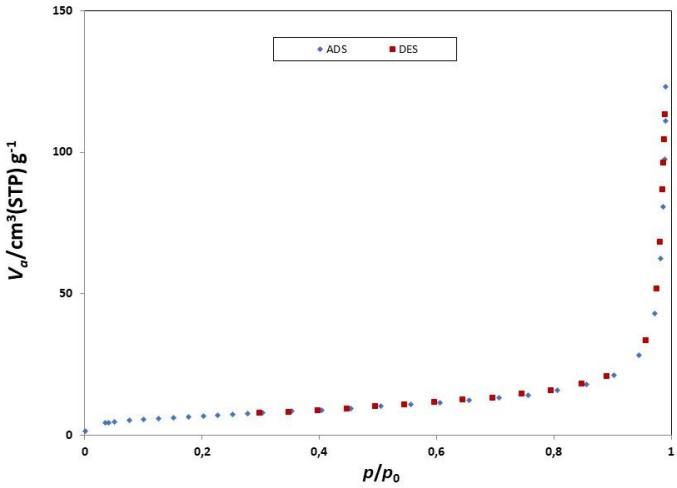

Figure 6.1. N_2 adsorption isotherm of MIL-178(Fe)-*RT* at 77 K [83].

Moreover, adsorption isotherms of single gas components (for both CO_2 and N_2) at 298 K are found Type I with a steeper slope at low pressure for CO_2 as compared to N_2 (**Figure 6.2 (a)**), which were then compared with their response in molecular simulation. **Figure 6.2 (c)** shows that the preferential adsorption site of CO_2 in MIL-178(Fe) remains the same for CO_2/N_2 mixture as with the CO_2 single component (**Figure 6.2 (b)**). This prediction motivated for an experimental study on MIL-178(Fe) in MMMs towards post-combustion CO_2 capture, i.e. for a binary gas mixture of CO_2/N_2 at 1.0 bar.

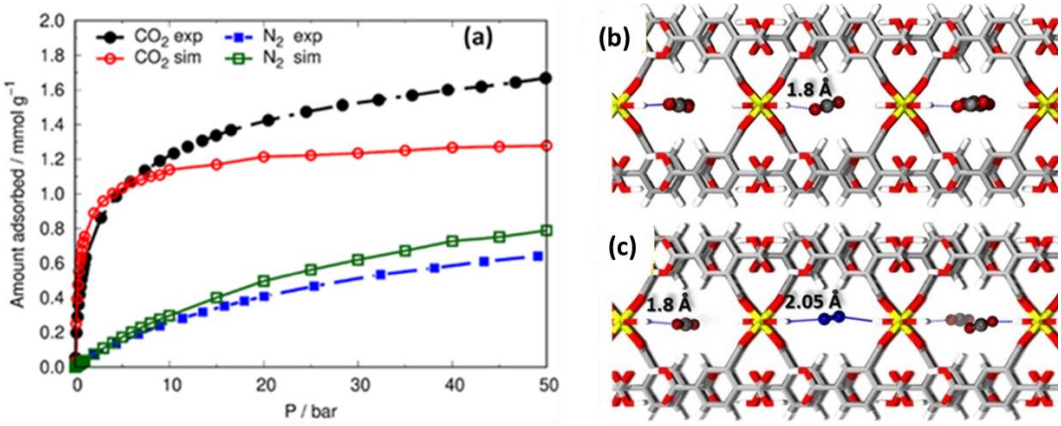

Figure 6.2. (a) GCMC calculated and experimental adsorption isotherms for the single components CO_2 and N_2 in MIL-178 at 298 K. Microscopic view of the GCMC preferential sittings at low pressure for (b) CO_2 molecules as single components and (c) both CO_2 and N_2 molecules in mixture, in the 1-D channel of MIL-178(Fe).

In this chapter, due to its high hydrothermal stability and scalability, MIL-178(Fe), synthesized under room temperature and green conditions, was used as a filler for the processing of mixed matrix membranes (MMMs). Its combination with the elastomeric block copolymer Pebax® 3533 led to defect-free composite membranes with an enhanced CO_2/N_2 post-combustion separation performance in comparison to the pristine membrane. Pebax® 3533 was preferred over the most studied Pebax® MH 1657 due to the fact that the former is not water/ethanol soluble. Therefore, Pebax® 3533 based membranes are prone to be more stable in the separation of a realistic humid flue gas [186].

6.2 Experimental

6.2.1 Materials

Pebax® 3533 (75 wt.% poly (tetramethylene oxide) (PTMO) and 25 wt.% aliphatic polyamide (PA12)) in the form of pellets was kindly provided by Arkema, France. Solvents, 1-propanol (Labbox, 99%) and 1-butanol (Scharlab, 99%) were used as received. MIL-178(Fe) was kindly provided by our French collaborator (research group of Nathalie Steunou and Christian Serre), which was hydrothermally prepared at RT from anhydrous $FeCl_3$ (Sigma Aldrich, 99%) and 1,2,4-benzene tricarboxylic acid (Sigma Aldrich, 95 %) by Benzaqui et. al. [83]. All research grade gases (greater than 99.995% of purity) used for the separation experiment were supplied by Abelló Linde S.A., Spain.

6.2.2. Membrane fabrication

Pebax® 3533 matrix-based membranes were fabricated following procedure explained in section 3.2.1. Wherein 1-propanol/1-butanol (75/25 (v/v)) mixture was used as solvent for membrane fabrication. Drying of the membrane was performed at RT for overnight.

6.3 Results and discussion

6.3.1 Characterization of mixed matrix membrane

Since MIL-178(Fe) particles present a good colloidal stability in 1-propanol and 1-butanol solvents (see **Figure 6.3**), MMMs were prepared by dispersing MIL-178(Fe)-*RT* in a solution of Pebax® 3533 in 1-propanol/1-butanol solvents mixture (see Experimental part for details). Pebax® 3533 is a poly (amide-6- *b*-tetramethylene oxide) block copolymer composed of 75 wt.% of a rubbery poly(tetramethylene oxide) (PTMO) block with high affinity towards CO_2 molecules and 25 wt.% of a glassy polyamide (PA) block providing mechanical strength [152,187,188]. This polymer has the advantage to be commercially available and soluble in non-toxic alcohol solvents. In the past few years [189], the series of Pebax polymers was used as continuous phase in MMMs owing to their promising separation performances resulting from their structural flexibility and solubility-selective gas separation [190,191]. Moreover, a few rubbery Pebax-MOF MMMs have shown better MOF-polymer interfacial properties in comparison to numerous MMMs based on rigid glassy polymers [135,192,193]. MIL-

178(Fe)-Pebax-X MMMs with different MIL-178(Fe) content (X=5-25 wt.%) were fabricated following a two-steps protocol (polymer dissolution and filler dispersion followed by casting), as explained in the experimental section.

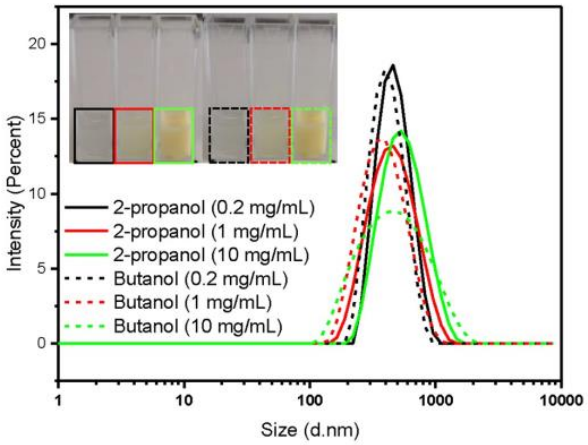

Figure 6.3. Size Distribution (diameter in nm) of MIL-178(Fe)-*RT* in 2-propanol and 1-butanol by dynamic light scattering at different concentrations (0.2, 1 and 10 mg.mL^{-1}). The inset shows photographs of the colloidal solutions of MIL-178(Fe)-*RT* in 2-propanol or butanol solvents.

PXRD patterns of the different MIL-178(Fe)-Pebax-X MMMs display the characteristic Bragg peaks of MIL-178(Fe), the intensity of which increases with the amount of MIL-178(Fe) (**Figure 6.5 (a)**). This indicates that the crystalline structure of MIL-178(Fe) is preserved upon their association with the polymer. The PXRD pattern of MMMs display also a broad peak at 2θ = 20° corresponding to the crystalline region of PTMO. MIL-178 (Fe) was analyzed with SEM and TEM with are shown in **Figure 6.4**. The morphology of the membranes was investigated by SEM. In contrast to pure Pebax® 3533 membrane that presents a smooth and homogeneous surface (**Figure 6.6 (a-b)**), the surface of MIL-178-Pebax-10 is rougher due to the embedding of well-dispersed MIL-178(Fe) platelets with a random orientation in the polymer matrix as shown in **Figure 6.6 (c-f)**. However, when the MOF content reached a loading of 15 wt.%, the morphology of the MMMs changes drastically (**Figure 6.5 (b)**). As shown in **Figure 6.5 (c, d)**, the top surface of MIL-178-Pebax-15 is smooth and exhibits a lamellar microstructure. Such layered structuration of the MIL-178-Pebax-15 MMM is also observed on cross-section SEM images **Figure 6.5 (e)**, and is certainly imparted by the stacking of MIL-178(Fe) platelets parallel to the substrate.

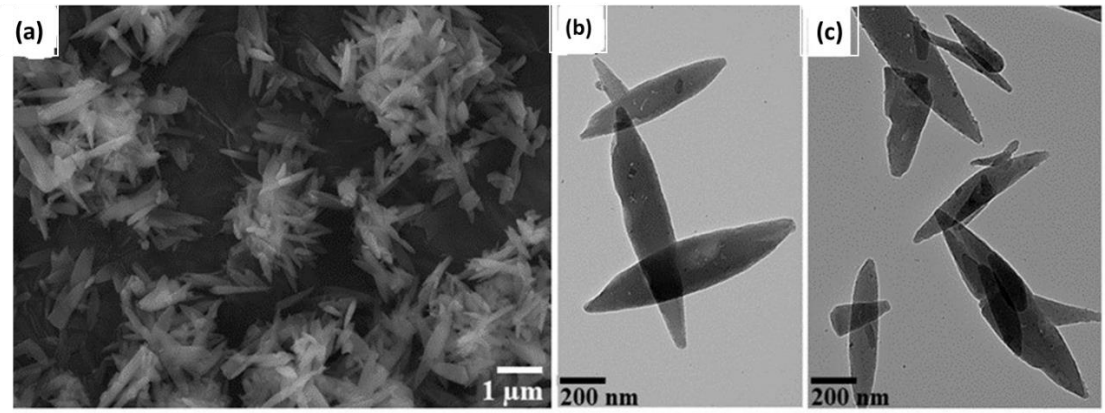

Figure 6.4. SEM images of (a) MIL-178(Fe)-*RT*, (c-d) TEM images of MIL-178(Fe)-*RT*.

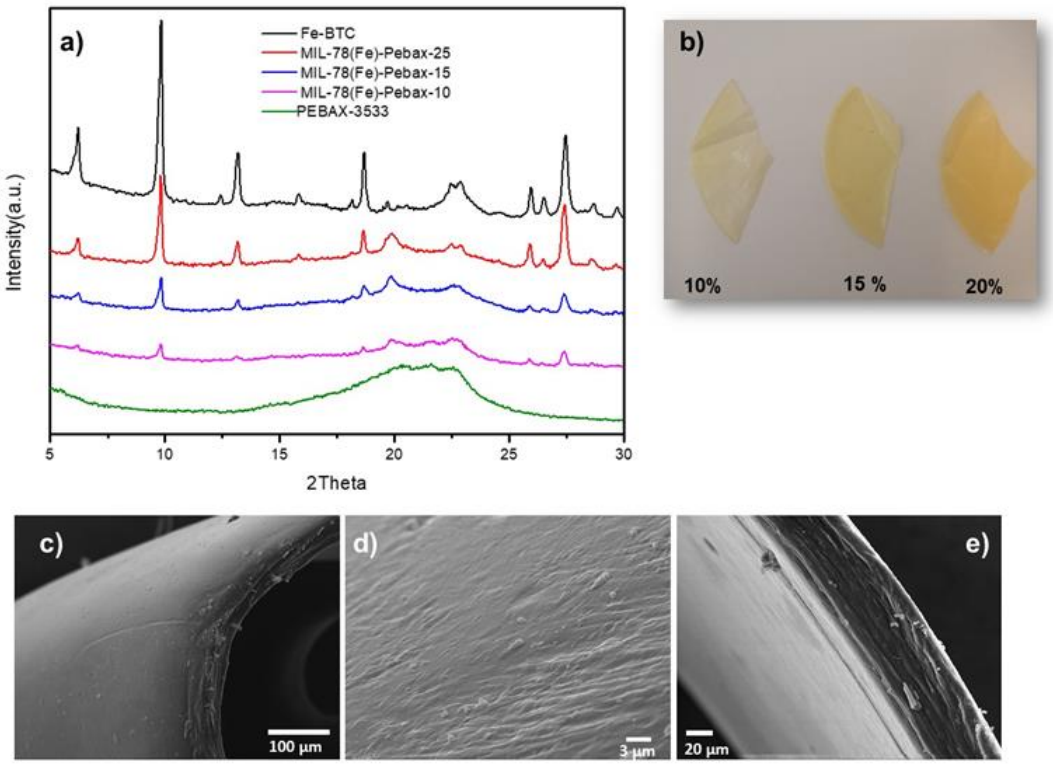

Figure 6.5. (a) PXRD of MIL-178(Fe)-Pebax 3533 MMMs in comparison with the pure polmer and MIL-178(Fe)-RT, (b) photographs of MMMs with different Mil-178(Fe) contents. (c, d) SEM images of the top surface and e) cross-section SEM image of MIL-78-Pebax-15 MMM.

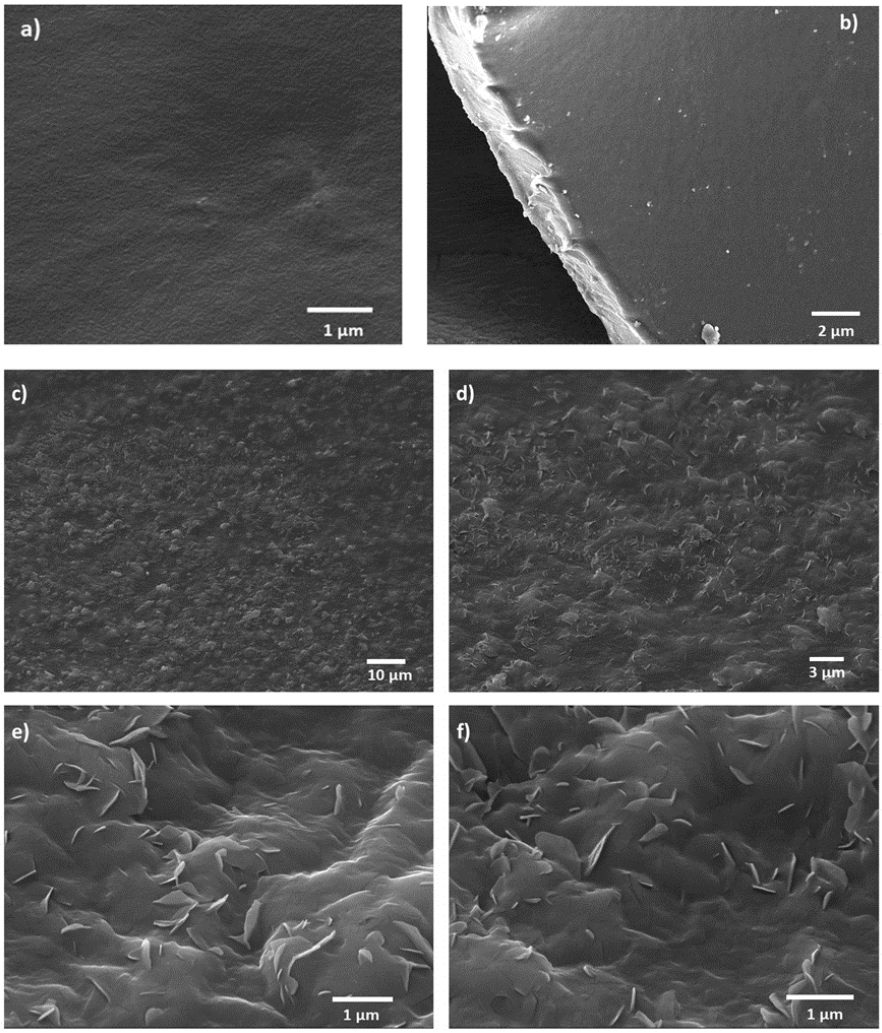

Figure 6.6. SEM images of the top surface of a-b) pure PEBAX-3533, and c-d) MIL-78-Pebax-10 MMM; e-f) cross-section image of MIL-78-Pebax-10 MMM

FT-IR spectra of MIL-178(Fe)-Pebax-X MMMs (**Figure 6.7**) present the characteristic vibration bands of both MIL-178(Fe) and Pebax® 3533, in agreement with the incorporation of the PCP in the polymer matrix and with the prevalence of the PCP crystallinity upon the MMM preparation. The FT-IR spectra of MIL-78(Fe)-Pebax-X membranes superimpose well with that of pure MIL-78(Fe) and Pebax® 3533. They display a series of vibration bands characteristic of the soft PEO block such as the peak at 1102 cm^{-1} corresponding to C-O-C group as well as those of the hard polyamide segment of the polymer (i. e. 3295, 1639 and 1735 cm^{-1} corresponding respectively to the hydrogen bonded -N-H-, H-N-C=O and O-C=O groups). The stretching vibration at 2929 cm^{-1} indicates the presence of aliphatic -C-H functions.The FT-IR spectra oft he membranes present also the characteristic vibration bands of MIL-178(Fe) (i. e. ν_s(C=O) = 1400 cm^{-1}, ν_{as}(C=O) = 1543 cm^{-1} and free carboxylic acid group at 1703 cm^{-1}).

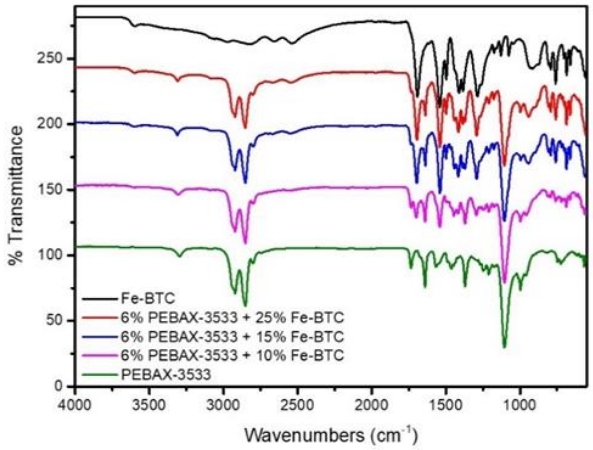

Figure 6.7. FT-IR spectra of pure PEBAX and Fe-BTC (MIL-78(Fe))-PEBAX 3533 MMMs with different MIL-78(Fe) contents

The thickness of the MMMs lies between 40 and 45 µm. The thermal stability of MIL-178(Fe)-Pebax-X MMMs was evaluated by TGA in comparison to the pure MIL-178(Fe) and bare polymer (see **Figure 6.8**). First, negligible weight loss below 250 °C shows the removal of any residual solvent in the MMM. The onset decomposition temperatures of MIL-178(Fe)-Pebax-10 and MIL-178(Fe)-Pebax- 15 MMMs is slightly higher than that of pure Pebax® 3533 (~ 220 °C for MMM vs. 180 °C for neat Pebax® 3533) as a result of the good thermal stability of MIL-178(Fe). In contrast, the thermal stability of MIL-178(Fe)-Pebax-25 is significantly lower than that of MMMs with a lower filler content and pure polymer. This suggests that the interfacial interactions between the MIL-178 (Fe) and Pebax® 3533 in MIL-178(Fe)-Pebax-25 are presumably lower than that of MIL-178(Fe)-Pebax-X with X=10 and 15. Nevertheless, the overall thermal stability of all MMMs is enough to meet the requirement for CO_2/N_2 separation. The residual amount above 500 °C of the MMMs is consistent with their respective MIL-178(Fe) contents.

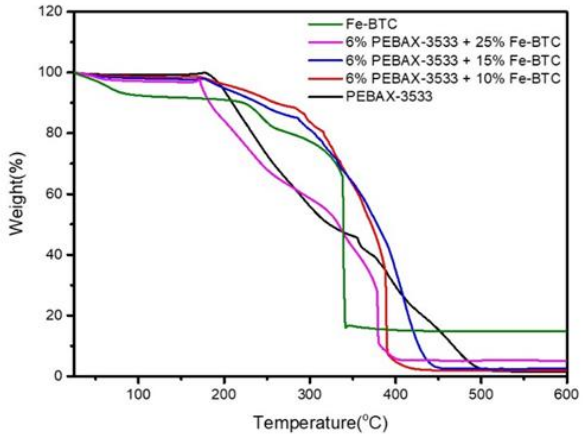

Figure 6.8. Thermogravimetric analysis of pure PEBAX, MIL-78(Fe)-*RT* and MIL-78(Fe)-PEBAX 3533 MMMs with different MIL-78(Fe) contents.

The DSC curves, characterized by a single endothermic peak corresponding to the melting of the PTMO phase ($T_{m,\,PTMO}$~10°C), have been used to quantify the degree of crystallinity of this phase (**Figure 6.9**). This was done for each MMM by calculating the ratio between the enthalpy of fusion (ΔHf) obtained by integration of the peak and the enthalpy of fusion corresponding to a purely crystalline PTMO phase as obtained from the literature ($\Delta Hf* \approx 200\ J/g$) [135]). The plot of the crystallinity degree as a function of the MIL-178(Fe)-*RT* concentration shows a continuous decrease from 33 % to 5 % when the MIL-178(Fe)-*RT* concentration varies from 0 to 20 % (**Figure 6.10**). Thus, it appears that MIL-178(Fe)-*RT* inhibits the crystallization of the PTMO phase, which should favor a significant softening of the Pebax® 3533 considering that this polymer contains 70 % of PTMO.

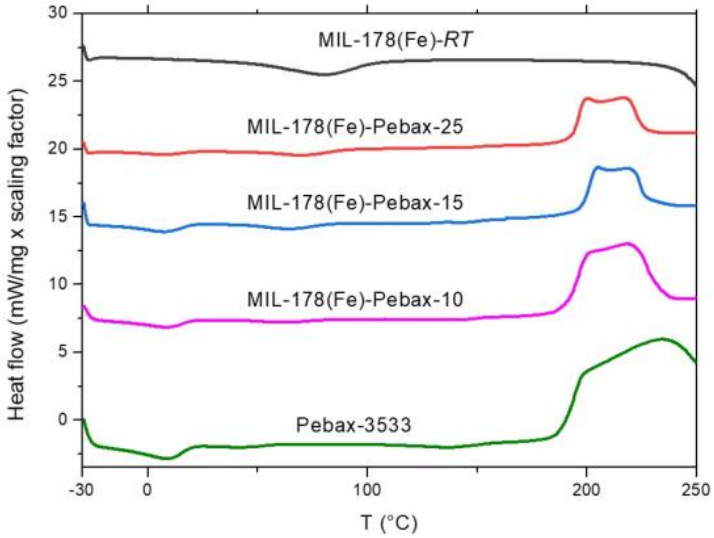

Figure 6.9. DSC curves of neat Pebax®-3533 and typical MIL-178(Fe)-Pebax-X MMM. The curves are shifted vertically for clarity

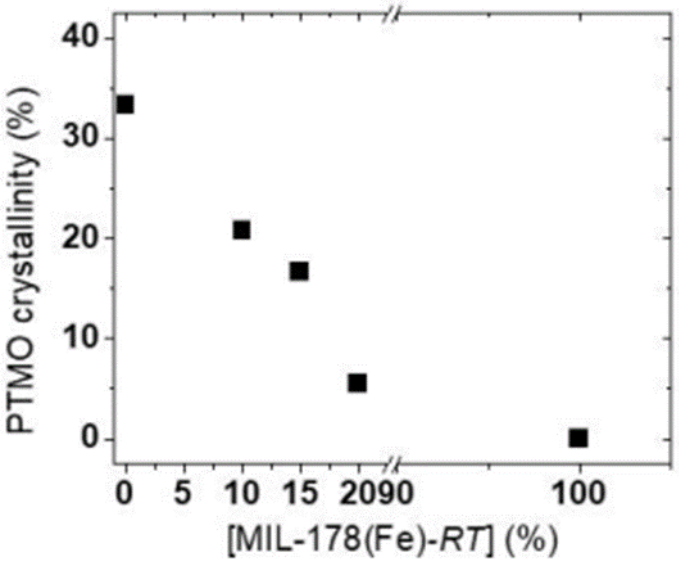

Figure 6.10. Crystallinity degree of PTMO as a function of the content of MIL-178(Fe)-RT

Therefore, the addition of MIL-178(Fe) fillers to Pebax® 3533 induces the presence of a larger amount of flexible PTMO chains. This is consistent with the mechanical properties of the membranes that were characterized at large deformation by performing tensile tests until failure**. Figure 6.11** shows the stress-strain curves for the MIL-178(Fe)-Pebax-X MMMs with X=10 and 15 in comparison to the pure Pebax® 3533 matrix. **Table 6.1** provides the values of the Young's modulus (E), the stress at break (σ_{break}) and elongation at break (e_{break}). Compared to the pure Pebax® 3533 matrix, the mechanical properties of MIL-178(Fe)-Pebax-X MMMs are significantly enhanced.

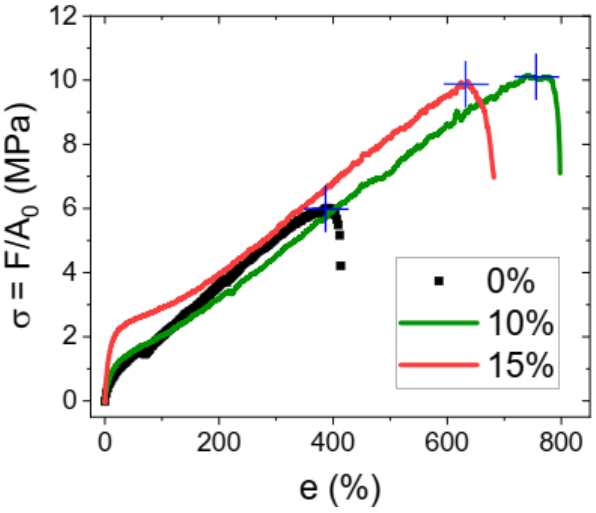

Figure 6.11. Representative stress-strain curves obtained by tensile testing to failure for MIL-178(Fe)-Pebax-X (X= 10 and 15 wt%) MMMs and a pure Pebax® 3533 membrane (X=0). The blue crosses indicate the position considered for the sample failure

Table 6.1. Young moduli (E), Stress at break (σ_{break}) and elongation at break (e_{break}) of the MIL-178(Fe)-Pebax-X MMMs with X = 10 and 15wt.% and of a pure Pebax® 3533 membrane (X=0).

Membranes	**E, MPa**	**σ_{break}, MPa**	**e_{break}, MPa**
Pebax 3533	5.5	6	394
MIL-178(Fe)-Pebax 3533-10	7.1	10.1	758
MIL-178(Fe)-Pebax 3533-15	17.2	9.8	632

These materials are much more extensible which is consistent with the presence of a larger amount of rubbery PTMO phase as shown by DSC. Note that the deformability of MIL-178(Fe)-Pebax-15 is slightly lower than that of MIL-178(Fe)-Pebax-10. This can be imparted by the increasing amount of MIL-178(Fe) particles that can act as reinforcing fillers of the polymer as is also shown by the higher value of Young's modulus of MIL-178(Fe)-Pebax-15 in comparison to those of the other MMMs. Finally, the long-term chemical stability of the MIL-178(Fe)-Pebax-X MMMs with X=10, 15 and 25 was confirmed by recording PXRD and FT-IR experiments after

ageing the composite membranes under humid ambient air for about 8 months, with no evidence of structural evolution (see **Figure 6.12**).

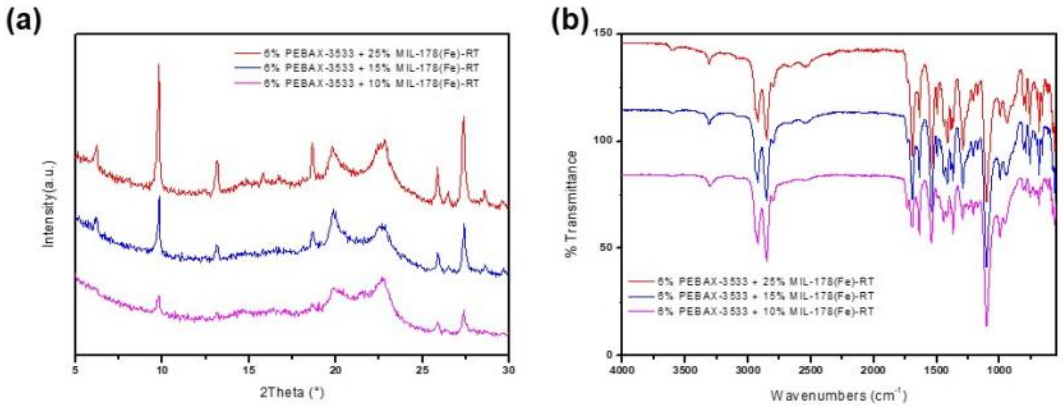

Figure 6.12. (a) PXRD pattern and (b) FT-IR spectra MIL-178(Fe)-Pebax-X (X= 10, 15 and 25 wt.%) MMMs after ageing under humid ambient conditions for 8 months.

6.3.2 CO_2 separation analysis

Gas separation measurements were carried out by feeding the post-combustion gaseous mixture of CO_2/N_2 (15/85 cm^3(STP) min^{-1}) at an operating pressure of 3 bars to the feed side at 35 °C. A schematic representation of the GC module is given in **Figure 3.5**. **Figure 5.7** and **Table 6.2** show the CO_2 permeability and CO_2/N_2 selectivity of MIL-178(Fe)-Pebax-X MMMs and pure Pebax® 3533. Remarkably, the addition of MIL-178(Fe) to Pebax® 3533 up to 10 wt. % of MIL-178(Fe) led to a significant increase of both the CO_2 permeability and CO_2/N_2 selectivity. The CO_2 permeability of MIL-178(Fe)-Pebax-10 (165 ± 4 Barrer) increased by a factor of 2 compared to the pure Pebax® 3533 (83 ± 6 Barrer) while the CO_2/N_2 selectivity of MIL-178(Fe)- Pebax-10 (16.0 ± 0.7) was improved by about 80 % in comparison to the pure polymer (9.0 ± 0.7). Further increase of MIL-178(Fe) content to 15 wt. % led to membranes with the highest CO_2 permeability (210 ± 15 Barrer) at the expense of a slight decrease of the CO_2/N_2 selectivity (14.0 ± 0.7). These results indicate that the inclusion of MIL-178(Fe) fillers in the Pebax® 3533 matrix can induce a high increase of both permeability and CO_2/N_2 selectivity values up to about 160 % and 80 %, respectively in comparison to the bare membranes. The promising performance of these MMMs can be explained by the high CO_2/N_2 selectivity of the bare MIL-178(Fe) and the good compatibility of the MOF filler with the polymer matrix. Moreover, the ultra-micropores of MIL-178(Fe) are presumably fully accessible to CO_2 molecules since the penetration of polymer chains is not likely to occur in the MOF channels (ϕ< 4.5 Å).

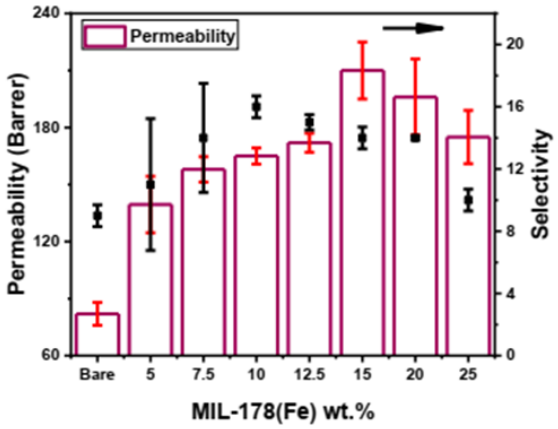

Figure 6.13. Permeation analysis of MMMs and their comparison with bare polymer membrane

Table S5.2. Permeation analysis results of the membranes with filler loading in the polymer matrix

MIL-178(Fe) load (wt. %)	**P CO_2 (Barrer)**	**Selectivity (CO_2/N_2)**
0	82 ± 6	9 ± 0.7
5	140 ± 15	11 ± 4
7.5	158 ± 7	14 ± 3.5
10	**165** ± 4	**16** ± **0.7**
12.5	172 ± 5	15 ± 0.5
15	210 ± 15	14 ± 0.7
20	196 ± 20	14 ± 0.1
25	175 ± 14	10 ± 0.7

To shed light on the solubility and diffusivity contributions of the gas permeation results, time lag experiments were carried out to obtain CO_2 and N_2 single gas permeabilities, and subsequently CO_2 and N_2 diffusivities and solubilities. It is worth to mention that CO_2 permeability and CO_2/N_2 selectivity values of bare membrane and MMM obtained by time lag and mixture separation analyses are in good concordance, as shown in **Table 6.3**. Time lag experiments have demonstrated that the inclusion of the MOF in the polymer increases the CO_2 solubility (**Table 6.3**). CO_2 solubility values are $7.3 \cdot 10^{-2}$ and $3.3 \cdot 10^{-1}$ (cm^3(STP)/($cm^3 \cdot$cmHg)) for the pure polymer membrane and the MIL-178(Fe)-Pebax-10 MMM, respectively. On the contrary, the CO_2 diffusivity decreases (and so does the N_2 diffusivity) from the pure polymer to the MIL- 178(Fe)-Pebax-10 MMM from $1.3 \cdot 10^{-7}$ to $3.8 \cdot 10^{-8}$ cm^2/s, in agreement with the narrow microporosity of MIL-178(Fe) and the tortuosity created in the MMM by the addition of the filler particles. Therefore, the enhanced permeability of MMM in comparison to the pure Pebax® 3533 can be partly explained by the increased content of the more permeable amorphous PTMO (lower crystallinity degree) as it was previously reported for a few MOF-Pebax MMMs [190].

Table 6.3. CO_2/N_2 permeation results at 35 ºC for pure Pebax® 3533 membrane and MIL-178(Fe)-Pebax -10 MMM. Comparison between single gas permeabilities (time lag) and 15/85 CO_2/N_2 mixture permeabilities and the corresponding CO_2/N_2 ideal and separation selectivities.

	Pure Pebax® 3533		**Pebax-10**	
Parameters	**GC results**	**Time lag results**	**GC results**	**Time lag results**
CO_2 Permeability (Barrer)	83 ± 6	96	165 ± 4	126
CO_2 Diffusivity (cm^2/s)		1.3×10^{-7}		3.8×10^{-8}
CO_2 Solubility ($cm^3(STP)/(cm^3\ cmHg)$)		7.3×10^{-2}		3.3×10^{-1}
N_2 Permeability (Barrer)	9.2	9.5	10.3	6.9
N_2 Diffusivity (cm^2/s)		1.1×10^{-6}		3.9×10^{-7}
N_2 Solubility ($cm^3(STP)/(cm^3\ cmHg)$)		8.2×10^{-4}		1.7×10^{-3}
Selectivity (CO_2/N_2)	9 ± 0.7	10	16 ± 0.7	18

6.4 Conclusions

A new water stable 1D microporous coordination polymer, MIL- 178(Fe), was applied, presenting interesting features for CO_2 capture such as hydrothermal and thermal stability as well as ultra-micropores decorated with polar OH groups acting as CO_2 adsorption sites. This material was synthesized through an easily-scalable and environmentally friendly protocol with nontoxic reactants, allowing to achieve the production of a large amount of this material with high yield. Monodisperse MIL-178(Fe) sub-micrometer sized particles were synthesized at room temperature and were used for the preparation of MMMs. MIL-178(Fe) presents a moderate CO_2 adsorption capacity at low pressure but retains a high CO_2/N_2 adsorption selectivity in the 1-3 bar pressure range due to the high affinity of CO_2 molecules toward μ_2-OH groups located on corner-sharing Fe octahedra chains. MMMs based on MIL- 178(Fe) and the Pebax® 3533 elastomer with a MIL-178 (Fe) loading up to 25 wt. % were cast, showing significantly enhanced CO_2/N_2 separation performance in comparison to the pure Pebax® 3533. Such results are likely due to the excellent dispersion of MIL-178(Fe) particles in the polymer matrix with the absence of any interfacial micro-voids defects, the enhancement of the MMM CO_2 solubility as well as the lower crystallinity degree of the Pebax matrix in comparison to the pure polymer.

Chapter 7: Optimization of MIL-178(Fe) and Pebax® 3533 loading in mixed matrix membranes for CO_2 capture

Outlines

Reproduced from "M.R. Hasan, H. Zhao, N. Steunou, C. Serre, M. Malankowska, C. Téllez, J. Coronas, Optimization of MIL-178(Fe) and Pebax® 3533 loading in mixed matrix membranes for CO_2 capture, Int. J. Greenh. Gas Control 121 (2022). https://doi.org/10.1016/j.ijggc.2022.103791" with permission from Elsevier Ltd.

7.1 Introduction

Anthropogenic activities necessitate substantial amount of fossil fuels which produce CO_2 with a 6% increment every year [138] causing global warming and unpredictable climatic changes to the environment. To mitigate such a drastic effect on the atmosphere, it has been agreed to limit the global temperature rise below 2 °C (Paris conference in 2015 [140], confirmed at the Glasgow COP26 in 2021 [159]).

Membranes of Pebax copolymers are interesting for CO_2 separation application since they consist of both glassy and rubbery segments, which offer high permeability for polar gases[194]. Additionally, MMMs show improved separation, mechanical and thermal properties, which enable them to be used as potential candidates for CO_2 separation [195]. Among all Pebax® codes, Pebax® MH 1657 is interesting for MMMs fabrication towards CO_2 separation application due to better selectivity, but its affinity to water may restrict its application under humid conditions (since coal-derived flue gases often contains oxygen, SO_x, NO_x and other minor components like water vapor) [196]. However, Pebax® 3533 is another interesting block copolymer composed of 75 wt.% of PE and 25 wt.% of PA. Due to its high solubility in alcoholic solvents (less polar in nature than water), this polymer would be prone to exhibit a long-term stability and durability under humid conditions and it has shown good performance in the separation of CO_2 containing mixtures [83,87].

MIL-178(Fe), a recently reported one dimensional Fe (III) based PCP whose combination with Pebax® 3533 leads an efficient membrane for CO_2 capture [83]. The reported MMMs were prepared at room temperature and were found mechanically stable with about 80 % improvement in terms of CO_2/N_2 selectivity (16.0 ± 0.7) compared to bare membrane (9.0 ± 0.7). More detailed investigation and optimization of the Pebax® 3533 and MIL-178(Fe) is interesting, since, for instance, solvent evaporation condition can alter gas separation performance, which was reported by Karamouz et al. [197]. Additionally, Martinez-Izquierdo et al. reported that a proper polymer concentration in the membrane casting solution can significantly improve CO_2 separation performance [152]. Moreover, filler loading in the MMM has a direct effect on the gas separation performance [160], as well as the use or ionic liquids [198] or the blending of Pebax® with other polymers [199], among other improvement options.

The objective of this chapter is to understand the impact of polymer-filler composition and drying conditions of MIL-178(Fe)/ Pebax® 3533 MMMs on CO_2 separation performance. For that purpose, we focus on the optimization of the MIL-178(Fe) and Pebax® 3533 concentration in MMMs for an efficient capture of CO_2 from both CO_2/N_2 and CO_2/CH_4 gas mixtures.

7.2 Experimental methods

7.2.1 Materials

Pebax® 3533 (75 wt.% poly (tetramethylene oxide) (PTMO) and 25 wt.% aliphatic polyamide (PA12)) in the form of pellets was kindly provided by Arkema, France. Solvents, 1-propanol (Labbox, 99%) and 1-butanol (Scharlab, 99%) were used as received. MIL-178(Fe) was kindly provided by our French collaborator (research

group of Profs. Nathalie Steunou and Christian Serre), which was prepared at RT from anhydrous $FeCl_3$ (Sigma Aldrich, 99%) and 1,2,4-benzene tricarboxylic acid (Sigma Aldrich, 95 %) by Benzaqui et. al. [72]. All research grade gases (greater than 99.995% of purity) used for the separation experiment were supplied by Abelló Linde S.A., Spain.

7.2.2. Membrane fabrication

Pebax® 3533 matrix-based membranes were fabricated following procedure explained in section 3.2.1. Wherein, 1-propanol/1-butanol (75/25 (v/v)) used as solvent for membrane fabrication. Drying of the membranes were permormed at 40 ºC for 24 h. Identification names of the fabricated membranes are given in **Table 7.1**.

Table 7.3. Membranes fabricated for this study.

Name	*Membrane type*	*Description*	*Thickness (µm)*
M1	Bare polymer	1 wt. % of Pebax® 3533	38 ± 2
M2	Bare polymer	2 wt. % of Pebax® 3533	55 ± 4
M3	Bare polymer	3 wt. % of Pebax® 3533	75 ± 5
M4	Bare polymer	4 wt. % of Pebax® 3533	88 ± 4
M5	Bare polymer	5 wt. % of Pebax® 3533	110 ± 5
M6	Bare polymer	6 wt. % of Pebax® 3533	128 ± 6
M5.3	MMM	5 wt. % of Pebax® 3533 + 3 wt. % MIL-178(Fe)	114 ± 3
M5.5	MMM	5 wt. % of Pebax® 3533 + 5 wt. % MIL-178(Fe)	116 ± 8
M5.10	MMM	5 wt. % of Pebax® 3533 + 10 wt. % MIL-178(Fe)	119 ± 4
M5.15	MMM	5 wt. % of Pebax® 3533 + 15 wt. % MIL-178(Fe)	123 ± 6

7.2.3 Characterization

Characterization techniques used for membranes and fillers are explained in chapter 3 (section 3.4 and 3.5). Apart from those, zeta potential of the membrane was measured by an alectrokinetic analyzer (SurPass 3, Anton Paar). The membranes were cut in the form of a rectangle (2 cm x 1 cm) and placed inside the SurPass flow cell. SMART L Fungilab rotational viscometer was used to investigate viscosity of the polymer solutions.

7.3 Result and discussion

7.3.1 Characterization of MOFs and membranes

Surface and cross section SEM images of bare polymeric membranes in **Figures 7.1 (A) and (D)** reveal the fabrication of defect free membranes. Similarly, cross section SEM images of MMMs consisting of MIL-178(Fe) within polymer matrix are represented in **Figure 7.1 (B)** and **7.1 (E)**, correspondingly. These images show the

presence of MIL-178(Fe) particles in the matrix and proper filler-polymer interaction. SEM and TEM images of MIL-178(Fe) (**Figures 7.1 (C)** and **7.1 (F)**). Additionally, cross-section images of the MMMs (M5.5, M5.10, M5.15) have been provided **Figure 7.2 (A) – C))**, where agglomeration tendency of fillers in the membranes intensified with an increase of the fillers dose.

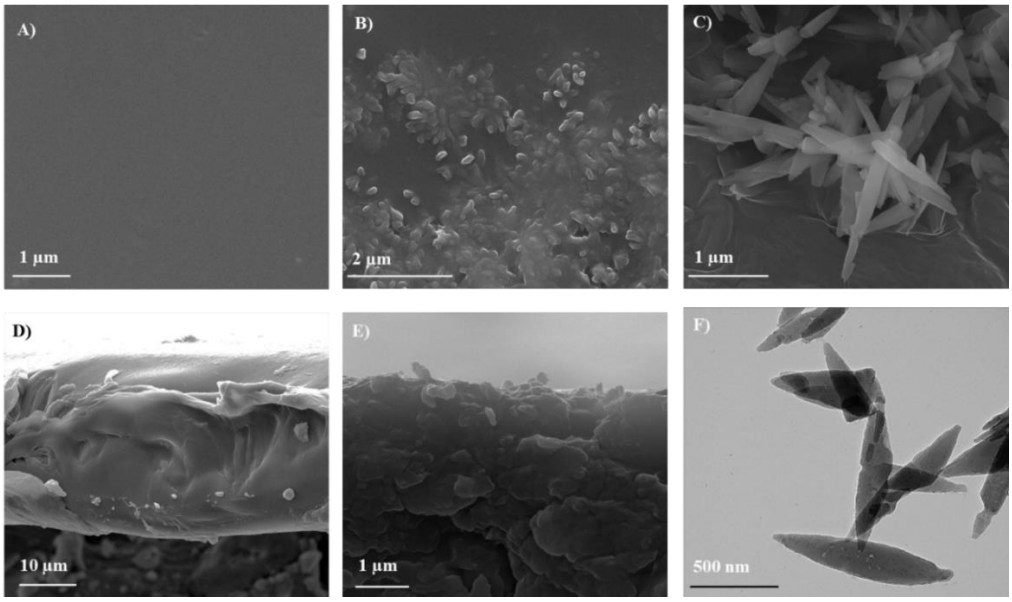

Figure 7.1. SEM images of: A) top surface of bare membrane (M5), B) top surface of MMM (M5.5), C) SEM image of MIL-178(Fe), D) cross-section image of bare membrane (M5), E) cross-section image of MMM (M5.5), and F) TEM image of MIL-178(Fe).

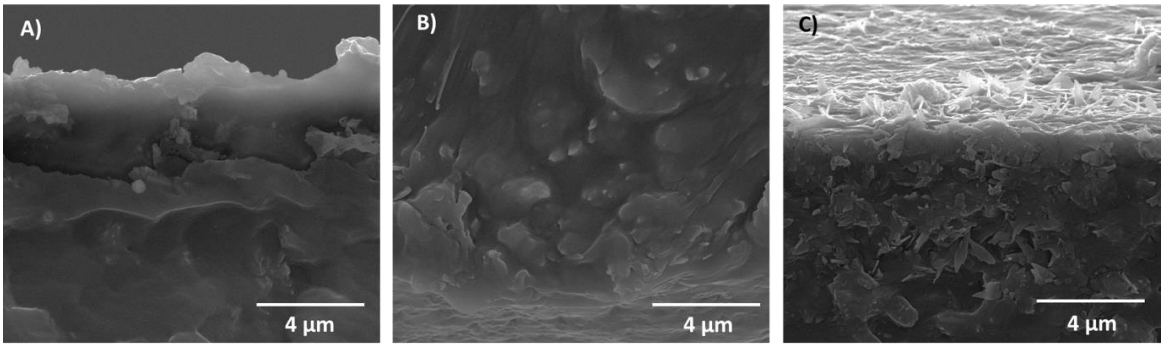

Figure 7.2. Cross-section SEM images of MMMs: A) M5.5, B) M5.10 and C) M5.15.

Moreover, zeta potential of the membranes was performed (shown in **Figure 7.3**), which reveals change of the surface charge over increase of pH. At lower pH, 3 wt. % and 5 wt. % filler load (M5.3 and M5.5) filler dose showed higher zeta potential than bare membrane (M5). Whereas, 10 wt. % filler dose (M5.10) showed reduced zeta potential than M5.5, but that value is still slightly higher than bare membrane. However, for 15 wt. % of the filler dose (M5.15), zeta potential result is even lower than for the bare membrane. Such changes suggest agglomeration tendency of the fillers at their higher dose, which reduces surface charge of the membrane, consequently, zeta potential being reduced.

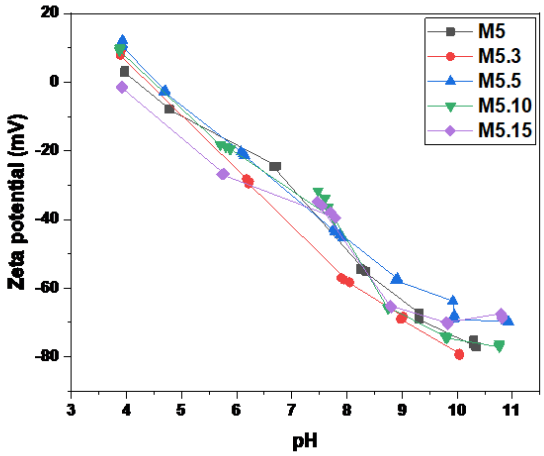

Figure 7.3. Zeta potential response of the membranes over increase of pH

Powder X-ray diffraction (PXRD) diffractogram of MIL-178(Fe) (**Figure 7.4 (A)**) is fully consistent with that previously reported by Benzaqui et al. [83]. PXRD diagrams of bare membrane and MMM show the concomitant presence of diffraction peaks of both the Pebax® 3533 and MIL-178(Fe) (**Figure 7.4 (A)**). This is consistent with the preservation of the crystallinity of the PCP once combined with the polymer. TGA of MIL-178(Fe) shows an early weight loss (4 wt. % of the total weight) bellow 100 °C due to the removal of moisture (**Figure 7.4 (B)**). Rapid degradation of the MOF is observed after 350 °C due to the thermal decomposition of MIL-178(Fe) which results in a ca. 18 wt. % residue of the initial weight which corresponds to the oxidation of the iron of the MOF structure to Fe_2O_3, as previously shown [83]. Bare polymeric membranes (M5) are found stable up to 220 °C, then they undergo thermal degradation (**Figure 7.4 (B)**). However, the thermal stability of the polymer matrix is improved upon the incorporation of MIL-178(Fe) since the TGA curves of MMMs (M5.3, M5.5, M5.10 and M5.15) clearly show their early stage stability beyond 300 °C. Additionally, an increase of fillers content in the membranes augments the quantity of residues, M5.5 and M5.15 producing residues of 2 wt. % and 3 wt. % of the initial wt., respectively.

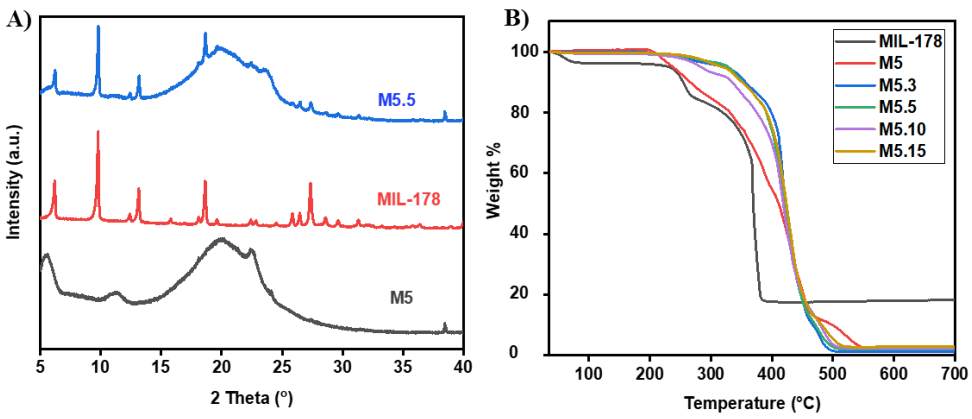

Figure 7.4. A) XRD diffractograms of bare polymer membrane, MIL-178(Fe) and MMM M5.5. B) TGA of MIL-178(Fe), bare polymer membrane and MMMs.

7.3.2 Gas permeation measurements

Gas permeation experiments were performed for two different gas mixtures (CO_2/N_2 and CO_2/CH_4) at the prescribed experimental conditions. Detailed interpretation of the acquired data is discussed in the subsequent sections.

7.3.2.1 CO_2/N_2 permeation measurement

We previously demonstrated that a MMM with 6/94 wt. % of Pebax® 3533/solvent in the casting solution (3 g total weight basis and drying condition at RT) and 10/90 wt. % MIL-178(Fe)/polymer produced maximum CO_2/N_2 selectivity, whereas a 15 wt. % MIL-178(Fe) loading showed best CO_2 permeability, although the polymer concentration was not optimized [83]. Since Martinez-Izquierdo et al. reported the effect of polymer concentration in bare membrane on CO_2 separation performance [152], this work focuses on, firstly, the optimization of the polymer matrix concentration and, secondly, the optimization of filler content to obtain membranes with better gas separation performance. In consequence, a set of bare membranes of different polymer concentrations was investigated for gas separation (see **Table 7.1**), while their performances are shown in **Figure 7.5 (A)**. In the current study, the total weight basis (of material to cast the membranes) has been changed from 3 g to 10 g, consequently the polymer content increased more than three times, resulting in thicker membranes that are expected to contain a low amount of defects. Besides, membranes prepared from low polymer concentrations (e.g. 1 wt. %) are thinner (see **Table 7.1**) due to the fact that the amount of casting solution is always the same, limited by the Petri dish volume. In any event, this higher amount of casting solution allows to enhance the separation performance of the polymer, as shown below. In these conditions, the permeation analysis with such membranes revealed that the bare membrane corresponding to 5 wt. % of polymer composition (named as M5) performs better in terms of both CO_2 permeability and CO_2/N_2 selectivity which are 277 Barrer and 20, respectively. An increasing trend of permeability and selectivity was observed for pristine membranes having polymer content from 1 wt. % to up to 5 wt. % (CO_2 permeability augments from 205 ± 4 Barrer to 277 ± 8 Barrer and CO_2/N_2 selectivity from 16 ± 1 to 20 ± 1.1). However, beyond this, both parameters showed a significant downturn to 262 ± 6 Barrer and 17.0 ± 2.0 (for M6). However, in the Chapter 6, the permeation performance of a 6 wt.% Pebax® 3533 bare membrane (on 3 g total wt. basis and dried at RT) corresponded to a CO_2 permeability of 83 ± 6 Barrer and a CO_2/N_2 selectivity of 9 ± 0.7 [200]. Such an increase of Pebax® 3533 content in bare membranes improves CO_2 separation in terms of both CO_2 permeability and CO_2/N_2 selectivity is justified by Kline. et al. where they have reported, increasing PEO unit content significantly improves CO_2 separation because of its unique affinity for CO_2 due to the interaction of polar ethylene oxide units with the high quadrupole moment of the highly polarizable CO_2 molecule [201]. Another empirical difference was related to the membrane drying temperature, being it RT in previous work [200]. With all these modifications (see **Table 7.2**), M5 having a higher polymer loading and improved drying condition at 40 ºC in the oven for 24 h allowed the achievement of a better CO_2

separation. Additionally, the viscosity of the polymer solution of the bare membranes (M3 to M6) was measured at 25 ºC (**Figure 7.6**). The sharp rise of polymer viscosity from membrane samples M5 to M6 suggests that a higher homogeneity in the filler distribution will be achieved in the MMMs with the 5 wt. % polymer concentration. This agrees with what was observed by Martinez-Izquierdo, who also found that when there is a sudden increase in viscosity with the Pebax® MH 1657 solution concentration the CO_2 separation properties of the membrane were markedly worsened in terms of permeation and selectivity due to changes in the crystallinity extend of the polymer [152]. Consequently, 5 wt. % polymer content (M5) was considered as the optimum composition and was selected for subsequent MMMs fabrication.

Table 7.2. Main changes in the membrane preparation conditions for optimum Pebax® 3533 membranes in this work and in chapter 6 [199].

	Chapter 6 [199]	***This work***
Polymer + solvent amount	3 g	10 g
Polymer concentration	6 wt. %	5 wt. %
Polymer solution viscosity at 50 r.p.m. and RT	169 mPa·s	72 mPa·s
Drying temperature	RT	40 ºC
Membrane thickness	43 µm	110 µm

Accordingly, in order to optimize the filler concentration in MMMs, a set of MMMs were prepared by dispersing MIL-178(Fe) in 5 wt. % Pebax® 3533 (which are named in **Table 7.1**) and were analyzed to reveal gas separation performance as shown in **Figure 7.5 (B)**. Such MMMs produced improved separation in terms of CO_2 permeability for MMMs M5.3, M5.5 and M5.10 compositions compared to the bare membrane (M5). Although, membranes M5.3 and M5.5 showed similar CO_2 permeability (14 % and 12 % overperformed compared to the bare membrane, respectively) considering both permeability and selectivity, MMM M5.5 outperformed (CO_2 permeability improved by 12 % and CO_2/N_2 selectivity enhanced by 25 %) the bare membrane (M5). On the other hand, 10 and 15 wt. % MIL-178(Fe) based MMMs show a decrease of both selectivity and permeability (with values even smaller than those of the bare membrane M5). Finally, considering both CO_2 permeability and CO_2/N_2 selectivity, M5.5 is the best performing membrane containing MIL-178(Fe) filler and Pebax® 3533 matrix. Membranes with their CO_2/N_2 separation performance and thicknesses are shortlisted in **Table 7.3**. Additionally, aging test (membranes was used for gas separation analysis, then preserved it for subsequent analysis upto 35 days) of the best performed MMM was performed where membrane CO_2 separation performance (both CO_2 permeability and CO_2/N_2 selectivity) slightly deteriorated over time shown in **Table 7.4**.

Table 7.3. Separation of the 15/85 CO_2/N_2 and 50/50 CO_2/CH_4 mixtures at 35 ºC of bare membranes and MMMs.

CO_2/N_2 separation			
Membranes	Thickness (µm)	Permeability CO_2 (Barrer)	Selectivity (CO_2/N_2)
M1	38 ± 2	205 ± 4	16.0 ± 1.0
M2	55 ± 4	214 ± 5	17.0 ± 1.0
M3	75 ± 5	232 ± 4	18.5 ± 0.5
M4	88 ± 4	251 ± 6	18.0 ± 0.7
M5	110 ± 5	277 ± 8	20.0 ± 1.1
M6	128 ± 6	262 ± 6	17.0 ± 2.0
M5.3	114 ± 3	315 ± 7	21.0 ± 1.0
M5.5	116 ± 8	312 ± 5	25.0 ± 0.5
M5.10	119 ± 4	286 ± 9	22.0 ± 1.0
M5.15	123 ± 6	275 ± 8	19.0 ± 0.7
CO_2/CH_4 separation			
Membranes	Thickness (µm)	Permeability CO_2 (Barrer)	Selectivity (CO_2/CH_4)
M5	110 ± 5	259 ± 4	4.6 ± 0.8
M5.5	116 ± 8	295 ± 7	8.7 ± 1.3

Table 7.4. Performance of the MMM (M5.5) over time

CO_2/N_2			
Day	Perm (CO_2) Barrer	Sel (CO_2/N_2)	Condition
1	308	25	Fresh MMM
2	293	24	Membrane removed from module after using 1st day use for 2 h
3	279	22.5	Membrane removed from module after using 2nd day for 2 h
7	272	21	Membrane removed from module after using 3rd day for 2 h
25	257	17.5	Membrane kept in the module after using 7th day for 2 h
30	252	17	Membrane removed from module after using 30th day for 2 h
35	249	17	Membrane from 30th day, dried at 40 ºC for 2 h

Concerning the role of PCP MIL-178(Fe) in the MMM improved separation ability, it has been demonstrated that its structure with narrow pore channels (pore diameter < 0.45 nm) and decorated with polar groups (μ_2-OH and $-CO_2H$ functionalities) favors the selective adsorption of CO_2 and in turn the CO_2 separation ability of the MMMs containing it [83]. In addition, previous time lag experiments depicted an important increase of the CO_2 solubility of the Pebax® 3533 polymer based MMM (by almost x5 when adding a 10 wt. % of the PCP)) when incorporating MIL-178(Fe) [83]. This compensates the loss of CO_2 diffusivity observed giving rise to the increase of separation performance already discussed.

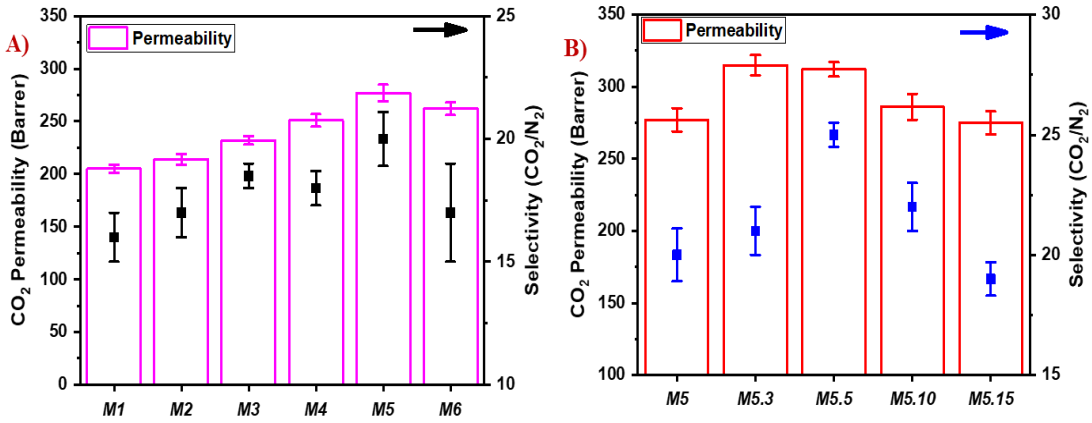

Figure 7.5. Separation of the 15/85 CO_2/N_2 mixture at 35 ºC: A) optimization of polymer concentration, (B) optimization of MMMs.

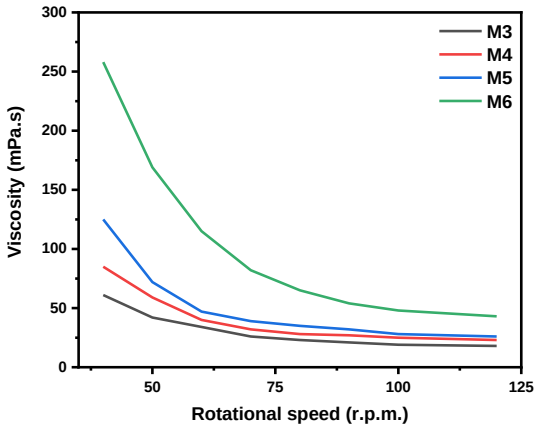

Figure 7.6. Effect of polymer concentration on the viscosity of the polymer solution at RT.

7.3.2.2 CO_2/CH_4 gas permeation measurement

MMM with the optimum concentration of MIL-178(Fe) (5 wt.%) and Pebax® 3533 was investigated for CO_2/CH_4 separation. The MMM (M5.5) was efficient and outperformed the bare membrane (M5) (**Table 7.3 and Figure 7.7**. This MMM was found to improve the CO_2 permeability and CO_2/CH_4 selectivity by 14 % and 89 %, respectively, in comparison to the bare membrane (M5). CO_2 permeability and CO_2/CH_4 selectivity of the bare membrane were 259 ± 4 Barrer and 4.7 ± 0.8,

respectively, whereas, for MMM both parameters were 295 ± 7 Barrer and 8.7 ± 1.3, respectively. Even if CH_4 (kinetic diameter of 0.38 nm) is a larger molecule than N_2 (0.364 nm) and CO_2 (0.33 nm), which would penalize its diffusivity through the membrane (particularly when filled it with the narrow pore material MIL-178(Fe)), the expected larger CH_4 membrane solubility (probably increased in the MMM by the PCP) due to its easy condensability reduces the separation selectivity of CO_2/CH_4 as compared to that of CO_2/N_2. However, comparison of the current CO_2 separation performance with literature which is presented in **Table 7.5**. Moreover, CO_2 separation performance of the MMM is compared with Robeson's upper bound 2008 which is presented in **Figure 7.8**

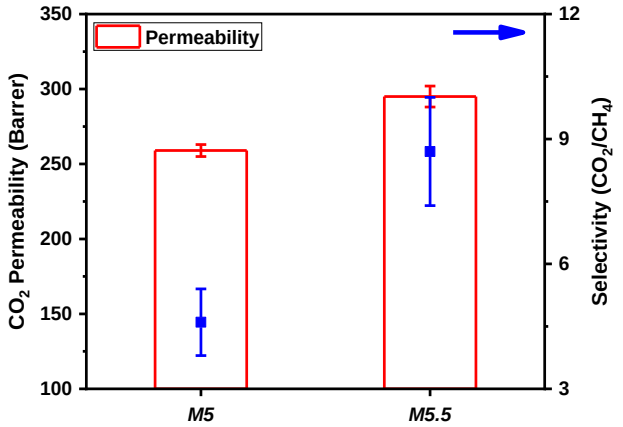

Figure 7.7. Separation of the 50/50 CO_2/CH_4 mixture at 35 ºC: MMM vs bare membrane.

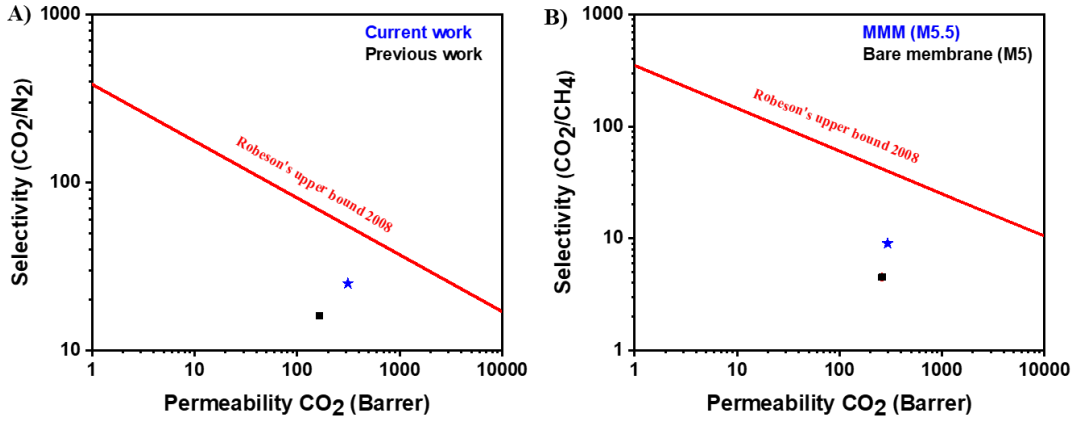

Figure 7.8. Separation performance of the membranes with respect to Robeson's upper bound 2008 [29] : A) for CO_2/N_2 and B) for CO_2/CH_4 separation.

Table 7.5. Comparison of the CO_2/N_2 selectivity and CO_2/CH_4 selectivity of current work with literature for different materials

Material	**CO_2/N_2 selectivity**	**Reference**
ZIF-94	36 (308 K)	[160]
IITKGP-13A	47 (295 K)	[202]
BUT-11 (AcOH)	24.1 (298 K)	[203]
PCN-61	15 (298 K)	[204]
MIL-96(Al)	36 (303 K)	[205]
PCN-80	12 (296 K)	[206]
Zn_2(BTetB)(py-CF3)2	37 (298 K)	[207]
Cu-BTC	20 (298 K)	[208]
ZIF-8(Zn)	8 (298 K)	[143]
MIL-178 (Fe)	16 (308 K)	[200]
Cu-BTC-S1	18.5 (303K)	[209]
MOF-74	21 - 28 (298K)	[210]
PCP (MIL-167)	25 (308 K)	**(Current work)**
Material	**CO_2/CH_4 selectivity**	**Reference**
ZIF-8	19.6 (308 K)	[211]
ZIF-8	8-9 (298 K)	[91]
ZIF-8 (s)	5 (298 K)	[212]
Cu-BTC-S1	23.5 (303)	[209]
MOF-74	14 - 19 (298K)	[210]
PCP (MIL-167)	9 - 11 (308 K)	**(Current work)**

7.4. Conclusion

Porous coordination polymer MIL-178(Fe) was incorporated in Pebax® 3533 matrix after the optimization of the polymer concentration to achieve an efficient CO_2/N_2 separation. MIL-178(Fe) is compatible with the polymer, thus defect free MMMs with good filler distribution were obtained as confirmed by SEM analysis. An optimized bare polymer membrane (5 wt.% of Pebax® 3533) was prepared by finely tuning different parameters such as the polymer solution viscosity, membrane thickness and drying conditions. This gave rise to an efficient gas separation performance with CO_2 permeability and CO_2/N_2 selectivity of 277 ± 8 Barrer and 20.0 ± 1.1, respectively. These conditions for the preparation of the bare membranes constituted the starting point for the preparation of MMMs. In consequence, the optimum loading of filler was obtained at 5 wt.% in the best matrix composition. This MMM outperformed the bare membrane in terms of both CO_2 permeability (312 ± 5 Barrer) and CO_2/N_2 selectivity (25.0 ± 0.5) by 12 % and 25 %, respectively. Interestingly, MIL-178(Fe) improved the separation performance of the MMM due to its chemical composition (with polar CO_2-philic groups) and narrow microporosity (pore diameter < 0.45 nm) which increases the CO_2 solubility of the Pebax® 3533 polymer based MMM, compensating the loss of CO_2 diffusivity. Additionally, the optimized MMM was applied for CO_2/CH_4 separation and compared with the bare polymer membrane where MMM was also found efficient to improve the CO_2 permeability and CO_2/CH_4 selectivity (lower than that corresponding to the CO_2/N_2 mixture because of the CH_4 large condensability as compared to that of N_2) by 14 % and 89 %, respectively.

Chapter 8: Summary and Conclusions

8.1 Summary

In recent years, membrane technologies are becoming an attractive solution for CCS applications, due to their low carbon footprint, economical feasibility, ease of operation and scale-up possibility. Within the available membrane technologies, their applications towards gas separation gaining commercial maturity and scientific verification are investigated in this doctoral thesis.

Within the available processes for gas separation, the separation of CO_2 has become one of the key goals to be achieved due to its great importance in the current climate crisis. Additionally, such membranes can be applicable to upgrade natural gas streams, especially those extracted from a depleting mine, since the CO_2 content increases in the production stream over the exhaustion of the resource (mines). The limitation of persisting membranes includes: their stability, durability, adaptation at the operating conditions, gas separation efficiency, etc. Therefore, an improvement in the membrane performance dealing with CO_2 separation is still a great scope of research.

Inter-chain free volumes resulted from cross-linking of polymer chains increase permeability of gases whose dimension is compatible with the membrane pores. Generally, an increase in temperature increases permeability of all gases of the feed, which results in a membrane to underperform. Additionally, such membranes can be affected by plasticization while CO_2 capture, which influences further reduction of the membrane separation performance. The most interesting membranes for CO_2 separation applications are the so-called MMMs ("mixed matrix membranes"), comprised of a polymeric continuous phase and a nano-scale dispersed phase. MOFs are a class of nano-fillers very interesting for MMM fabrication due to their exceptional characteristics such as crystallinity, their high specific surface area, adsorption capacity, molecular sieving ability, flexibility, functionalization capacity and their organic-inorganic character that allows them to have greater affinity to polymeric compounds than an inorganic nanoparticle. In this context, this doctoral thesis aimed to develop membranes using MOF based MMMs towards gas separations.

There are several MOFs available for MMMs fabrication, which are found promising for CO_2 separation application. Due to an intensive impact of the waste chemicals produced from synthesis process, to the environment, the first aim attempted to reuse them (mother liquor) to ensure a green synthesis approach (in terms of lower environmental impact). Such approach also increased MOFs conversion efficiency from their raw chemicals. As a case study (chapter 4), this research aimed to synthesise ZIF-94 in green manner, wherein ZIF-94 obtained from recycling of mother liquor was incorporated in a membrane (Pebax® MH 1657 as a polymer matrix) and compared with freshly synthesised ZIF-94. These membranes were tested in the separation of CO_2/N_2 gas from their mixture. Where both classes of ZIFs were found comparable in terms of their effect in MMMs towards CO_2 separation application. In the same line, chapter 5 was devoted to recycling of MMM to extract its key components (MOF and polymer) and reused them in MMMs

Another the promising filler called MIL-178(Fe), which is one-dimensionaland has a high CO_2 absorption capacity, was studied, firstly to check its adaptability in

MMMs with Pebax® 3533 which was tested in the separation of CO_2/N_2 gas from their mixture (chapter 6). The performance of MIL-178(Fe) was compared with the theoretically possible separation performance. The optimization of the composition was carried out (Pebax® 3533 and MIL-178 (Fe)) in chapter 7, since, as literature suggests, polymer and fillers composition have intensive impact on the gas separation performance. These membranes were tested in the separation of CO_2/N_2 and CO_2/CH_4 from their mixtures, which is interesting for CO_2 separation application and natural gas upgrading.

The main conclusions drawn are detailed below.

8.2 Conclusions

The purpose of this thesis was to investigate MOF-based mixed matrix membranes and to apply them for gas mixture separation. As part of the research plan, the project was divided in several chapters. Recycling of mother liquor to increase ZIF-94 production efficiency as well as to decrease environmental impact was found a promising study. Both fresh and recycled ZIF-94 was found comparable in MMM to separate CO_2 from a mixture of CO_2/N_2. Additionally, MILs another class of trivalent cation-based MOFs are widely applied in photocatalysis are for the very first time applied in CCS application. In this sense, MIL-178(Fe) was investigated with Pebax® 3533 to fabricate MMM, which was found efficient in the separation of CO_2/N_2 and CO_2/CH_4 from their mixtures, which is interesting for CO_2 separation application and natural gas upgrading. Moreover, this thesis aimed towards reduction of carbon footprint raised from disposal of ZIF-94 based MMMs by isolating both components (filler and matrix). Moreover, these recycled components are found compatible in MMMs which were efficient to separate CO_2 from a mixture of CO_2/N_2. The most relevant conclusions are presented below for each of the results chapters.

Synthesis of ZIF-94 from recycled mother liquors: study of the influence of its loading on post-combustion CO_2 capture with Pebax® based mixed matrix membranes

- A synthesis methodology was developed to produce ZIF-94 nanocrystals from recycling of its mother liquors, wherein two key parameters were modified: pH and temperature.
- In all the conditions pure, crystalline ZIF-94 was obtained.
- The most promising results, considering crystallinity, yield of the reaction and BET specific surface area, were obtained when both, the initial synthesis (BET: 463 m^2/g, particle size: 43 nm) and the mother liquor (Product A.4; BET: 483 m^2/g; particle size: 34 nm), were carried out at pH = 10.
- After the successful synthesis of ZIF-94 from the recycled mother liquors, the fabrication of a defect-free mixed matrix membrane was successfully conducted with Pebax® MH 1657 as a continues phase and synthesized ZIF-94 as a dispersed phase.

- ZIF-94 fillers obtained at different conditions, having different particle sizes and slightly different BET specific surface area values, were incorporated inside the polymeric membrane and the resulted MMMs were applied for the CO_2/N_2 separation.
- The optimum composition of MMMs was found to be 9 wt. % Pebax® MH 1657 and 10 wt. % ZIF-94 loading.
- ZIF-94 of ca. 180 nm in particle size was found to be the best filler in terms of selectivity 36 ± 7 and permeability 137 ± 31 Barrer, whereas ZIF-94 of ca. 40 nm produced maximum permeability of 150 ± 7 Barrer (with selectivity of 28 ± 4).
- What was said above suggests that the fabricated membranes were found to be stable at the operating condition since no damage, cracks or non-selective gaps in the membrane was observed.

Study on the recycling of zeolitic imidazolate frameworks and polymer Pebax® MH 1657 from their mixed matrix membranes applied to CO_2 capture

- In this work, a methodology was developed to recycle ZIF-94 and Pebax® MH 1657 from their MMM with a recovery yield of 97.8 ± 0.5 % for polymer and 76 ± 2.5 % for ZIF-94. This method was also applicable for the recycling of ZIF-8 with a recovery yield of 74.8 ± 4.0 %.
- The recycled nanocrystals were undistorted in terms of size, shape and crystallinity. Fresh and recycled ZIF-94 have comparable BET SSA values, those are 427 ± 7 m^2/g and 412 ± 6 m^2/g respectively. Moreover, particle diameters were 148 ± 44 nm and 164 ± 32 nm respectively (within the experimental error).
- Similarly, fresh ZIF-8 and recycled ZIF-8 show BET specific surface areas of 1507 ± 30 m^2/g and 1325 ± 26 m^2/g, respectively, and their mean particle sizes correspond to 120 ± 30 nm and 110 ± 20 nm respectively.
- The MMMs containing recovered MOFs and fresh polymer matrix produced an acceptable gas separation performance with CO_2 permeability and CO_2/N_2 selectivity of 174 ± 3 Barrer and 25.6 ± 0.6, respectively. These values are comparable to those achieved with MMMs obtained from totally fresh MOF and polymer materials (permeability of 134 ± 6 Barrer and selectivity 29 ± 0.8).
- The previous parameters suggest successful recovery of precious components (MOFs) from MMMs. Although, recycled materials are found compatible in MMMs, still, estimation of energy consumption, recycling of the solvents and life cycle assessment are considered as future objective of the project which will reveal complete insight of the recycling of MMMs.
- Finally, this work reinforces the industrial application of MMMs with less carbon footprint.

Mixed matrix membranes for CO_2 capture from Microporous Iron Coordination Polymer MIL-178(Fe) and Pebax® 3533

- A new water stable 1D microporous coordination polymer, MIL- 178(Fe) was developed by Benzaqui et. al (our collaborator) [83], presents interesting features for CO_2 capture with membranes.
- MIL-178(Fe) was found well dispersed in MMMs. Moreover, MMMs were found mechanically stable.
- The characterization of the CO_2/N_2 gas sorption properties of MIL-178(Fe) revealed that MIL-178(Fe) presents a moderate CO_2 adsorption capacity at low pressure but retains a high CO_2/N_2 selectivity in the 1-3 bar pressure range due to the high affinity of CO_2 molecules toward μ2-OH groups located on corner-sharing Fe octahedra chains.
- MMMs based on MIL- 178(Fe) and the Pebax®-3533 elastomer with a PCP loading up to 25 wt% were cast, showing significantly enhanced CO_2/N_2 separation performance in comparison to the pure Pebax®- 3533.
- The good permeation results are likely due to the excellent dispersion of MIL-178(Fe) particles in the polymer matrix with the absence of any interfacial micro-voids defects, the enhancement of the MMM CO_2 solubility as well as the lower crystallinity degree of the Pebax matrix in comparison to the pure polymer.
- Time lag data for single gas mesurements are in good agreement with mixture separation analyses for both CO_2 permeability and CO_2/N_2 selectivity values of bare membrane and MMM. Time lag experiments have demonstrated that the inclusion of the MOF in the polymer increases the CO_2 solubility.

Optimization of MIL-178(Fe) and Pebax® 3533 loading in mixed matrix membranes for CO_2 capture

- Porous coordination polymer MIL-178(Fe) was incorporated in Pebax® 3533 matrix after the optimization of the polymer concentration to achieve an efficient CO_2/N_2 separation.
- MIL-178(Fe) was compatible with the polymer, thus defect free MMMs with good filler distribution were obtained as confirmed by SEM analysis.
- An optimized bare polymer membrane (5 wt. % of Pebax® 3533) was prepared by finely tuning different parameters such as the polymer solution viscosity, membrane thickness and drying conditions. This gave rise to an efficient gas separation performance with CO_2 permeability and CO_2/N_2 selectivity of 277 ± 8 Barrer and 20.0 ± 1.1, respectively. These conditions for the preparation of the bare membranes constituted the starting point for the preparation of MMMs.
- In consequence, the optimum loading of filler was obtained at 5 wt. % in the best matrix composition. This MMM outperformed the bare membrane in terms of both CO_2 permeability (312 ± 5 Barrer) and CO_2/N_2 selectivity (25.0 ± 0.5) by 12 % and 25 %, respectively.

- Interestingly, MIL-178(Fe) improved the separation performance of the MMM due to its chemical composition (with polar CO_2-philic groups) and narrow microporosity (pore diameter < 0.45 nm) which increases the CO_2 solubility of the Pebax® 3533 polymer based MMM, compensating the loss of CO_2 diffusivity.
- Additionally, the optimized MMM was applied for CO_2/CH_4 separation and compared with the bare polymer membrane where MMM was also found efficient to improve the CO_2 permeability and CO_2/CH_4 selectivity (lower than that corresponding to the CO_2/N_2 mixture because of the CH_4 large condensability as compared to that of N_2) by 14 % and 89 %, respectively.

Chapter 9: Bibliography

References:

[1] Marshall Shepherd, Water Vapor Vs Carbon Dioxide: Which "Wins" In Climate Warming?, Https://Www.Forbes.Com/Sites/Marshallshepherd/2016/06/20/Water-Vapor-vs-Carbon-Dioxide-Which-Wins-in-Climate-Warming/?Sh=4f35ce273238. (2016).

[2] SETIS - SET Plan information system, Https://Setis.Ec.Europa.Eu/What-Set-Plan_en. (n.d.).

[3] F. Hervás Soriano, F. Mulatero, EU Research and Innovation (R&I) in renewable energies: The role of the Strategic Energy Technology Plan (SET-Plan), Energy Policy. 39 (2011) 3582–3590. https://doi.org/10.1016/j.enpol.2011.03.059.

[4] C.J. Rhodes, The 2015 Paris climate change conference: COP21, Sci Prog. 99 (2016) 97–104. https://doi.org/10.3184/003685016X14528569315192.

[5] COP27 held in Egypt, Https://En.Wikipedia.Org/Wiki/2022_United_Nations_Climate_Change_Conference. (2022).

[6] S.D. Kenarsari, D. Yang, G. Jiang, S. Zhang, J. Wang, A.G. Russell, Q. Wei, M. Fan, Review of recent advances in carbon dioxide separation and capture, RSC Adv. 3 (2013) 22739–22773. https://doi.org/10.1039/c3ra43965h.

[7] Z. Dai, L. Ansaloni, L. Deng, Recent advances in multi-layer composite polymeric membranes for CO2 separation: A review, Green Energy Environ. 1 (2016) 146–161. https://doi.org/10.1016/j.gee.2016.08.001.

[8] S.P. Kaldis, G.T. Pantoleontos, D.E. Koutsonikolas, Membrane technology in IGCC processes for precombustion CO_2 capture, in: Current Trends and Future Developments on (Bio-) Membranes: Carbon Dioxide Separation/Capture by Using Membranes, (2018) 329–357. https://doi.org/10.1016/B978-0-12-813645-4.00012-X.

[9] E.S. Rubin, H. Mantripragada, A. Marks, P. Versteeg, J. Kitchin, The outlook for improved carbon capture technology, Prog Energy Combust Sci. 38 (2012) 630–671. https://doi.org/10.1016/j.pecs.2012.03.003.

[10] M. Gharaie, Design and Optimization of Energy Systems with Effective Carbon Control, PhD Thesis, University of Manchester, 2013.

[11] Y. Tan, E. Croiset, M.A. Douglas, K. v. Thambimuthu, Combustion characteristics of coal in a mixture of oxygen and recycled flue gas, Fuel. 85 (2006) 507–512. https://doi.org/10.1016/j.fuel.2005.08.010.

[12] M. Harasimowicz, P. Orluk, G. Zakrzewska-Trznadel, A.G. Chmielewski, Application of polyimide membranes for biogas purification and enrichment, J Hazard Mater. 144 (2007) 698–702. https://doi.org/10.1016/j.jhazmat.2007.01.098.

[13] N. Abatzoglou, S. Boivin, A review of biogas purification processes, Biofuel Bioprod Biorefin. 3 (2009) 42–71. https://doi.org/10.1002/bbb.117.

[14] O.W. Awe, Y. Zhao, A. Nzihou, D.P. Minh, N. Lyczko, A Review of Biogas Utilisation, Purification and Upgrading Technologies, Waste Biomass Valorization. 8 (2017) 267-283. https://doi.org/10.1007/s12649-016-9826-4.

[15] S. Rasi, A. Veijanen, J. Rintala, Trace compounds of biogas from different biogas production plants, Energy. 32 (2007) 1375-1380. https://doi.org/10.1016/j.energy.2006.10.018.

[16] M.E. Diego, M. Akram, J.M. Bellas, K.N. Finney, M. Pourkashanian, Making gas-CCS a commercial reality: The challenges of scaling up, Greenhouse Gases: Science and Technology. 7 (2017) 778-801. https://doi.org/10.1002/ghg.1695.

[17] Y. Tan, W. Nookuea, H. Li, E. Thorin, J. Yan, Cryogenic technology for biogas upgrading combined with carbon capture-a review of systems and property impacts, in: Energy Procedia, (2017) 3741-3746. https://doi.org/10.1016/j.egypro.2017.12.270.

[18] T.C. Merkel, M. Zhou, R.W. Baker, Carbon dioxide capture with membranes at an IGCC power plant, J Memb Sci. 389 (2012) 441-450. https://doi.org/10.1016/j.memsci.2011.11.012.

[19] P. Bernardo, E. Drioli, G. Golemme, Membrane gas separation: A review/state of the art, Ind Eng Chem Res. 48 (2009) 4638–4663. https://doi.org/10.1021/ie8019032.

[20] R.W. Baker, Future directions of membrane gas separation technology, Ind Eng Chem Res. 41 (2002) 5-10. https://doi.org/10.1021/ie0108088.

[21] R. Castro-Muñoz, M. Zamidi Ahmad, M. Malankowska, J. Coronas, A new relevant membrane application: CO2 direct air capture (DAC), Chem Eng J. 446 (2022) 137047. https://doi.org/10.1016/j.cej.2022.137047.

[22] M.Z. Ahmad, T.A. Peters, N.M. Konnertz, T. Visser, C. Téllez, J. Coronas, V. Fila, W.M. de Vos, N.E. Benes, High-pressure CO_2/CH_4 separation of Zr-MOFs based mixed matrix membranes, Sep Purif Technol. 230 (2020) 115858. https://doi.org/10.1016/j.seppur.2019.115858.

[23] Y. Osada, T. Nakagawa, Membrane science and technology, 1992. https://doi.org/10.1201/9781482277203 (accessed January 16, 2023).

[24] Membrane, Https://En.Wikipedia.Org/Wiki/Membrane. (n.d.). https://en.wikipedia.org/wiki/Membrane (accessed February 23, 2023).

[25] P. Cote, Z. Alam, J. Penny, Hollow fiber membrane life in membrane bioreactors (MBR), Desalination. 288 (2012) 145–151. https://doi.org/10.1016/j.desal.2011.12.026.

[26] Z. Dai, L. Ansaloni, L. Deng, Recent advances in multi-layer composite polymeric membranes for CO_2 separation: A review, Green Energy and Environ. 1 (2016) 102-128. https://doi.org/10.1016/j.gee.2016.08.001.

[27] S. Bertelle, T. Gupta, D. Roizard, C. Vallières, E. Favre, Study of polymer-carbon mixed matrix membranes for CO_2 separation from flue gas, Desalination. 199 (2006) 1581-1597. https://doi.org/10.1016/j.desal.2006.03.207.

[28] C. v. Funk, D.R. Lloyd, Zeolite-filled microporous mixed matrix (ZeoTIPS) membranes: Prediction of gas separation performance, J Memb Sci. 313 (2008) 224-231. https://doi.org/10.1016/j.memsci.2008.01.002.
[29] L.M. Robeson, The upper bound revisited, J Memb Sci. 320 (2008) 390–400. https://doi.org/10.1016/j.memsci.2008.04.030.
[30] D.R. Paul, D.R. Kemp, Diffusion time lag in polymer membranes containing adsorptive fillers., J Polym Sci, Part C, Polym Symp. (1973) 79-93. https://doi.org/10.1002/polc.5070410109.
[31] J.M. Duval, B. Folkers, M.H.V. Mulder, G. Desgrandchamps, C.A. Smolders, Adsorbent filled membranes for gas separation. Part 1. Improvement of the gas separation properties of polymeric membranes by incorporation of microporous adsorbents, J Memb Sci. 80 (1993) 189-198. https://doi.org/10.1016/0376-7388(93)85143-K.
[32] S. Kulprathipanja, R. Neuzil, N. Li, Separation of gases by means of mixed matrix membranes, 5,127,925, 1992.
[33] T.M. Gür, Permselectivity of zeolite filled polysulfone gas separation membranes, J Memb Sci. 93 (1994) 283-289. https://doi.org/10.1016/0376-7388(94)00102-2.
[34] P. Tanvidkar, S. Appari, B.V.R. Kuncharam, A review of techniques to improve performance of metal organic framework (MOF) based mixed matrix membranes for CO_2/CH_4 separation, Rev Environ Sci Biotechnol. 21 (2022) 539–569. https://doi.org/10.1007/s11157-022-09612-5.
[35] M. Sánchez-Serratos, J.R. Álvarez, E. González-Zamora, I.A. Ibarra, Porous coordination polymers (Pcps): New platforms for gas storage, J Mex Chem Soc. 60 (2016) 43-57. https://doi.org/10.29356/jmcs.v60i2.72.
[36] Y. Horiuchi, T. Toyao, M. Matsuoka, Metal–Organic Framework (MOF) and Porous Coordination Polymer (PCP)-Based Photocatalysts: In: Yamashita, H., Li, H. (eds) Nanostructured Photocatalysts. Nanostructure Science and Technology. Springer, Cham, (2016) 479-489. https://doi.org/10.1007/978-3-319-26079-2_27.
[37] H.C. Zhou, J.R. Long, O.M. Yaghi, Introduction to metal-organic frameworks, Chem Rev. 112 (2012) 673–674. https://doi.org/10.1021/cr300014x.
[38] H. Li, M. Eddaoudi, M. O'Keeffe, O.M. Yaghi, Design and synthesis of an exceptionally stable and highly porous metal- organic framework, Nature. 402 (1999) 276-279. https://doi.org/10.1038/46248.
[39] F. Serpaggi, G. Férey, Hybrid open frameworks (MIL-n): Synthesis and crystal structure of MIL-17 - A rare-earth dicarboxylate with a relatively open framework, $[Pr(H_2O)]_2[O_2C(CH_2)_2CO_2]_3 \cdot H_2O$, Microporous Mesoporous Mater. 32 (1999) 311-318. https://doi.org/10.1016/S1387-1811(99)00120-1.
[40] H. Furukawa, M.A. Miller, O.M. Yaghi, Independent verification of the saturation hydrogen uptake in MOF-177 and establishment of a benchmark for hydrogen adsorption in metal-organic frameworks, J Mater Chem. 17 (2007) 3197-3204. https://doi.org/10.1039/b703608f.
[41] H. Furukawa, N. Ko, Y.B. Go, N. Aratani, S.B. Choi, E. Choi, A.Ö. Yazaydin, R.Q. Snurr, M. O'Keeffe, J. Kim, O.M. Yaghi, Ultrahigh porosity in metal-organic frameworks, Science (1979). 329 (2010) 424-428. https://doi.org/10.1126/science.1192160.
[42] Y.R. Lee, M.S. Jang, H.Y. Cho, H.J. Kwon, S. Kim, W.S. Ahn, ZIF-8: A comparison of synthesis methods, Chem Eng J. 271 (2015) 276-280. https://doi.org/10.1016/j.cej.2015.02.094.
[43] P.L. Llewellyn, S. Bourrelly, C. Serre, A. Vimont, M. Daturi, L. Hamon, G. de Weireld, J.S. Chang, D.Y. Hong, Y.K. Hwang, S.H. Jhung, G. Férey, High uptakes of CO_2 and CH_4 in mesoporous metal-organic frameworks MIL-100 and MIL-101, Langmuir. 24 (2008) 7245-7250. https://doi.org/10.1021/la800227x.
[44] Z. Hu, Y. Wang, B.B. Shah, D. Zhao, CO_2 Capture in Metal-Organic Framework Adsorbents: An Engineering Perspective , Adv Sustain Syst. 3 (2019) 1800080. https://doi.org/10.1002/adsu.201800080.
[45] M. Ding, R.W. Flaig, H.L. Jiang, O.M. Yaghi, Carbon capture and conversion using metal-organic frameworks and MOF-based materials, Chem Soc Rev. 48 (2019) 2783-2828. https://doi.org/10.1039/c8cs00829a.
[46] R. Luo, M. Chen, X. Liu, W. Xu, J. Li, B. Liu, Y. Fang, Recent advances in CO_2 capture and simultaneous conversion into cyclic carbonates over porous organic polymers having accessible metal sites, J Mater Chem A. 8 (2020) 18408–18424. https://doi.org/10.1039/d0ta06142e.
[47] R.L. Siegelman, E.J. Kim, J.R. Long, Porous materials for carbon dioxide separations, Nat Mater. 20 (2021) 1060-1072. https://doi.org/10.1038/s41563-021-01054-8.
[48] S. Aguado, J. Canivet, D. Farrusseng, Facile shaping of an imidazolate-based MOF on ceramic beads for adsorption and catalytic applications, ChemComm. 46 (2010) 7999–8001. https://doi.org/10.1039/c0cc02045a.
[49] N. Keser Demir, B. Topuz, L. Yilmaz, H. Kalipcilar, Synthesis of ZIF-8 from recycled mother liquors, Microporous Mesoporous Mater. 198 (2014) 291–300. https://doi.org/10.1016/j.micromeso.2014.07.052.
[50] W. Morris, N. He, K.G. Ray, P. Klonowski, H. Furukawa, I.N. Daniels, Y.A. Houndonougbo, M. Asta, O.M. Yaghi, B.B. Laird, A combined experimental-computational study on the effect of topology on carbon dioxide adsorption in zeolitic imidazolate frameworks, J Phys Chem C. 116 (2012) 24084–24090. https://doi.org/10.1021/jp307170a.
[51] J. Canivet, J. Bonnefoy, C. Daniel, A. Legrand, B. Coasne, D. Farrusseng, Structure-property relationships of water adsorption in metal-organic frameworks, New J Chem. 38 (2014) 3102–3111. https://doi.org/10.1039/c4nj00076e.
[52] M. Eddaoudi, J. Kim, N. Rosi, D. Vodak, J. Wachter, M. O'Keeffe, O.M. Yaghi, Systematic design of pore size and functionality in isoreticular MOFs and their application in methane storage, Science, 295 (2002) 469-472. https://doi.org/10.1126/science.1067208.

[53] B. Zornoza, C. Tellez, J. Coronas, J. Gascon, F. Kapteijn, Metal organic framework based mixed matrix membranes: An increasingly important field of research with a large application potential, Microporous Mesoporous Mater. (2013) 67-78. https://doi.org/10.1016/j.micromeso.2012.03.012.
[54] J. Gascon, U. Aktay, M.D. Hernandez-Alonso, G.P.M. van Klink, F. Kapteijn, Amino-based metal-organic frameworks as stable, highly active basic catalysts, J Catal. 261 (2009) 75-87. https://doi.org/10.1016/j.jcat.2008.11.010.
[55] P. Horcajada, C. Serre, M. Vallet-Regí, M. Sebban, F. Taulelle, G. Férey, Metal-organic frameworks as efficient materials for drug delivery, Angewandte Chemie - International Edition. 45 (2006) 5974-5978. https://doi.org/10.1002/anie.200601878.
[56] K.S. Park, Z. Ni, A.P. Côté, J.Y. Choi, R. Huang, F.J. Uribe-Romo, H.K. Chae, M. O'Keeffe, O.M. Yaghi, Exceptional chemical and thermal stability of zeolitic imidazolate frameworks, Proc Natl Acad Sci U S A. 103 (2006) 10186-10191. https://doi.org/10.1073/pnas.0602439103.
[57] X.C. Huang, Y.Y. Lin, J.P. Zhang, X.M. Chen, Ligand-directed strategy for zeolite-type metal-organic frameworks: Zinc(II) imidazolates with unusual zeolitic topologies, Angewandte Chemie - International Edition. 45 (2006) 1557-1559. https://doi.org/10.1002/anie.200503778.
[58] H. Hayashi, A.P. Côté, H. Furukawa, M. O'Keeffe, O.M. Yaghi, Zeolite A imidazolate frameworks, Nat Mater. 6 (2007) 501-506. https://doi.org/10.1038/nmat1927.
[59] A. Perea-Cachero, J. Sánchez-Laínez, Á. Berenguer-Murcia, D. Cazorla-Amorós, C. Téllez, J. Coronas, A new zeolitic hydroxymethylimidazolate material and its use in mixed matrix membranes based on 6FDA-DAM for gas separation, J Memb Sci. 544 (2017) 88-97. https://doi.org/10.1016/j.memsci.2017.09.009.
[60] SOD and RHO Framework Type Structure, Https://Asia.Iza-Structure.Org/IZA-SC/Ftc_table.Php. (n.d.). https://asia.iza-structure.org/IZA-SC/ftc_table.php (accessed February 24, 2023).
[61] J.H. Park, S.H. Park, S.H. Jhung, Microwave-syntheses of zeolitic imidazolate framework material, ZIF-8, J Korean Chem Soc. 53 (2009) 553-559. https://doi.org/10.5012/jkcs.2009.53.5.553.
[62] A. Martinez Joaristi, J. Juan-Alcañiz, P. Serra-Crespo, F. Kapteijn, J. Gascon, Electrochemical synthesis of some archetypical Zn 2+, Cu 2+, and Al 3+ metal organic frameworks, Cryst Growth Des. 12 (2012) 3489–3498. https://doi.org/10.1021/cg300552w.
[63] P.J. Beldon, L. Fábián, R.S. Stein, A. Thirumurugan, A.K. Cheetham, T. Friščić, Rapid room-temperature synthesis of zeolitic imidazolate frameworks by using mechanochemistry, Angewandte Chemie - International Edition. 49 (2010) 9640-9643. https://doi.org/10.1002/anie.201005547.
[64] Q. Shi, Z. Chen, Z. Song, J. Li, J. Dong, Synthesis of ZIF-8 and ZIF-67 by steam-assisted conversion and an investigation of their tribological behaviors, Angewandte Chemie - International Edition. 50 (2011) 672-675. https://doi.org/10.1002/anie.201004937.
[65] D. Fairen-Jimenez, S.A. Moggach, M.T. Wharmby, P.A. Wright, S. Parsons, T. Düren, Opening the gate: Framework flexibility in ZIF-8 explored by experiments and simulations, J Am Chem Soc. 133 (2011) 8900-8902. https://doi.org/10.1021/ja202154j.
[66] A.M. Marti, M. Van, K.J. Balkus, Tuning the crystal size and morphology of the substituted imidazole material, SIM-1, J Porous Mater. 21 (2014) 889–902. https://doi.org/10.1007/s10934-014-9840-5.
[67] F. Cacho-Bailo, M. Etxeberría-Benavides, O. Karvan, C. Téllez, J. Coronas, Sequential amine functionalization inducing structural transition in an aldehyde-containing zeolitic imidazolate framework: application to gas separation membranes, CrystEngComm. 19 (2017) 1545-1554. https://doi.org/10.1039/c7ce00086c.
[68] D.I. Kolokolov, H. Jobic, A.G. Stepanov, M. Plazanet, M. Zbiri, J. Ollivier, V. Guillerm, T. Devic, C. Serre, G. Férey, Comparison of the dynamics of MIL-53(Cr) and MIL-47(V) frameworks using neutron scattering and DFT methods, Eur Phys J. 189 (2010) 263–271. https://doi.org/10.1140/epjst/e2010-01331-y.
[69] A. Sabetghadam, X. Liu, M. Benzaqui, E. Gkaniatsou, A. Orsi, M.M. Lozinska, C. Sicard, T. Johnson, N. Steunou, P.A. Wright, C. Serre, J. Gascon, F. Kapteijn, Influence of Filler Pore Structure and Polymer on the Performance of MOF-Based Mixed-Matrix Membranes for CO_2 Capture, Chem Eur J. 24 (2018) 7949–7956. https://doi.org/10.1002/chem.201800253.
[70] T. Zhou, Y. Sang, X. Wang, C. Wu, D. Zeng, C. Xie, Pore size dependent gas-sensing selectivity based on ZnO@ZIF nanorod arrays, Sens Actuators B Chem. 258 (2018) 1099–1106. https://doi.org/10.1016/j.snb.2017.12.024.
[71] M. Etxeberria-Benavides, O. David, T. Johnson, M.M. Łozińska, A. Orsi, P.A. Wright, S. Mastel, R. Hillenbrand, F. Kapteijn, J. Gascon, High performance mixed matrix membranes (MMMs) composed of ZIF-94 filler and 6FDA-DAM polymer, J Memb Sci. 550 (2018) 198–207. https://doi.org/10.1016/j.memsci.2017.12.033.
[72] F. Cacho-Bailo, I. Matito-Martos, J. Perez-Carbajo, M. Etxeberría-Benavides, O. Karvan, V. Sebastián, S. Calero, C. Téllez, J. Coronas, On the molecular mechanisms for the H_2/CO_2 separation performance of zeolite imidazolate framework two-layered membranes, Chem Sci. 8 (2017) 325–333. https://doi.org/10.1039/c6sc02411d.
[73] A. Noguera-Díaz, J. Villarroel-Rocha, V.P. Ting, N. Bimbo, K. Sapag, T.J. Mays, Flexible ZIFs: probing guest-induced flexibility with CO_2, N_2 and Ar adsorption, J Chem Technol Biotechnol. 94 (2019) 3787–3792. https://doi.org/10.1002/jctb.5947.
[74] G. Zhong, D. Liu, J. Zhang, Applications of Porous Metal-Organic Framework MIL-100(M) (M = Cr, Fe, Sc, Al, V), Cryst Growth Des. 18 (2018) 7730-7744. https://doi.org/10.1021/acs.cgd.8b01353.

[75] S. Yang, X. Li, G. Zeng, M. Cheng, D. Huang, Y. Liu, C. Zhou, W. Xiong, Y. Yang, W. Wang, G. Zhang, Materials Institute Lavoisier (MIL) based materials for photocatalytic applications, Coord Chem Rev. 438 (2021) 213874. https://doi.org/10.1016/j.ccr.2021.213874.
[76] L. Han, H. Qi, D. Zhang, G. Ye, W. Zhou, C. Hou, W. Xu, Y. Sun, A facile and green synthesis of MIL-100(Fe) with high-yield and its catalytic performance, New J Chem. 41 (2017) 13504-13509. https://doi.org/10.1039/c7nj02975f.
[77] P. Mishra, H.P. Uppara, B. Mandal, S. Gumma, Adsorption and separation of carbon dioxide using MIL-53(Al) metal-organic framework, Ind Eng Chem Res. (2014) 19747-19753. https://doi.org/10.1021/ie5006146.
[78] Z. Lionet, T.H. Kim, Y. Horiuchi, S.W. Lee, M. Matsuoka, Linker Engineering of Iron-Based MOFs for Efficient Visible-Light-Driven Water Oxidation Reaction, J Phys Chem C. (2019) 27501-27508. https://doi.org/10.1021/acs.jpcc.9b06838.
[79] C. Xu, R. Fang, R. Luque, L. Chen, Y. Li, Functional metal–organic frameworks for catalytic applications, Coord Chem Rev. 388 (2019) 268-292. https://doi.org/10.1016/j.ccr.2019.03.005.
[80] W.T. Xu, L. Ma, F. Ke, F.M. Peng, G.S. Xu, Y.H. Shen, J.F. Zhu, L.G. Qiu, Y.P. Yuan, Metal-organic frameworks MIL-88A hexagonal microrods as a new photocatalyst for efficient decolorization of methylene blue dye, Dalton Trans. 43 (2014) 3792-3798. https://doi.org/10.1039/c3dt52574k.
[81] M. Cheng, C. Lai, Y. Liu, G. Zeng, D. Huang, C. Zhang, L. Qin, L. Hu, C. Zhou, W. Xiong, Metal-organic frameworks for highly efficient heterogeneous Fenton-like catalysis, Coord Chem Rev. 368 (2018) 80-92. https://doi.org/10.1016/j.ccr.2018.04.012.
[82] Q. Wang, Q. Gao, A.M. Al-Enizi, A. Nafady, S. Ma, Recent advances in MOF-based photocatalysis: Environmental remediation under visible light, Inorg Chem Front. 7 (2020) 300-339. https://doi.org/10.1039/c9qi01120j.
[83] M. Benzaqui, M. Wahiduzzaman, H. Zhao, M.R. Hasan, T. Steenhaut, A. Saad, J. Marrot, P. Normand, J.M. Grenèche, N. Heymans, G. De Weireld, A. Tissot, W. Shepard, Y. Filinchuk, S. Hermans, F. Carn, M. Manlankowska, C. Téllez, J. Coronas, G. Maurin, N. Steunou, C. Serre, A robust eco-compatible microporous iron coordination polymer for CO_2 capture, J Mater Chem A. 10 (2022) 8535-8545. https://doi.org/10.1039/d1ta10385g.
[84] J. Ahmad, W.U. Rehman, K. Deshmukh, S.K. Basha, B. Ahamed, K. Chidambaram, Recent Advances in Poly (Amide-B-Ethylene) Based Membranes for Carbon Dioxide (CO_2) Capture: A Review, Polym-Plast Technol Mater. 58 (2019) 366-383. https://doi.org/10.1080/03602559.2018.1482921.
[85] T.C. Merkel, V.I. Bondar, K. Nagai, B.D. Freeman, I. Pinnau, Gas sorption, diffusion, and permeation in poly(dimethylsiloxane), J Polym Sci B Polym Phys. 38 (2000) 415-434. https://doi.org/10.1002/(SICI)1099-0488(20000201)38:3<415::AID-POLB8>3.0.CO;2-Z.
[86] A. Tena, S. Shishatskiy, V. Filiz, Poly(ether-amide) vs. poly(ether-imide) copolymers for post-combustion membrane separation processes, RSC Adv. 5 (2015) 22310–22318. https://doi.org/10.1039/c5ra01328c.
[87] L. Martínez-Izquierdo, M. Malankowska, C. Téllez, J. Coronas, Phase inversion method for the preparation of Pebax® 3533 thin film membranes for CO_2/N_2 separation, J Environ Chem Eng. 9 (2021) 105624. https://doi.org/10.1016/j.jece.2021.105624.
[88] H. Lin, B.D. Freeman, Materials selection guidelines for membranes that remove CO_2 from gas mixtures, J Mol Struct. 739 (2005) 57-74. https://doi.org/10.1016/j.molstruc.2004.07.045.
[89] M.E. Rezac, T. John, P.H. Pfromm, Effect of copolymer composition on the solubility and diffusivity of water and methanol in a series of polyether amides, J Appl Polym Sci. 65 (1997) 1983-1993. https://doi.org/10.1002/(SICI)1097-4628(19970906)65:10<1983::AID-APP16>3.0.CO;2-Y.
[90] T. Li, Y. Pan, K.V. Peinemann, Z. Lai, Carbon dioxide selective mixed matrix composite membrane containing ZIF-7 nano-fillers, J Memb Sci. 425–426 (2013). https://doi.org/10.1016/j.memsci.2012.09.006.
[91] V. Nafisi, M.B. Hägg, Development of dual layer of ZIF-8/PEBAX-2533 mixed matrix membrane for CO_2 capture, J Memb Sci. 459 (2014) 244–255. https://doi.org/10.1016/j.memsci.2014.02.002.
[92] W. Zheng, R. Ding, K. Yang, Y. Dai, X. Yan, G. He, ZIF-8 nanoparticles with tunable size for enhanced CO_2 capture of Pebax based MMMs, Sep Purif Technol. (2019) 111-119. https://doi.org/10.1016/j.seppur.2018.04.010.
[93] A. Ehsani, M. Pakizeh, Synthesis, characterization and gas permeation study of ZIF-11/Pebax® 2533 mixed matrix membranes, J Taiwan Inst Chem Eng. 66 (2016) 414–423. https://doi.org/10.1016/j.jtice.2016.07.005.
[94] F. Dorosti, A. Alizadehdakhel, Fabrication and investigation of PEBAX/Fe-BTC, a high permeable and CO_2 selective mixed matrix membrane, Chem Eng Res Des. 136 (2018). https://doi.org/10.1016/j.cherd.2018.01.029.
[95] J.G. Wijmans, R.W. Baker, The solution-diffusion model: a review, J Memb Sci. 107 (1995) 1-21. https://doi.org/10.1016/0376-7388(95)00102-I.
[96] J.R. Li, R.J. Kuppler, H.C. Zhou, Selective gas adsorption and separation in metal-organic frameworks, Chem Soc Rev. 38 (2009) 1477-1504. https://doi.org/10.1039/b802426j.
[97] S.A. Stern, The "Barrer" permeability unit, J Polym Sci A-2: Polym Phys. 6 (1968) 1933-1934. https://doi.org/10.1002/pol.1968.160061108.
[98] W.J. Koros, G.K. Fleming, Membrane-based gas separation, J Memb Sci. 83 (1993) 1-80. https://doi.org/10.1016/0376-7388(93)80013-N.
[99] W.J. Koros, D.R. Paul, Design considerations for measurement of gas sorption in polymers by pressure decay, J Polym Sci B Polym Phys. 14 (1976) 1903-1907. https://doi.org/10.1002/pol.1976.180141014.

[100] R.M. Barrer, J.A. Barrie, J. Slater, Sorption and diffusion in ethyl cellulose. Part III. Comparison between ethyl cellulose and rubber, J Polym Sci. 27 (1958) 177-197. https://doi.org/10.1002/pol.1958.1202711515.
[101] R.W. Baker, Membrane Transport Theory, in: Membrane Technology and Applications, (2012) 15-96. https://doi.org/10.1002/9781118359686.ch2.
[102] S.S. Jordan, W.J. Koros, A Free Volume Distribution Model of Gas Sorption and Dilation in Glassy Polymers, Macromolecules. 28 (1995) 2228-2235. https://doi.org/10.1021/ma00111a017.
[103] A.R. Berens, H.B. Hopfenberg, Diffusion of organic vapors at low concentrations in glassy PVC, polystyrene, and PMMA, J Memb Sci. 10 (1982) 283-303. https://doi.org/10.1016/S0376-7388(00)81415-5.
[104] T. Yang, Y. Xiao, T.S. Chung, Poly-/metal-benzimidazole nano-composite membranes for hydrogen purification, Energy Environ Sci. 4 (2011) 4171-4180. https://doi.org/10.1039/c1ee01324f.
[105] J.S. Chiou, J.W. Barlow, D.R. Paul, Plasticization of glassy polymers by CO_2, J Appl Polym Sci. 30 (1985) 2633-2642. https://doi.org/10.1002/app.1985.070300626.
[106] S. v. Wroblewski, Ueber die Natur der Absorption der Gase, Ann Phys. 244 (1879) 29-52. https://doi.org/10.1002/andp.18792440903.
[107] T.H. Kim, W.J. Koros, G.R. Husk, K.C. O'Brien, Relationship between gas separation properties and chemical structure in a series of aromatic polyimides, J Memb Sci. 37 (1988) 45-62. https://doi.org/10.1016/S0376-7388(00)85068-1.
[108] R.H.B. Bouma, A. Checchetti, G. Chidichimo, E. Drioli, Permeation through a heterogeneous membrane: The effect of the dispersed phase, J Memb Sci. 128 (1997) 141-149. https://doi.org/10.1016/S0376-7388(96)00303-1.
[109] A. Fuoco, M.R. Khdhayyer, M.P. Attfield, E. Esposito, J.C. Jansen, P.M. Budd, Synthesis and transport properties of novel MOF/PIM-1/MOF sandwich membranes for gas separation, Membranes (Basel). 7 (2017) 1-17. https://doi.org/10.3390/membranes7010007.
[110] T.T. Moore, W.J. Koros, Non-ideal effects in organic-inorganic materials for gas separation membranes, J Mol Struct. 739 (2005) 87-98. https://doi.org/10.1016/j.molstruc.2004.05.043.
[111] M. Moaddeb, W.J. Koros, Gas transport properties of thin polymeric membranes in the presence of silicon dioxide particles, J Memb Sci. 125 (1997) 143-163. https://doi.org/10.1016/S0376-7388(96)00251-7.
[112] S. LOEB, S. SOURIRAJAN, Sea Water Demineralization by Means of an Osmotic Membrane, Saline Water Conversion—II, (1963) 117-132. https://doi.org/10.1021/ba-1963-0038.ch009.
[113] A. Car, C. Stropnik, W. Yave, K. v. Peinemann, PEG modified poly(amide-b-ethylene oxide) membranes for CO_2 separation, J Memb Sci. 307 (2008) 88-95. https://doi.org/10.1016/j.memsci.2007.09.023.
[114] P.A. Gurr, J.M.P. Scofield, J. Kim, Q. Fu, S.E. Kentish, G.G. Qiao, Polyimide polydimethylsiloxane triblock copolymers for thin film composite gas separation membranes, J Polym Sci A Polym Chem. 52 (2014) 3372-3382. https://doi.org/10.1002/pola.27401.
[115] J. Mulder, Basic Principles of Membrane Technology, Springer Science & Business Media. (2012).
[116] L.M. Robeson, Correlation of separation factor versus permeability for polymeric membranes, J Memb Sci. 62 (1991) 165-185. https://doi.org/10.1016/0376-7388(91)80060-J.
[117] B. Comesaña-Gándara, J. Chen, C.G. Bezzu, M. Carta, I. Rose, M.C. Ferrari, E. Esposito, A. Fuoco, J.C. Jansen, N.B. McKeown, Redefining the Robeson upper bounds for CO_2/CH_4 and CO_2/N_2 separations using a series of ultrapermeable benzotriptycene-based polymers of intrinsic microporosity, Energy Environ Sci. 12 (2019) 2733-2740. https://doi.org/10.1039/c9ee01384a.
[118] J.J. Krol, M. Boerrigter, G.H. Koops, Polyimide hollow fiber gas separation membranes: Preparation and the suppression of plasticization in propane/propylene environments, J Memb Sci. 184 (2001) 275-285. https://doi.org/10.1016/S0376-7388(00)00640-2.
[119] A. Bos, I.G.M. Pünt, M. Wessling, H. Strathmann, Suppression of CO_2-plasticization by semiinterpenetrating polymer network formation, J Polym Sci B Polym Phys. 36 (1998) 1547-1556. https://doi.org/10.1002/(SICI)1099-0488(19980715)36:9<1547::AID-POLB12>3.0.CO;2-5.
[120] A. Bos, I.G.M. Pünt, M. Wessling, H. Strathmann, Plasticization-resistant glassy polyimide membranes for CO_2/CO_4 separations, Sep Purif Technol. 14 (1998). https://doi.org/10.1016/S1383-5866(98)00057-4.
[121] H. Kawakami, M. Mikawa, S. Nagaoka, Gas permeability and selectivity through asymmetric polyimide membranes, J Appl Polym Sci. 62 (1996) 965-971. https://doi.org/10.1002/(SICI)1097-4628(19961114)62:7<965::AID-APP2>3.0.CO;2-Q.
[122] F. Cacho-Bailo, G. Caro, M. Etxeberría-Benavides, O. Karvan, C. Téllez, J. Coronas, MOF-polymer enhanced compatibility: Post-annealed zeolite imidazolate framework membranes inside polyimide hollow fibers, RSC Adv. 6 (2016) 5881–5889. https://doi.org/10.1039/c5ra26076k.
[123] L. Rosu, I. Sava, D. Rosu, Modification of the surface properties of a polyimide film during irradiation with polychromic light, Appl Surf Sci. 257 (2011) 6996-7002. https://doi.org/10.1016/j.apsusc.2011.03.054.
[124] K. Vanherck, G. Koeckelberghs, I.F.J. Vankelecom, Crosslinking polyimides for membrane applications: A review, Prog Polym Sci. 38 (2013) 874-896. https://doi.org/10.1016/j.progpolymsci.2012.11.001.
[125] S. Quan, S. Li, Z. Wang, X. Yan, Z. Guo, L. Shao, A bio-inspired CO_2-philic network membrane for enhanced sustainable gas separation, J Mater Chem A. 3 (2015) 13758-13766. https://doi.org/10.1039/c5ta03232f.
[126] J. Yuan, D. Mecerreyes, M. Antonietti, Poly(ionic liquid)s: An update, Prog Polym Sci. 38 (2013) 1009-1036. https://doi.org/10.1016/j.progpolymsci.2013.04.002.

[127] H. Eguchi, D.J. Kim, W.J. Koros, Chemically cross-linkable polyimide membranes for improved transport plasticization resistance for natural gas separation, Polymer (Guildf). 58 (2015) 121-129. https://doi.org/10.1016/j.polymer.2014.12.064.
[128] F. Carrillo, S. Gupta, M. Balooch, S.J. Marshall, G.W. Marshall, L. Pruitt, C.M. Puttlitz, Nanoindentation of polydimethylsiloxane elastomers: Effect of crosslinking, work of adhesion, and fluid environment on elastic modulus, J Mater Res. 20 (2005) 2820-2830. https://doi.org/10.1557/JMR.2005.0354.
[129] N. Stafie, D.F. Stamatialis, M. Wessling, Effect of PDMS cross-linking degree on the permeation performance of PAN/PDMS composite nanofiltration membranes, Sep Purif Technol. 45 (2005) 220-231. https://doi.org/10.1016/j.seppur.2005.04.001.
[130] S.K. Sia, G.M. Whitesides, Microfluidic devices fabricated in poly(dimethylsiloxane) for biological studies, Electrophoresis. 24 (2003) 3563-3576. https://doi.org/10.1002/elps.200305584.
[131] T. Fujii, PDMS-based microfluidic devices for biomedical applications: Microelectron Eng, (2002) 907-914. https://doi.org/10.1016/S0167-9317(02)00494-X.
[132] S. Sridhar, B. Smitha, T.M. Aminabhavi, Separation of carbon dioxide from natural gas mixtures through polymeric membranes - A review, Sep Purifi Rev. 36 (2007) 113-174. https://doi.org/10.1080/15422110601165967.
[133] D. Madhav, M. Malankowska, J. Coronas, Synthesis of nanoparticles of zeolitic imidazolate framework ZIF-94 using inorganic deprotonators, New J Chem. (2020) 20449-20457. https://doi.org/10.1039/d0nj04402d.
[134] J. Sánchez-Laínez, B. Zornoza, S. Friebe, J. Caro, S. Cao, A. Sabetghadam, B. Seoane, J. Gascon, F. Kapteijn, C. le Guillouzer, G. Clet, M. Daturi, C. Téllez, J. Coronas, Influence of ZIF-8 particle size in the performance of polybenzimidazole mixed matrix membranes for pre-combustion CO2 capture and its validation through interlaboratory test, J Memb Sci. 515 (2016) 45–53. https://doi.org/10.1016/j.memsci.2016.05.039.
[135] I.J.W. Bowman, D.S. Brown, R.E. Wetton, Crystal density, crystallinity and heat of fusion of poly (tetramethylene oxide), Polymer (Guildf). 10 (1969) 715-718. https://doi.org/10.1016/0032-3861(69)90097-4.
[136] Z.A. Alothman, A review: Fundamental aspects of silicate mesoporous materials, Materials. 5 (2012) 2874-2902. https://doi.org/10.3390/ma5122874.
[137] H. Yang, Z. Xu, M. Fan, R. Gupta, R.B. Slimane, A.E. Bland, I. Wright, Progress in carbon dioxide separation and capture: A review, J Environ Sci. 20 (2008) 14–27. https://doi.org/10.1016/S1001-0742(08)60002-9.
[138] Z. Dai, R.D. Noble, D.L. Gin, X. Zhang, L. Deng, Combination of ionic liquids with membrane technology: A new approach for CO2 separation, J Memb Sci. 497 (2016) 1–20. https://doi.org/10.1016/j.memsci.2015.08.060.
[139] A. Tellez-Rio, A. Vallejo, S. García-Marco, D. Martin-Lammerding, J.L. Tenorio, R.M. Rees, G. Guardia, Conservation Agriculture practices reduce the global warming potential of rainfed low N input semi-arid agriculture, European Journal of Agronomy. 84 (2017) 95–104. https://doi.org/10.1016/j.eja.2016.12.013.
[140] K. Xie, Q. Fu, G.G. Qiao, P.A. Webley, Recent progress on fabrication methods of polymeric thin film gas separation membranes for CO2 capture, J Memb Sci. 572 (2019) 38–60. https://doi.org/10.1016/j.memsci.2018.10.049.
[141] X. Gong, Y. Wang, T. Kuang, ZIF-8-Based Membranes for Carbon Dioxide Capture and Separation, ACS Sustain Chem Eng. 5 (2017) 11204–11214. https://doi.org/10.1021/acssuschemeng.7b03613.
[142] J. Yuan, H. Zhu, J. Sun, Y. Mao, G. Liu, W. Jin, Novel ZIF-300 Mixed-Matrix Membranes for Efficient CO2 Capture, ACS Appl Mater Interfaces. 9 (2017) 38575–38583. https://doi.org/10.1021/acsami.7b12507.
[143] Z. Zhang, S. Xian, H. Xi, H. Wang, Z. Li, Improvement of CO2 adsorption on ZIF-8 crystals modified by enhancing basicity of surface, Chem Eng Sci. 66 (2011) 4878–4888. https://doi.org/10.1016/J.CES.2011.06.051.
[144] Y. Pan, H. Li, X.X. Zhang, Z. Zhang, X.S. Tong, C.Z. Jia, B. Liu, C.Y. Sun, L.Y. Yang, G.J. Chen, Large-scale synthesis of ZIF-67 and highly efficient carbon capture using a ZIF-67/glycol-2-methylimidazole slurry, Chem Eng Sci. 137 (2015) 504–514. https://doi.org/10.1016/j.ces.2015.06.069.
[145] N. Tannert, S. Gökpinar, E. Hastürk, S. Nießing, C. Janiak, Microwave-assisted dry-gel conversion-a new sustainable route for the rapid synthesis of metal-organic frameworks with solvent re-use, Dalton Trans. 47 (2018) 9850–9860. https://doi.org/10.1039/c8dt02029a.
[146] S. Gökpinar, T. Diment, C. Janiak, Environmentally benign dry-gel conversions of Zr-based UiO metal-organic frameworks with high yield and the possibility of solvent re-use, Dalton Trans. 46 (2017) 9895–9900. https://doi.org/10.1039/c7dt01717k.
[147] M. García-Palacín, J.I. Martínez, L. Paseta, A. Deacon, T. Johnson, M. Malankowska, C. Téllez, J. Coronas, Sized-Controlled ZIF-8 Nanoparticle Synthesis from Recycled Mother Liquors: Environmental Impact Assessment, ACS Sustain Chem Eng. 8 (2020) 2973–2980. https://doi.org/10.1021/acssuschemeng.9b07593.
[148] N. Jamil, N.H. Alias, M.Z. Shahruddin, N.H. Othman, A green in situ synthesis of hybrid graphene-based zeolitic imidazolate framework-8 nanofillers using recycling mother liquor, Key Eng Mater. 797 (2019) 48–54. https://doi.org/10.4028/www.scientific.net/KEM.797.48.

[149] F. Şahin, B. Topuz, H. Kalıpçılar, Synthesis of ZIF-7, ZIF-8, ZIF-67 and ZIF-L from recycled mother liquors, Microporous Mesoporous Mater. 261 (2018) 259–267. https://doi.org/10.1016/j.micromeso.2017.11.020.
[150] Q. Shi, Z. Song, X. Kang, J. Dong, Y. Zhang, Controlled synthesis of hierarchical zeolitic imidazolate framework-GIS (ZIF-GIS) architectures, CrystEngComm. 14 (2012) 8280–8285. https://doi.org/10.1039/c2ce26170g.
[151] C. Ying-Bo, Z. Lin-Fei, W. Biao, H. Xiao-Yu, L. Dong-Qing, Z. Feng-Xiao, Z. Yu-Feng, Structural evolution of zeolitic imidazolate framework-8(ZIF-8), J Tianjin Polytech Univ. 35 (2016) 1–4. https://doi.org/10.3969/j.issn.1671-024x.2016.05.001.
[152] L. Martínez-Izquierdo, M. Malankowska, J. Sánchez-Laínez, C. Téllez, J. Coronas, Poly(ether-block-amide) copolymer membrane for CO_2/N_2 separation: The influence of the casting solution concentration on its morphology, thermal properties and gas separation performance, R Soc Open Sci. 6 (2019) 190866. https://doi.org/10.1098/rsos.
[153] T. Johnson, M.M. Łozińska, A.F. Orsi, P.A. Wright, S. Hindocha, S. Poulston, Improvements to the production of ZIF-94; A case study in MOF scale-up, Green Chem. 21 (2019) 5665–5670. https://doi.org/10.1039/c9gc00783k.
[154] Z. Su, Y.R. Miao, G. Zhang, J.T. Miller, K.S. Suslick, Bond breakage under pressure in a metal organic framework, Chem Sci. 8 (2017) 8004–8011. https://doi.org/10.1039/c7sc03786d.
[155] A. Sabetghadam, X. Liu, M. Benzaqui, E. Gkaniatsou, A. Orsi, M.M. Lozinska, C. Sicard, T. Johnson, N. Steunou, P.A. Wright, C. Serre, J. Gascon, F. Kapteijn, Influence of Filler Pore Structure and Polymer on the Performance of MOF-Based Mixed-Matrix Membranes for CO_2 Capture, Chem Eur J. 24 (2018) 7949–7956. https://doi.org/10.1002/chem.201800253.
[156] A. Noguera-Díaz, J. Villarroel-Rocha, V.P. Ting, N. Bimbo, K. Sapag, T.J. Mays, Flexible ZIFs: probing guest-induced flexibility with CO_2, N_2 and Ar adsorption, J Chem Technol Biotechnol. 94 (2019) 3787–3792. https://doi.org/10.1002/jctb.5947.
[157] K.G. Ray, D.L. Olmsted, J.M.R. Burton, Y. Houndonougbo, B.B. Laird, M. Asta, Gas membrane selectivity enabled by zeolitic imidazolate framework electrostatics, Chem Mater. 26 (2014) 3976–3985. https://doi.org/10.1021/cm5015477.
[158] R. Selyanchyn, M. Ariyoshi, S. Fujikawa, Thickness Effect on CO_2 /N_2 Separation in Double Layer Pebax-1657®/PDMS Membranes, Membranes (Basel). 8 (2018) 1-13. https://doi.org/10.3390/membranes8040121.
[159] COP26: green technologies could turn the tide, Nat Rev Mater. 6 (2021) 959. https://doi.org/10.1038/s41578-021-00390-0.
[160] M.R. Hasan, L. Paseta, M. Malankowska, C. Téllez, J. Coronas, Synthesis of ZIF-94 from Recycled Mother Liquors: Study of the Influence of Its Loading on Postcombustion CO 2 Capture with Pebax Based Mixed Matrix Membranes, Adv Sustain Syst. (2021) 2100317. https://doi.org/10.1002/adsu.202100317.
[161] Y. Nishi, M. Inagaki, Gas Adsorption/Desorption Isotherm for Pore Structure Characterization, Tsinghua University Press Limited, (2016) 243-267. https://doi.org/10.1016/b978-0-12-805256-3.
[162] Y. Wang, G. Yang, H. Guo, X. Meng, G. Kong, Z. Kang, R. Guillet-Nicolas, S. Mintova, Preparation of HKUST-1/PEI mixed-matrix membranes: Adsorption-diffusion coupling control of small gas molecules, J Memb Sci. 643 (2022) 120070. https://doi.org/10.1016/j.memsci.2021.120070.
[163] V. Herynek, M. Babič, O. Kaman, H. Charvátová, M. Veselá, O. Buchholz, M. Vosmanská, D. Kubániová, J. Kohout, U.G. Hofmann, L. Šefc, Maghemite nanoparticles coated by methacrylamide-based polymer for magnetic particle imaging, J Nanoparticle Res. 23 (2021) 52. https://doi.org/10.1007/s11051-021-05164-x.
[164] D. Muñoz-Gil, F.M.L. Figueiredo, High surface proton conduction in nanostructured ZIF-8, Nanomaterials. 9 (2019) 1–14. https://doi.org/10.3390/nano9101369.
[165] L.S. Lai, Y.F. Yeong, K.K. Lau, A.M. Shariff, Effect of Synthesis Parameters on the Formation of ZIF-8 under Microwave-assisted Solvothermal, Procedia Eng. 148 (2016) 35–42. https://doi.org/10.1016/j.proeng.2016.06.481.
[166] M. García-Palacín, J.I. Martínez, L. Paseta, A. Deacon, T. Johnson, M. Malankowska, C. Téllez, J. Coronas, Sized-Controlled ZIF-8 Nanoparticle Synthesis from Recycled Mother Liquors: Environmental Impact Assessment, ACS Sustain Chem Eng. 8 (2020) 2973–2980. https://doi.org/10.1021/acssuschemeng.9b07593.
[167] Y. Chen, M. Yu, R. Wang, Porous zeolitic imidazolate framework loaded mn as an efficient catalyst for the selective catalytic reduction of nox with nh3, Aerosol Air Qual Res. 21 (2021) 1–12. https://doi.org/10.4209/AAQR.210201.
[168] T. Mudalige, H. Qu, D. Van Haute, S.M. Ansar, A. Paredes, T. Ingle, Characterization of Nanomaterials: Tools and Challenges, Nanomaterials for Food Applications. (2019) 313–353. https://doi.org/10.1016/B978-0-12-814130-4.00011-7.
[169] Y. Kushida, Y. Makita, T. Kawakami, K. Hoshiko, H. Nakagawa, Y. Nishimura, Y. Yamaguchi, New polymer design by DLS analysis of development defect detection, J Photopolym Sci Technol. 21 (2008) 641–646. https://doi.org/10.2494/photopolymer.21.641.
[170] F. Cacho-Bailo, C. Téllez, J. Coronas, Interactive Thermal Effects on Metal–Organic Framework Polymer Composite Membranes, Chem Eur J. 22 (2016) 9533–9536. https://doi.org/10.1002/chem.201601530.
[171] A.S. Embaye, L. Martínez-Izquierdo, M. Malankowska, C. Téllez, J. Coronas, Poly(ether-block-amide) Copolymer Membranes in CO_2 Separation Applications, Energy Fuels. (2021) 17085-17102. https://doi.org/10.1021/acs.energyfuels.1c01638.

[172] Q. Xia, H. Wang, B. Huang, X. Yuan, J. Zhang, J. Zhang, L. Jiang, T. Xiong, G. Zeng, State-of-the-Art Advances and Challenges of Iron-Based Metal Organic Frameworks from Attractive Features, Synthesis to Multifunctional Applications, Small. 15 (2019) 1803088. https://doi.org/10.1002/smll.201803088.
[173] S. Zhang, Y. Zhang, F. Baig, T.F. Liu, Synthesis and Applications of Stable Iron-Based Metal-Organic Framework Materials, Cryst Growth Des. 21 (2021) 3100-3122. https://doi.org/10.1021/acs.cgd.0c01500.
[174] S. Patra, S. Sene, C. Mousty, C. Serre, A. Chaussé, L. Legrand, N. Steunou, Design of Laccase-Metal Organic Framework-Based Bioelectrodes for Biocatalytic Oxygen Reduction Reaction, ACS Appl Mater Interfaces. 8 (2016) 20012-20022. https://doi.org/10.1021/acsami.6b05289.
[175] S. Sene, M.T. Marcos-Almaraz, N. Menguy, J. Scola, J. Volatron, R. Rouland, J.M. Grenèche, S. Miraux, C. Menet, N. Guillou, F. Gazeau, C. Serre, P. Horcajada, N. Steunou, Maghemite-nanoMIL-100(Fe) Bimodal Nanovector as a Platform for Image-Guided Therapy, Chem. 3 (2017) 303-322. https://doi.org/10.1016/j.chempr.2017.06.007.
[176] S. Cui, M. Qin, A. Marandi, V. Steggles, S. Wang, X. Feng, F. Nouar, C. Serre, Metal-Organic Frameworks as advanced moisture sorbents for energy-efficient high temperature cooling, Sci Rep. 8 (2018) 15284. https://doi.org/10.1038/s41598-018-33704-4.
[177] A. Permyakova, S. Wang, E. Courbon, F. Nouar, N. Heymans, P. D'Ans, N. Barrier, P. Billemont, G. de Weireld, N. Steunou, M. Frère, C. Serre, Design of salt-metal organic framework composites for seasonal heat storage applications, J Mater Chem A. 5 (2017) 12889-12898. https://doi.org/10.1039/c7ta03069j.
[178] C. Serre, C. Mellot-Draznieks, S. Surblé, N. Audebrand, Y. Filinchuk, G. Férey, Role of solvent-host interactions that lead to very large swelling of hybrid frameworks, Science (1979). 315 (2007) 1828-1831. https://doi.org/10.1126/science.1137975.
[179] Z. Guo, J. Yu, G. Li, Z. Si, H. Guo, H. Zhang, A three-dimensional metal-organic framework based on a triazine derivative: Syntheses, structure analysis, and sorption studies, CrystEngComm. 11 (2009) 2254-2256. https://doi.org/10.1039/b903932e.
[180] M. Pang, A.J. Cairns, Y. Liu, Y. Belmabkhout, H.C. Zeng, M. Eddaoudi, Highly monodisperse M III-based soc -MOFs (M = in and Ga) with cubic and truncated cubic morphologies, J Am Chem Soc. 134 (2012) 13176–13179. https://doi.org/10.1021/ja3049282.
[181] D. Lenzen, J.G. Eggebrecht, P.G.M. Mileo, D. Fröhlich, S. Henninger, C. Atzori, F. Bonino, A. Lieb, G. Maurin, N. Stock, Unravelling the water adsorption in a robust iron carboxylate metal-organic framework, ChemComm. 56 (2020) 9628-9631. https://doi.org/10.1039/d0cc03489d.
[182] F. Steinke, A. Javed, S. Wöhlbrandt, M. Tiemann, N. Stock, New isoreticular phosphonate MOFs based on a tetratopic linker, Dalton Trans. 50 (2021) 13572-13579. https://doi.org/10.1039/d1dt02610k.
[183] E. Soubeyrand-Lenoir, C. Vagner, J.W. Yoon, P. Bazin, F. Ragon, Y.K. Hwang, C. Serre, J.S. Chang, P.L. Llewellyn, How water fosters a remarkable 5-fold increase in low-pressure CO 2 uptake within mesoporous MIL-100(Fe), J Am Chem Soc. 134 (2012) 10174–10181. https://doi.org/10.1021/ja302787x.
[184] S. Wongsakulphasatch, W. Kiatkittipong, J. Saupsor, J. Chaiwiseshphol, P. Piroonlerkgul, V. Parasuk, S. Assabumrungrat, Effect of Fe open metal site in metal-organic frameworks on post-combustion CO_2 capture performance, Greenhouse Gases Sci Technol. 7 (2017) 383-394. https://doi.org/10.1002/ghg.1662.
[185] S. Wang, C. Serre, Toward Green Production of Water-Stable Metal-Organic Frameworks Based on High-Valence Metals with Low Toxicities, ACS Sustain Chem Eng. 7 (2019) 11911-11927. https://doi.org/10.1021/acssuschemeng.9b01022.
[186] J. Embaye, Alua Selomon Martinez-Izquierdo, Lidia Malankawska, Magdalena Tellez, Carlos Coronas, Poly(ether-block-amide) copolymer membranes in CO_2 separation applications, Energy Fuels. 35 (2021) 17085–17102. https://doi.org/10.1021/acs.energyfuels.1c01638.
[187] J.H. Kim, S.Y. Ha, Y.M. Lee, Gas permeation of poly(amide-6-b-ethylene oxide) copolymer, J Memb Sci. 190 (2001) 179–193. https://doi.org/10.1016/S0376-7388(01)00444-6.
[188] L. Wang, Y. Li, S. Li, P. Ji, C. Jiang, Preparation of composite poly(ether block amide) membrane for CO_2 capture, J Energy Chem. 23 (2014) 717–725. https://doi.org/10.1016/S2095-4956(14)60204-7.
[189] S. Meshkat, S. Kaliaguine, D. Rodrigue, Comparison between ZIF-67 and ZIF-8 in Pebax® MH-1657 mixed matrix membranes for CO_2 separation, Sep Purif Technol. 235 (2020) 116150. https://doi.org/10.1016/j.seppur.2019.116150.
[190] S. Meshkat, S. Kaliaguine, D. Rodrigue, Mixed matrix membranes based on amine and non-amine MIL-53(Al) in Pebax® MH-1657 for CO_2 separation, Sep Purif Technol. 200 (2018) 177–190. https://doi.org/10.1016/j.seppur.2018.02.038.
[191] M. Benzaqui, R. Semino, F. Carn, S.R. Tavares, N. Menguy, M. Giménez-Marqués, E. Bellido, P. Horcajada, T. Berthelot, A.I. Kuzminova, M.E. Dmitrenko, A. v. Penkova, D. Roizard, C. Serre, G. Maurin, N. Steunou, Covalent and Selective Grafting of Polyethylene Glycol Brushes at the Surface of ZIF-8 for the Processing of Membranes for Pervaporation, ACS Sustain Chem Eng. 7 (2019) 6629-6639. https://doi.org/10.1021/acssuschemeng.8b05587.
[192] C. Song, R. Li, Z. Fan, Q. Liu, B. Zhang, Y. Kitamura, CO_2/N_2 separation performance of Pebax/MIL-101 and Pebax /NH_2-MIL-101 mixed matrix membranes and intensification via sub-ambient operation, Sep Purif Technol. 238 (2020) 116500. https://doi.org/10.1016/j.seppur.2020.116500.
[193] N. Habib, Z. Shamair, N. Tara, A.S. Nizami, F.H. Akhtar, N.M. Ahmad, M.A. Gilani, M.R. Bilad, A.L. Khan, Development of highly permeable and selective mixed matrix membranes based on Pebax®1657 and NOTT-300 for CO_2 capture, Sep Purif Technol. 234 (2020) 116101. https://doi.org/10.1016/j.seppur.2019.116101.

[194] E. Seddigh, M. Azizi, E.S. Sani, D. Mohebbi-Kalhori, Investigation of poly(ether-b-amide)/nanosilica membranes for CO 2/CH4 separation, Chinese J Polym Sci (English Edition). 32 (2014) 402–410. https://doi.org/10.1007/s10118-014-1416-y.
[195] B. Seoane, J. Coronas, I. Gascon, M.E. Benavides, O. Karvan, J. Caro, F. Kapteijn, J. Gascon, Metal-organic framework based mixed matrix membranes: A solution for highly efficient CO_2 capture?, Chem Soc Rev. 44 (2015) 2421–2454. https://doi.org/10.1039/c4cs00437j.
[196] T.C. Merkel, H. Lin, X. Wei, R. Baker, Power plant post-combustion carbon dioxide capture: An opportunity for membranes, J Memb Sci. 359 (2010) 126–139. https://doi.org/10.1016/j.memsci.2009.10.041.
[197] F. Karamouz, H. Maghsoudi, R. Yegani, Synthesis and characterization of high permeable PEBA membranes for CO2/CH4 separation, J Nat Gas Sci Eng. 35 (2016) 980–985. https://doi.org/10.1016/j.jngse.2016.09.036.
[198] F. Pardo, G. Zarca, A. Urtiaga, Effect of feed pressure and long-term separation performance of Pebax-ionic liquid membranes for the recovery of difluoromethane (R32) from refrigerant mixture R410A, J Memb Sci. 618 (2021) 118744. https://doi.org/10.1016/J.MEMSCI.2020.118744.
[199] M. Kheirtalab, R. Abedini, M. Ghorbani, A novel ternary mixed matrix membrane comprising polyvinyl alcohol (PVA)-modified poly (ether-block-amide)(Pebax®1657)/graphene oxide nanoparticles for CO_2 separation, Process Saf Environ Prot. 144 (2020) 208–224. https://doi.org/10.1016/J.PSEP.2020.07.027.
[200] M. Benzaqui, M. Wahiduzzaman, H. Zhao, M.R. Hasan, T. Steenhaut, A. Saad, J. Marrot, P. Normand, J.-M. Grenèche, N. Heymans, G. de Weireld, A. Tissot, W. Shepard, Y. Filinchuk, S. Hermans, F. Carn, M. Manlankowska, C. Téllez, J. Coronas, G. Maurin, N. Steunou, C. Serre, A robust eco-compatible microporous iron coordination polymer for CO_2 capture, J Mater Chem A. 10 (2022) 8535–8545. https://doi.org/10.1039/d1ta10385g.
[201] G.K. Kline, J.R. Weidman, Q. Zhang, R. Guo, Studies of the synergistic effects of crosslink density and crosslink inhomogeneity on crosslinked PEO membranes for CO_2-selective separations, J Memb Sci. 544 (2017) 25–34. https://doi.org/10.1016/j.memsci.2017.09.002.
[202] S. Chand, A. Pal, R. Saha, P. Das, R. Sahoo, P.K. Chattaraj, M.C. Das, Two Closely Related Zn(II)-MOFs for Their Large Difference in CO2 Uptake Capacities and Selective CO_2 Sorption, Inorg Chem. 59 (2020) 7056–7066. https://doi.org/10.1021/acs.inorgchem.0c00551.
[203] B. Wang, H. Huang, X.L. Lv, Y. Xie, M. Li, J.R. Li, Tuning CO2 selective adsorption over N_2 and CH_4 in UiO-67 analogues through ligand functionalization, Inorg Chem. 53 (2014) 9254–9259. https://doi.org/10.1021/ic5013473.
[204] B. Zheng, J. Bai, J. Duan, L. Wojtas, M.J. Zaworotko, Enhanced CO2 binding affinity of a high-uptake rht-type metal-organic framework decorated with acylamide groups, J Am Chem Soc. 133 (2011) 748–751. https://doi.org/10.1021/ja110042b.
[205] M. Benzaqui, R.S. Pillai, A. Sabetghadam, V. Benoit, P. Normand, J. Marrot, N. Menguy, D. Montero, W. Shepard, A. Tissot, C. Martineau-Corcos, C. Sicard, M. Mihaylov, F. Carn, I. Beurroies, P.L. Llewellyn, G. de Weireld, K. Hadjiivanov, J. Gascon, F. Kapteijn, G. Maurin, N. Steunou, C. Serre, Revisiting the Aluminum Trimesate-Based MOF (MIL-96): From Structure Determination to the Processing of Mixed Matrix Membranes for CO2 Capture, Chem Mater. 29 (2017) 10326–10338. https://doi.org/10.1021/acs.chemmater.7b03203.
[206] W. Lu, D. Yuan, T.A. Makal, J.R. Li, H.C. Zhou, A highly porous and robust (3,3,4)-connected metal-organic framework assembled with a 90° bridging-angle embedded octacarboxylate ligand, Angewandte Chemie - International Edition. 51 (2012) 1580–1584. https://doi.org/10.1002/anie.201106615.
[207] Y.S. Bae, O.K. Farha, J.T. Hupp, R.Q. Snurr, Enhancement of CO2/N2 selectivity in a metal-organic framework by cavity modification, J Mater Chem. 19 (2009) 2131–2134. https://doi.org/10.1039/b900390h.
[208] Z. Liang, M. Marshall, A.L. Chaffee, CO2 adsorption-based separation by metal organic framework (Cu-BTC) versus zeolite (13X), Energy Fuels. 23 (2009) 2785–2789. https://doi.org/10.1021/ef800938e.
[209] L. Ge, W. Zhou, V. Rudolph, Z. Zhu, Mixed matrix membranes incorporated with size-reduced Cu-BTC for improved gas separation, J Mater Chem A. 1 (2013) 6350–6358. https://doi.org/10.1039/c3ta11131h.
[210] N. Tien-Binh, H. Vinh-Thang, X.Y. Chen, D. Rodrigue, S. Kaliaguine, Crosslinked MOF-polymer to enhance gas separation of mixed matrix membranes, J Memb Sci. 520 (2016) 941–950. https://doi.org/10.1016/j.memsci.2016.08.045.
[211] M. Askari, T.S. Chung, Natural gas purification and olefin/paraffin separation using thermal cross-linkable co-polyimide/ZIF-8 mixed matrix membranes, J Memb Sci. 444 (2013) 173–183. https://doi.org/10.1016/j.memsci.2013.05.016.
[212] W.S. Chi, S. Hwang, S.J. Lee, S. Park, Y.S. Bae, D.Y. Ryu, J.H. Kim, J. Kim, Mixed matrix membranes consisting of SEBS block copolymers and size-controlled ZIF-8 nanoparticles for CO2 capture, J Memb Sci. 495 (2015) 479–488. https://doi.org/10.1016/j.memsci.2015.08.016.

Chapter 10: Appendices

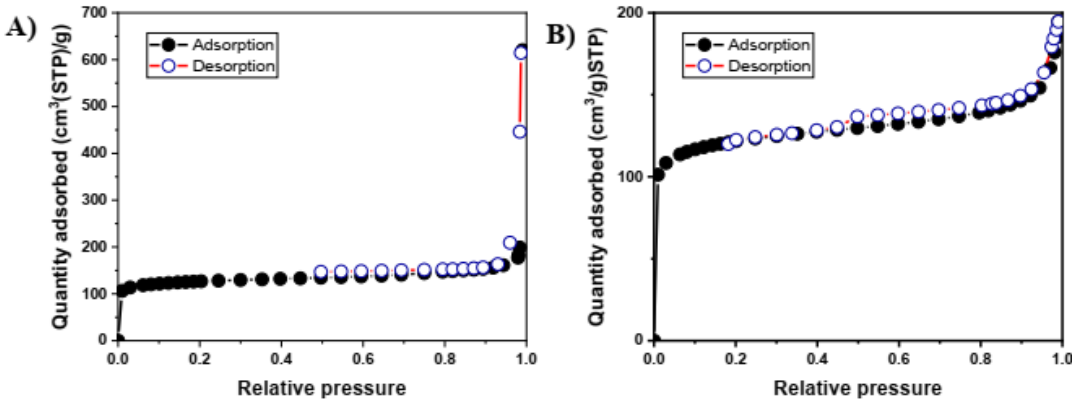

Figure A.1. N_2 adsorption - desorption isotherms of: (A) fresh ZIF-94 (B), recycled ZIF-94

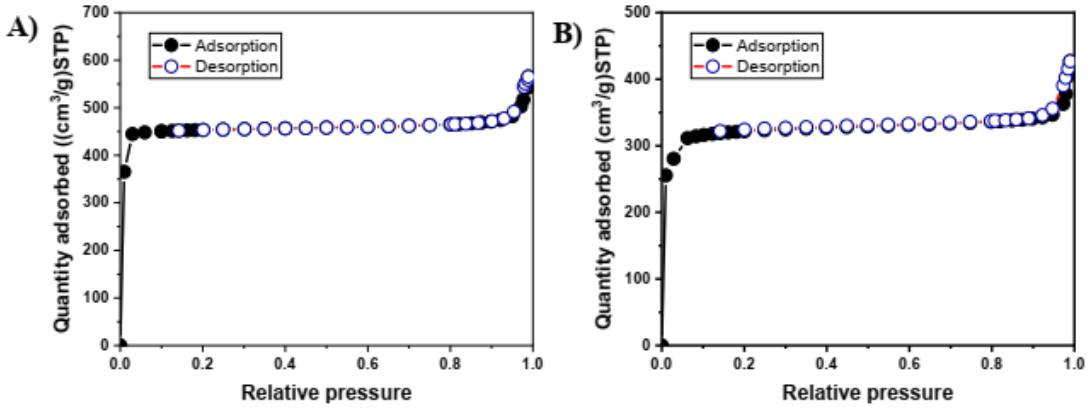

Figure A.2. N_2 adsorption - desorption isotherm of (A) fresh ZIF-8 (B) recycled ZIF-8

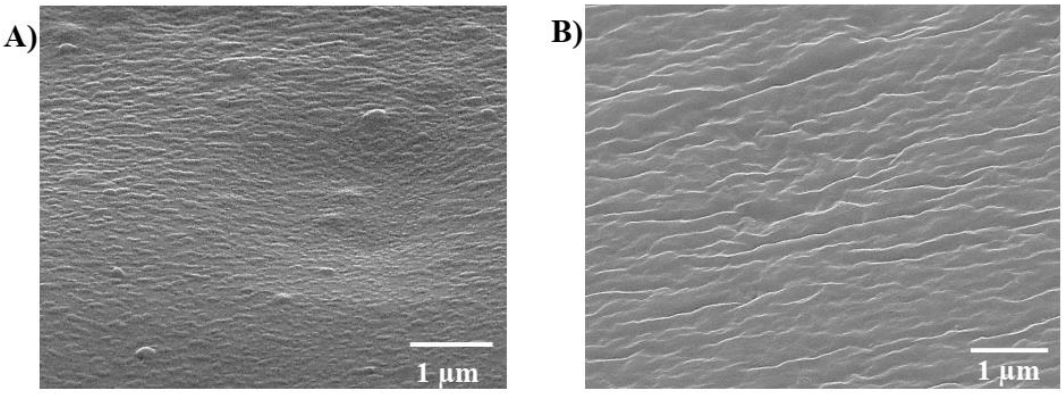

Figure A.3. Cross section SEM images of: (A) fresh bare polymer membrane, (B) recycled bare polymer membrane.

Element	Weight (%)	Atomic (%)
C (K)	41.28 ± 2.94	73.99
O (K)	12.35 ± 1.60	16.63
Zn (L)	0.00	0.00
Pd (L)	46.37 ± 3.09	9.38
Totals	100.00	100

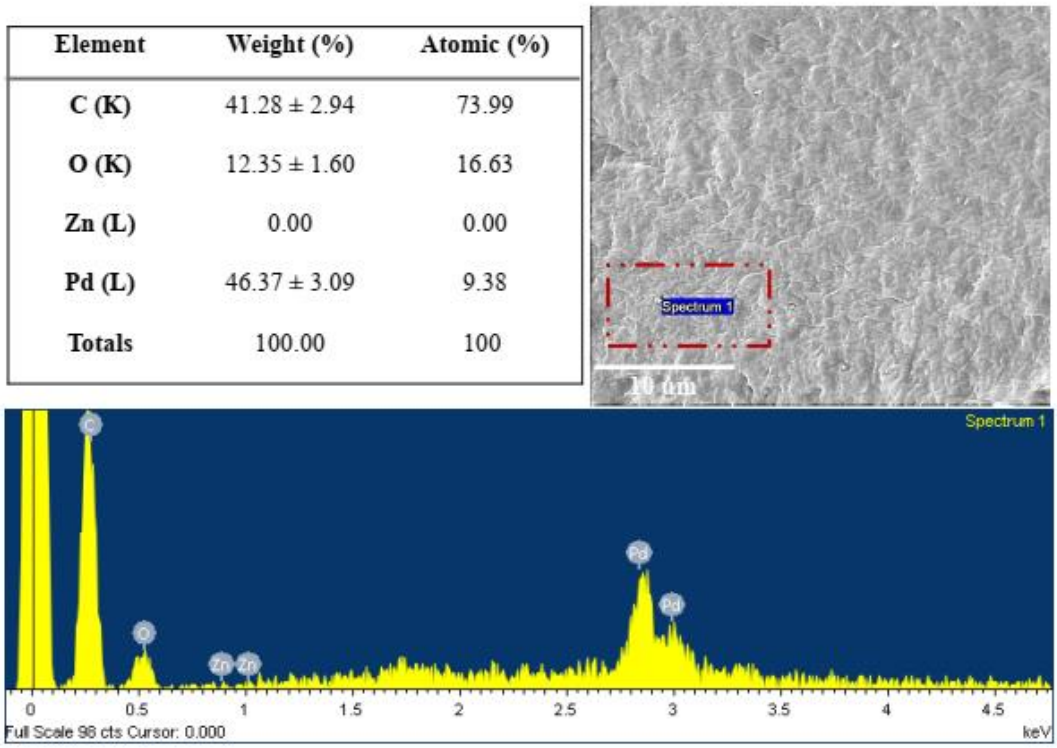

Figure A.4. EDX analyses (on the cross-section surface) of recycled polymer from ZIF-94 based MMM

Element	Weight (%)	Atomic (%)
C (K)	66.38 ± 1.89	84.61
O (K)	12.97 ± 1.00	12.42
Zn (L)	0.00	0.00
Pd (L)	20.65 ± 1.85	2.97
Totals	100.00	100

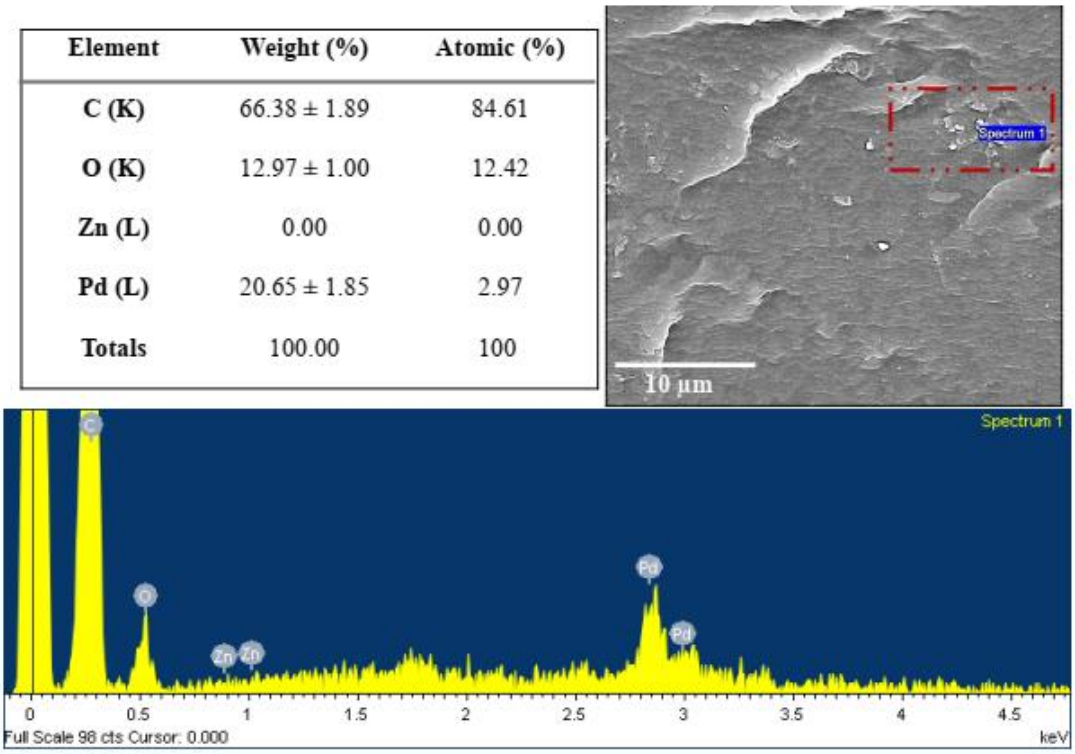

Figure A.5. EDX analyses (on the cross-section surface) of recycled polymer from ZIF-8 based MMM

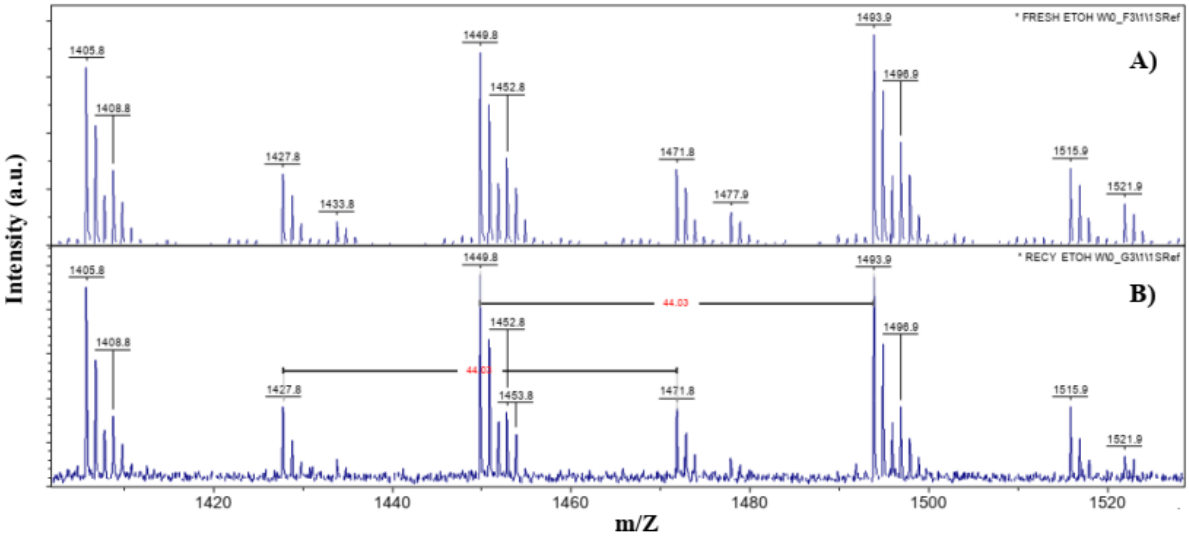

Figure A.6. Molecular weight analysis of polymer membrane: (A) fresh polymer, (B) recycled polymer from bare membrane